WAVE INDUCED OCEAN DIFFUSION

BADAL K. PAL

WAVE INDUCED OCEAN DIFFUSION

BY

Badal K. Pal

A thesis submitted to the School of Graduate
Studies in partial fulfillment of the
requirements for the degree of
Doctor of Philosophy

Department of Physics
Memorial University of Newfoundland
February 1992

St. John's Newfoundland

ISBN 0-315-73333-0

ABSTRACT

Eddy-diffusion in the ocean is studied by using drifter data in the Atlantic Equatorial Undercurrent. The drifter trajectories are analysed to include a detailed analysis of the space and time scales of the relative motion. The ratio of Lagrangian integral length scale to the standard deviation of drifter positions ranged from C_ℓ=0.02 to 0.36. However, on average it was 0.12 in the meridional direction, thus confirming the Fahrbach et al.'s (1986) calculations of the meridional diffusion of salt from the Equatorial Undercurrent. Integral time scales were found to decrease with increasing velocity. It was shown that measurement errors have little effect upon estimation of eddy-diffusivities but biased Lagrangian integral time and length scales (smaller than they should have been). The Eulerian integral time-scale for relative velocities is only slightly greater than the Lagrangian integral time-scale. Joint space-time correlations indicated that the eddy velocity changes rapidly compared with time-scales required to advect a particle over the eddy length-scale.

A perturbation analysis of the 3-D Lagrangian equations of motion is used to examine the diffusion induced by a random field of surface gravity waves in an inviscid and viscous ocean. At second order, the inviscid solutions give a random field of shearing motion in the horizontal plane. For the viscous case, the Lagrangian equations of motion are solved for a spectrum of nondecaying surface gravity waves and a spectrum of decaying surface gravity waves. At second order, the zero-frequency nondecaying and decaying solutions show random field of

shearing motion in both horizontal and vertical plane. For zero angle of interaction between the primary waves, the horizontal velocity due to viscous decaying wave solution is large near the surface compared to the inviscid and viscous forcing solutions. The three solutions converge below the depth of the viscous boundary layer for zero angle of interaction. For interaction with non-zero angle between the primary waves, the viscous decaying solutions go to inviscid solutions below the depth of the viscous boundary layer. The viscous nondecaying wave solutions decay more slowly with depth and remain different from the inviscid and viscous decaying wave solutions.

The inviscid solutions exhibit horizontal diffusion identical to Herterich and Hasselmann (1982). The viscous (decaying and nondecaying) solutions show both horizontal and vertical diffusion. The inclusion of viscosity causes a significant change in the horizontal inviscid eddy-diffusivity. Near the surface, the single-particle viscous decaying diffusivity D_{11}^{VD} is larger than the inviscid diffusivity D_{11}^{IN} and viscous nondecaying diffusivity D_{11}^{VF} by factors of 1.2 and 1.7 respectively for viscosity $\nu = 1.0 \times 10^{-2} m^2/s$. Changing viscosity has very small effect on the horizontal diffusivity.

The vertical eddy-diffusivity is found to be much smaller than the eddy-viscosity. A linear increase of vertical eddy-diffusivity with the viscosity is observed. The single-particle horizontal eddy-diffusivities increase with wind-speed raised to the power of 3. The single-particle vertical eddy-diffusivity does not show any power-law dependence with the wind-speed.

ACKNOWLEDGEMENTS

I sincerely thank my supervisor Dr. Brian G. Sanderson for his guidance, support and encouragement throughout my studies. He suggested the topic of this thesis to me and offered numerous ideas during the course of the work.

I gratefully thank Dr. E. Fahrbach for making available to me data for this analysis.

I am indebted to Dr. Richard Greatbatch and Dr. Gordon Mertz for their helpful comments and advice. Dr. Greatbatch in particular made important suggestions in deriving the general boundary conditions for the viscous problem. Thanks are also due to Dr. Alex Hay and Dr. Brad de Young for many discussions.

I thank Mr. A. Goulding for helping with computer related problems.

I specially thank Dr. D. Rendell, Dr. F. A. Aldrich, Dr. C. Sharp, Mrs. J. Barron and Mrs. B. Burke for their help in dealing with administrative matters.

I am deeply appreciative of the financial assistance from the Memorial University of Newfoundland in the form of University Fellowship and teaching assistantship, and from Dr. Sanderson's operating Grant funded by Natural Sciences and Engineering Research Council of Canada.

Finally, I thank my wife Manisha for her understanding, encouragement and support during my graduate studies.

TABLE OF CONTENTS

ABSTRACT ii

ACKNOWLEDGEMENTS iv

TABLE OF CONTENTS v

LIST OF FIGURES viii

LIST OF TABLES xi

LIST OF SYMBOLS xii

CHAPTER 1. INTRODUCTION 1

CHAPTER 2. PATCH DIFFUSION COMPUTED FROM LAGRANGIAN DATA 7

2.1. INTRODUCTION 7

2.2. CALCULATION OF EDDY DIFFUSIVITIES 9

2.3. EULERIAN ANALYSIS OF RELATIVE VELOCITIES 21

2.4. SUMMARY 34

CHAPTER 3. RESIDUAL MOTIONS ASSOCIATED WITH INVISCID GRAVITY WAVES 36

3.1. INTRODUCTION 36

3.2. MATHEMATICAL FORMULATION 38

3.3. SOLUTION OF THE FIRST ORDER EQUATIONS 41

3.4. SOLUTION OF THE SECOND ORDER EQUATIONS 43

3.5. SUMMARY 50

CHAPTER 4. RESIDUAL MOTIONS ASSOCIATED WITH VISCOUS GRAVITY WAVES 51

4.1. INTRODUCTION 51

4.2. MATHEMATICAL FORMULATION 54

4.3. BOUNDARY CONDITIONS 57

4.4. SOLUTION FOR NONDECAYING VISCOUS GRAVITY WAVES 63

4.4.1. THE FIRST ORDER SOLUTIONS 63

4.4.2. THE SECOND ORDER SOLUTIONS 72

4.5. SOLUTION FOR DECAYING VISCOUS GRAVITY WAVES 88

4.5.1. THE FIRST ORDER SOLUTIONS 88

4.5.2. THE SECOND ORDER SOLUTIONS 92

4.5.3. SUMMARY 114

CHAPTER 5. CALCULATION OF EDDY DIFFUSIVITIES 116

5.1. INTRODUCTION 116

5.2. MATHEMATICAL DERIVATION 117

5.3. NUMERICAL CALCULATION 127

CHAPTER 6. SUMMARY AND CONCLUSIONS 151

BIBLIOGRAPHY 158

LIST OF FIGURES

Figure 2-1: Plot of $K_{11}(t)$ and $K_{22}(t)$ for experiment CIPREA. Error bars represent plus and minus one standard deviation. 12

Figure 2-2: Plots of Lagrangian autocorrelation and helicity $(R_{12}^{E}-R_{21}^{E})/2$ for velocities relative to the cluster centroid. Error bars represent plus and minus one standard deviation. 16

Figure 2-3: Plots of Eulerian autocorrelation coefficients of velocities relative to the centroid. Error bars represent plus and minus one standard deviation. H is $(R_{12}^{E}-R_{21}^{E})/2$ 25

Figure 2-4: Contour plots showing f^* and g^* as functions of time and space lags, for experiments CIPREA (4a) and D2 (4b). Line shading indicates negative correlations. Unshaded areas have correlations in the range 0.0 to 0.1. Dotted shading indicates correlations greater than 0.1. 30

Figure 2-5: Plots of spatial correlations $f(r)$, $g(r)$ for experiments CIPREA and D2. 33

Figure 3-1: Surface waves with wavenumbers k and k travel in the θ and θ' directions respectively. The resulting zero-frequency second-order interaction causes motion with wave number components $k\gamma_1$, $k\gamma_2$, which have a resultant in the Θ_r direction. The zero-frequency velocity is in the horizontal plane and is parallel to the angle bisector (dashed line). It is also sheared in the horizontal plane as indicated by the sinusoidally varying flow pattern. 49

Figure 4-1: Balance of forces on an elevated fluid surface. 58

Figure 4-2: Interaction of two primary waves to give a horizontally and vertically sheared mean flow. The arrows show the magnitude and direction of current as a function of position (a,b,c). (a) A horizontal section through the surface c=0. Plot shows u_2^{VF} and v_2^{VF} velocities are sheared in the horizontal plane. (b) A vertical section in the (b,c) plane. Plot shows v_2^{VF} and w_2^{VF} are sheared with respect to b and c. The parameters used are ω = 1.43 s^{-1}, θ = 45°, θ' = - 45°, a=b=20 m and ν = 0.01 m^2/s, amplitude = 1 m. 87

Figure 4-3: Plots of inviscid (3.63, 3.61), viscous nondecaying (4.102-4.104) and viscous decaying (4.145a-c) solutions versus depth. Note that magnitude and direction of the velocities vary as θ and θ' change. Parameters used in the calculations are shown on the plots. 112

Figure 5-1: Plots of single particle horizontal diffusivities as a function of exponent n of the directionality function (eqn. 5.39). (a) inviscid case, (b) D_{ii}^{VF} with viscosity $\nu = 1.0\times10^{-6}\ m^2/s$, (c) D_{ii}^{VF} with viscosity $\nu = 1.0\times10^{-2}\ m^2/s$ and (d) D_{ii}^{VD} with $\nu = 1.0\times10^{-2}\ m^2/s$. 130

Figure 5-2: Single-particle diffusivity D_{ii}^{IN}, D_{ii}^{VF}, D_{ii}^{VD} plotted as a function of depth for $\nu = 1.0\times10^{-6}\ m^2/s$ and t=100 s. 134

Figure 5-3: Single-particle diffusivities D_{11}^{IN} and D_{11}^{VF} plotted as a function of wind speed U. The following parameters are used : c=0, $\nu = 1.0\times10^{-6}\ m^2/s$. 136

Figure 5-4: Single-particle vertical diffusivities D_{33}^{VF} and D_{33}^{VD} plotted as a function of depth. The following parameters were used : U=10 m/s, $\nu = 1.0\times10^{-2}\ m^2/s$, t= 100 s 138

Figure 5-5: Single-particle diffusivities D_{33}^{VF} as function of depth for $\nu = 1.0\times10^{-6}$ m^2/s. Contributions from different terms in (5.44) are shown. The top line corresponds to *term*1 and total D_{33}^{VF}. The middle line (dashed) and the bottom line (solid) are due to *term*2 and *term*3 respectively. 140

Figure 5-6: Plots of D_{33}^{VF} versus viscosity for depth c=-4.0 m. The top line corresponds to *term*1 and total D_{33}^{VF}. The middle line (dashed) and the lowest line (solid) are due to *term*2 and *term*3. 142

Figure 5-7: Plot of single-particle vertical diffusivity D_{33}^{VF} as a function of wind speed U. 143

Figure 5-8: Single-particle, two-particle and patch-diffusivity plotted as a function of horizontal separation scale r. (a) inviscid case, (b) viscous forcing with $\nu = 1.0\times10^{-2}$ m^2/s and (c) viscous forcing with $\nu = 1.0\times10^{-2}$ m^2/s. Parameters used were c=0.0, λ=200 m. 145

Figure 5-9: Two-particle diffusivities $D_{11}^{IN(2)}$ and $D_{11}^{VF(2)}$ as a function of vertical separation r_3 for c=0. The solid line is for $D_{11}^{IN(2)}$ and the broken lines are due to $D_{11}^{VF(2)}$ for $\nu = 1.0\times10^{-6}$ and $\nu = 1.0\times10^{-2}$ m^2/s respectively. 147

Figure 5-10: Two-particle diffusivity $D_{33}^{VF(2)}$ as a function of vertical separation r_3 for c=0.05 m. The solid line is due to $\nu = 1.0\times10^{-6}$ and the broken line is due to $\nu = 1.0\times10^{-2}$ m^2/s respectively. 149

List of Tables

Table 2-1: Zonal and meridional components of the time-averaged eddy diffusivity tensor. K_{ii} is for a model in which all motion relative to the centroid is considered diffusive. K_{ii}^{d} is for a model in which motion relative to the centroid is considered to have a component due to time-varying spatially uniform Lagrangian deformations, as well as diffusive motion. K_{ii}^{F} are eddy diffusivities calculated by Fahrbach et. al.(1986), and C_{ei} are coefficients calculated from K_{ii} and K_{ii}^{F}. Units for $(K)s{:}m^2s^{-1}$ 11

Table 2-2: Time-averaged values of the standard deviation of drifter positions σ_x and σ_y relative to the cluster centroid, magnitude of relative velocities U'_i, Lagrangian integral time-scale τ_i^*, eddy diffusivities K_{ii}, and ratio of Lagrangian integral length scale to the standard deviation of drifter positions C_{ex} and C_{ey}. The numbers enclosed in parantheses are corrected for measurement error. 19

Table 2-3: integral time-scales: Lagrangian τ_u^*, τ_v^*; Eulerian Cartesian components τ_{EL}^* and τ_{ET}^*. All values are in minutes and are corrected for measurement error. 29

LIST OF SYMBOLS

a, b, c	Lagrangian coordinates
A^{IN}, B^{IN}	coefficients of inviscid solutions
A^{VF} B^{VF} C^{VF}	coefficients of viscous nondecaying solutions
A^{VD} B^{VD} C^{VD}	coefficients of viscous decaying solutions
C_e	ratio of integral length scale to standard deviation
$d\xi_1$	first order spectral density function of vertical displacement
$d\xi_x, d\xi_y$	first order spectral density function of horizontal displacement
$d\xi_p$	first order pressure spectral density function
D_{ij}^{IN}	inviscid single-particle diffusivity tensor
D_{ij}^{VF}	viscous nondecaying single-particle diffusivity tensor
D_{ij}^{VD}	viscous decaying single-particle diffusivity tensor
$D_{ij}^{IN(2)}$	inviscid two-particle diffusivity tensor for horizontal separation r
$D_{ij}^{VF(2)}$	viscous nondecaying two-particle diffusivity tensor for horizontal separation r
$D'^{IN(2)}_{ij}$	inviscid two-particle diffusivity tensor for vertical separation r_3
$D'^{VF(2)}_{ij}$	viscous nondecaying two-particle diffusivity tensor for vertical separation r_3
$D_{ij}^{IN(p)}$	inviscid patch diffusivity tensor
$D_{ij}^{VF(p)}$	viscous nondecaying patch diffusivity tensor

$D_{ij}^{IN(pa)}$	inviscid patch average diffusivity tensor
$D_{ij}^{VF(pa)}$	viscous nondecaying patch average diffusivity tensor
$f(r), g(r)$	spatial correlation along coordinate axes
f^*, g^*	correlation as a function of space and time lag along longitudinal and transverse direction
$F(s)$	Laplace transform of the function f(t)
$F(\tau)$	time lagged longitudinal correlation
$f(\omega)$	frequency dependent part of the spectrum
g	gravity
$G(\tau)$	time lagged transverse correlation
h_L	helicity
h^*	helicity due to correlation between longitudinal and transverse component of motion
$\hat{\imath}, \hat{\jmath}, \hat{k}$	unit vectors
k	wave number
K_{ij}	centroid position subtracted eddy-diffusivity tensor
K_{ij}^d	centroid position and deformation subtracted eddy-diffusivity tensor
K^F	Eddy-diffusivity calculated by Fahrbach et. al.
l	viscous length scale
l_1^*	Lagrangian integral length scale
$m_{1,2}$	roots of the homogeneous differential equation
$\hat{n}$	unit vector normal to the surface
n	directionality parameter
p_0	surface pressure

p_1	first order pressure solution
p_2	second order pressure solution
r_1, r_2	horizontal separation
r_3	vertical separation
R_{ij}	Lagrangian correlation
R_{ij}^{j}	joint space-time correlation
R_{ij}^{E}	Eulerian correlation
R	auto correlation function of the measured velocity
R_{Tr}	auto correlation function of the true velocity
$S_1(\omega,\theta)$	wave spectrum
t	time
$\hat{t}$	unit vector tangential to the surface
u	measured velocity
u_e	measurement error in the velocity
u_{Tr}	true velocity
U'_i	rms velocity
$u_2^{IN}, v_2^{IN}, w_2^{IN}$	second order inviscid solutions
$u_2^{VF}, v_2^{VF}, w_2^{VF}$	second order viscous nondecaying solutions
$u_2^{VFp}, v_2^{VFp}, w_2^{VFp}$	second order viscous nondecaying particular solutions
$u_2^{VD}, v_2^{VD}, w_2^{VD}$	second order viscous decaying solutions
$U_2^{VDh}, V_2^{VDh}, W_2^{VDh}$	Laplace transform of the second order homogeneous viscous decaying solutions
$u_2^{VDp}, v_2^{VDp}, w_2^{VDp}$	second order viscous decaying particular solutions

$x_1^{IN}, y_1^{IN}, z_1^{IN}$	first order inviscid solutions
$x_1^{VD}, y_1^{VD}, z_1^{VD}$	first order viscous decaying solutions
$x_1^{VF}, y_1^{VF}, z_1^{VF}$	first order viscous nondecaying solutions
x'_{in}	position with respect to centroid of the nth drifter along the i th direction
x'_{in}	velocity with respect to centroid of the n th drifter along i th direction
x_{in}''	residual displacement when centroid position and position due to linear deformation are extracted
$\delta = 4\nu k^2$	viscous wave decay time scale
∇^2	Laplacian operator
ε	wave slope
$\varepsilon_1 = kl$	nondimensinal quantity
η	free surface
θ	angle made by the wave number vector with the x-axis
ν	eddy-viscosity
ρ	density
σ_{ij}	internal stress tensor
τ	time lag
τ^*	Lagrangian integral time scale
τ^*_{Eu}, τ^*_{Ev}	cartesian components of Eulerian integral time scale
τ^*_{EL}, τ^*_{ET}	longitudinal and transverse components of integral time scale

τ_i'	first order wind stress
τ_i''	second order wind stress
ω_o, ω_R	real part of the frequency
ω_I	Imaginary part of the frequency

Chapter 1

INTRODUCTION

Oceanic eddy-diffusion is a complex physical phenomenon that is caused by a great number of different dynamical processes. Generally we constrain ourselves to describing the gross statistics of dispersing material. In the past, eddy-diffusivities have been evaluated from the statistics of clusters of drifters. The underlying assumption of the approach was that the dispersive motion of the particles can be understood by knowing only the statistical properties (e.g., mixing length, energy) of diffusive motion. Various dynamic processes can be related to the statistical properties of this motion (Sanderson and Okubo, 1988; Herterich and Hasselmann, 1982).

Taylor (1922) kinematically formulated the basic concept of the theory of dispersion in homogeneous stationary turbulence in terms of Lagrangian velocity correlation. Stommel (1949) showed that the classical Fickian diffusion equation can not properly describe the relative spread of a cluster of particles with respect to its center of mass. Instead, he found that Richardson's (1926) model of the distance-neighbour concentration describes the oceanic diffusion reasonably well. A review of oceanic diffusion models was given by Okubo (1962). He showed that for a radially symmetric two-dimensional diffusion of passive contaminants the solution to the diffusion equation may be expressed in terms of a diffusion velocity (Joseph and Sendner, 1958) or in terms of the rate of turbulent energy transfer-parameter (Ozmidov, 1958). The former class of solutions are characterized by maximum

concentrations that decrease with time as t^{-2} and the horizontal variances increase as t^2, while the later class of solutions find that they are t^{-3} and t^3 respectively. However, observations show that the horizontal variances increase with time at a power between 2 and 3 (Okubo, 1971). Davis (1982) examined the relationship between the transport of scalar properties and the statistics of particle motion and developed a model for predicting statistics of particle dispersal from Eulerian statistics of velocity. Kawai (1985) measured horizontal velocity gradients in the seas around Japan and United States and observed that the magnitude of divergence and vorticity vary as scale raised to the power of -0.67 for the mesoscale (3 m to 30 km). Krauss and Boning (1987) used one hundred and thirteen satellite tracked buoys in order to calculate Lagrangian statistics of eddy field in the northern North Atlantic. They noticed that the horizontal variance of particle motion is in good agreement with a t^2-law during the first day after release and increases linearly with time during 10 to 60 days. The spectral slope was found to follow a -2 or -3 power law. A -2 power law of the spectral slope was observed by Collin de Verdiere (1983) in the eastern North Atlantic. More recently Osborne et al. (1989) and Sanderson et al. (1990) have shown both absolute and relative dispersion to be fractal. Sanderson and Booth (1991) have formulated a fractal model that provides a better fit to the data than the Taylor model - the Taylor model being a special case of the fractal model.

The theory of shear flow dispersion began with Taylor's (1953) realization that the sheared velocity profile in a pipe would interact with cross-channel molecular diffusion to produce augmented along-channel dispersion. Sometimes it is appropriate (e.g., in estuaries Wilson and Okubo, 1978) to consider the oceanic motion as a large scale shear and small scale eddies. The combined effect of diffusion across the shear produces augmented horizontal diffusion in the along stream direction.

Bowden (1965) considered horizontal diffusion due to shear effect in alternating currents, steady currents and wind driven currents. Young et al. (1982) considered advection diffusion in the oscillatory, sheared velocity field comprised of internal waves.

Zimmerman (1986) reviewed cascade shear-dispersion and Lagrangian chaos models of the horizontal dispersion by tidal and residual currents. In the cascade shear-model tide induced turbulence is an essential aspect of the dispersion process. Turbulence interacts with vertical shear producing horizontal dispersion. In turn, that mechanism interacts with horizontal shear of residual currents giving rise to a large effective dispersion in the residual current direction. The Lagrangian chaos model explains the possibility of dispersion without recourse to large scale turbulence. However, it is a purely kinematic model based on the Euler Lagrange transformation. The superposition of deterministic Eulerian modes in the velocity field, that have different length and time scales can give rise to Lagrangian trajectories that are chaotic functions of time.

Most of the above models are limited to semi-empirical scaling arguments based on dimensional analysis or are largely kinematic in that details of the motion are not analytic solutions of dynamical equations. The main philosophy of the proposed study is that much of the horizontal dispersion of the drifters can be described using solutions of the equations of motion. Much of the work that has adopted this approach has been done in a Lagrangian coordinate system. From a mathematical stand point, the Lagrangian representation of the Navier-Stokes equations appears more complex than the Eulerian form. Furthermore, the Navier-Stokes equations in Lagrangian form have not been studied as extensively as the Eulerian form. However, since one follows the motion of fluid particles in the Lagrangian description, the Lagrangian approach has advantage over the Eulerian method for

describing the diffusion (Okubo, 1967). If an Eulerian coordinate system is used then one is always confronted with an Euler-Lagrange transformation in order to obtain eddy-diffusivities. Also the free boundary conditions are often more simple in a Lagrangian framework.

The Lagrangian form of the diffusion equation was first given by Corrsin (1962). An exact analytical solution of the Lagrangian diffusion equation has been found for time dependent, spatially uniform Lagrangian deformations and eddy-diffusivities (Okubo et al., 1983). Later, Sanderson and Okubo (1986) extended this analysis to include nonlinear Lagrangian deformations.

Pierson (1962) solved the Lagrangian form of the Navier-Stokes equations by means of a perturbation technique. He showed that the solution of the first order equations yield two- and three- dimensional motions that have some of the properties of mixing and turbulence. Okubo (1967) applied solutions to the viscous Lagrangian equations of motion and evaluated the eddy-diffusion caused by these solutions. This approach is fundamentally different from all prior work in that it found solutions to the equations of motion that caused eddy-diffusion directly.

Tamai (1972) studied diffusion due to a random field of deep water gravity waves using a perturbation analysis of the equations of motion. He considered two-dimensional motion in the vertical plane, and therefore observed no eddy-diffusion in the second order in the perturbation analysis. In the third order interactions Tamai (1972) found solutions that were valid for short times and caused eddy-diffusion. But his estimates are too small to account for experimentally measured values. Herterich and Hasselmann (1982) considered the horizontal diffusion of tracers in the presence of a random field of ocean surface gravity waves. Instead of solving the Lagrangian equations of motion, they constructed Eulerian velocities (for second order interactions)

following the procedure of Hasselmann (1961) and applied Euler-Lagrange transformation to obtain Lagrangian velocities (from the Eulerian velocities). These solutions exhibited horizontal eddy-diffusion as a particular case of zero frequency interactions but no vertical eddy-diffusion. Recently, Sanderson and Okubo (1988) solved the inviscid, nonrotating equations of motion in Lagrangian coordinates for a random field of internal waves. Their study was appropriate for coastal waters, in that they used normal modes rather than considering waves propagating vertically. In the second order of their analysis, they found solutions which gave horizontal eddy-diffusion. In particular they found that an approximation to the Munk (1981) spectrum resulted in a pair diffusivity varying as scale raised to the power of 4/3. The solutions also show that the velocity field is a random function of space.

In this thesis we will study oceanic diffusion by analysing data as well as making a theoretical study of mixing by surface waves. Fahrbach et al. (1986) conducted four experiments in the Atlantic Equatorial undercurrent in order to estimate the salt loss from the undercurrent. They analysed their data by applying a technique which has a recently discovered error (Sanderson et al., 1988). Chapter 2 contains a re-analysis of Fahrbach et al.'s drifter trajectories and calculates eddy-diffusivities by applying the appropriate corrections. The analysis is further extended to include a detailed study of the space and time scales of relative motion (Sanderson and Pal, 1990).

The results of the above work indicate that at scales of O (10 - 5000 m) particle dispersion is related to internal waves. Herterich and Hasselmann (1982) show that surface gravity waves can result in horizontal diffusivities that fit the small scale O(10 - 100 m) portion of Okubo's (1971) diffusivity diagram. Sanderson and Okubo (1988) related the horizontal eddy-diffusivities to nonrotating internal wave dynamics. Both Herterich and Hasselmann and Sanderson and Okubo obtained

solutions that diffuse material only in the horizontal plane, no diffusion in the vertical plane. The question to be asked is: can we obtain any vertical diffusion from the interaction of random waves? One major objective of this thesis is, therefore, to explore the possibility of relating random wave motion due to deep water surface gravity waves with vertical diffusion.

Chapter 3 deals with the solution of the 3-D Lagrangian equations of motion for surface gravity waves in an inviscid nonrotating ocean. At second order, the inviscid solutions show a random field of shearing motion in the horizontal plane, but no vertical motion.

In Chapter 4, the inviscid solutions are extended to include viscosity. The viscous 3-D Lagrangian equations of motion are solved analytically for a spectrum of nondecaying and decaying surface gravity waves in a homogeneous nonrotating ocean. At second order, the viscous (nondecaying and decaying) solutions show a random field of shearing motion in both the horizontal and vertical planes.

The solutions obtained in Chapter 3 and Chapter 4 are used to calculate single-particle, two-particle and patch eddy-diffusivities following the technique of Herterich and Hasselmann (1982) and are presented in Chapter 5. The resulting equations are then numerically integrated to obtain estimates of eddy-diffusivities. Eddy-diffusivities for an inviscid fluid are then compared with the corresponding quantities for a fluid with a range of eddy-viscosities.

Chapter 2

PATCH DIFFUSION COMPUTED FROM LAGRANGIAN DATA

2.1. INTRODUCTION

Katz et al. (1980) calculated a salt budget for the Atlantic Equatorial Undercurrent. They estimated that most of the salt loss is due to vertical mixing above and below the equatorial current. However, they did not have direct measurements of horizontal salt transport perpendicular to the core caused by eddy-diffusion. Fahrbach et al. (1986) used four drifter cluster experiments to measure relative diffusivities and determined that meridional horizontal eddy-diffusion accounts for about 20% of the salt loss. They calculated eddy diffusivities using the method of Okubo and Ebbesmeyer (1976). This method has two shortcomings. First it invokes an arbitrary constant C_c (taken to be 0.1 by analogy with Ozmidov, 1960) that is the ratio of the Lagrangian integral length scale to the standard deviation of drifter positions about the cluster centroid. Second the number of degrees of freedom for the residual velocities is given incorrectly, as discussed by Sanderson et al. (1988).

Fahrbach et al. (1986) calculated residual velocities by extracting motion due to time averaged velocity gradients from the velocities relative to the cluster centroid. They used these residual velocities to calculate horizontal eddy diffusivities. In this case the horizontal salt transport would be due to the combined effects of direct

eddy-diffusion as well as interaction of eddy-diffusion with velocity gradients (Okubo et al. 1983). However Fahrbach et al. (1986) used these horizontal eddy diffusivities in a pure eddy-diffusion model, without consideration of the shear-diffusion effect.

Although each of the three points mentioned above are only likely to affect the horizontal salt transport in a minor way it is worthwhile to reanalyze the data. In so doing we confirm the conclusions of Fahrbach et al. (1986), and also obtain insight into the spatial and temporal structure of the dispersive motion.

A detailed description of the cluster experiments is given in Fahrbach et al. (1986). The four drifter clusters were named CIPREA, D1, D2, D3 and consisted of 6, 9, 8, 5 drifters respectively. The drogues were set at depths in the range 70 to 90 m, depending upon the estimated depth of the salinity core. The ship's radar was used to measure relative drifter positions every 30 minutes for periods ranging from 39 to 50 hours. Experiments D1, D2, D3 were carried out at about 21°W, whereas experiment CIPREA was conducted in the Gulf of Guinea at about 4°W.

In section 2.2 we use a variation of the method of Okubo et al. (1976) with modifications recommended by Sanderson et al. (1988) to calculate eddy diffusivities from residual velocities relative to the centroid motion. We then calculate the Lagrangian autocorrelation coefficient of velocity relative to the centroid as a function of lag. This yields Lagrangian integral time/length scales, eddy diffusivities and values for C_e (Taylor 1921). Section 2.3 provides a more detailed analysis of the structure of motion relative to the cluster centroid. We compute the Eulerian space-time correlation function by correlating the motion of a drifter at position $\mathbf{x}$ at time t with the motion of a different particle at $\mathbf{x}+\mathbf{r}$ at time $t+\tau$. The analysis is done by resolving motion into components

that are transverse and along the direction of the space lag vector $\mathbf{r}$ (Middleton and Garrett 1986, Poulain and Niiler 1989).

2.2. CALCULATION OF EDDY DIFFUSIVITIES

In this section we calculate relative eddy diffusivities from drifter positions and velocities, relative to the cluster centroid. Positions/velocities relative to the cluster centroid will be referred to as relative positions/velocities throughout the following work. The absolute positions of drifters are not known with nearly the same precision as relative drifter positions, so it is inappropriate to attempt to calculate single particle (absolute) diffusivities. Consider positions in a Lagrangian coordinate system fixed to the cluster centroid so that x_{in} $(i=1,2)$ is the i'th coordinate of the n'th particles relative position. Here the x_1 and x_2 axes are positive towards the east and north respectively. The position of the n'th drifter in a cluster can be written as the following function of its Lagrangian relative position coordinates $a_{in}=x_{in}(t=0)$, and subsequent displacement x'_{in}

$$x_{in}=a_{in}+x'_{in}. \tag{2.1}$$

In a cluster of N drifters we note that

$$\sum_{n=1}^{N} x_{in}=\sum_{n=1}^{N} a_{in}=\sum_{n=1}^{N} x'_{in}=0$$

since all positions are relative to the centroid.

Considering a model for drifter motion that consists of advection with the patch centroid and diffusion relative to the patch centroid, then a time-dependent eddy-diffusivity tensor can be defined in a manner analogous to Okubo et al. (1976) and Sanderson et al. (1988)

$$K_{ij}(t)=\left(\sum_{n=1}^{N} x'_{in}\dot{x}'_{jn}\right)/(N-1), \quad i,j=1,2 \tag{2.2}$$

where $\dot{x}'_{jn}$ the time derivative of x'_{jn}.

Eddy diffusivity tensors calculated using (2.2) turn out to be rapidly fluctuating functions of time, as illustrated by the representative example in Figure 2.1. However if the relative trajectories are quasi-stationary (quasi-stationarity is discussed later), then averaging $K_{ij}(t)$ with respect to time will yield eddy diffusivities $\overline{K_{ij}}$ that are independent of t and might be compared with eddy diffusivities K^F found by Fahrbach et al. (1986). These and values of C_e derived from a ratio of $\overline{K}/(10K^F)$ are presented in Table 2.1.

Eddy diffusivities for CIPREA and for the x direction in D2 are a factor of about 5 greater than those of Fahrbach et al. (1986), indicating values for C_e that are substantially larger than 0.1. However eddy diffusivities for the other experiments are similar to, or smaller than those of Fahrbach et al. (1986), indicating that the assumption $C_e \approx 0.1$ is reasonable. It should be stressed that these values of C_e are not rigorously defined since Fahrbach et al. (1986) did not define residual displacements x'_i in the same way we did. Our reason for using a different method for calculating residual displacements will now be discussed.

It is conceivable that the large values of $\overline{K}_{ii}$ are caused by larger scale deformation of clusters. We therefore compute the diffusivity tensor $K^d_{ij}(t)$ from residuals x''_i that are left when both the centroid displacement and displacements due to time-varying spatially- uniform Lagrangian deformations are extracted (Okubo et al., 1976; Sanderson et al., 1988).

Table 2-1: Zonal and meridional components of the time-averaged eddy diffusivity tensor. K_{ii} is for a model in which all motion relative to the centroid is considered diffusive. K_{ii}^d is for a model in which motion relative to the centroid is considered to have a component due to time-varying spatially uniform Lagrangian deformations, as well as diffusive motion. K_{ii}^F are eddy diffusivities calculated by Fahrbach et al.(1986), and C_{ei} are coefficients calculated from K_{ii} and K_{ii}^F. Units for $(K)s: m^2 s^{-1}$

	$\bar{K}_{11}$ (m^2/s)	$\bar{K}_{22}$ (m^2/s)	$\bar{K}_{11}^d$ (m^2/s)	$\bar{K}_{22}^d$ (m^2/s)	K_{11}^F (m^2/s)	K_{22}^F (m^2/s)	C_{e1}	C_{e2}
CIPREA	22	32	33	50	4.7	4.0	0.5	0.8
D1	16	5.9	9.3	6.1	16.6	8.3	0.1	0.07
D2	109	7.5	107	1.7	18.4	17.2	0.6	0.04
D3	14	19	40	17	13.7	20.2	0.1	0.09

$$x_{in} = a_{in} + \left(\frac{\partial x_i}{\partial a_j}\right)_o a_{jn} + x''_{in} \tag{2.3}$$

$$K_{ij}^d(t) = \left(\sum_{n=1}^{N} x''_{in} \dot{x}''_{jn}\right)/(N-3) \tag{2.4}$$

Summation with respect to j is implied in (2.3) and the spatially uniform Lagrangian deformation is represented by $\left(\frac{\partial x_i}{\partial a_j}\right)_o$. Average values of $\bar{K}_{ii}^d$ are presented in Table 2.1. If (2.3) is a better model for the velocity field than (2.2), then we would expect $\bar{K}_{ii}^d$ to be significantly less than $\bar{K}_{ii}$. This

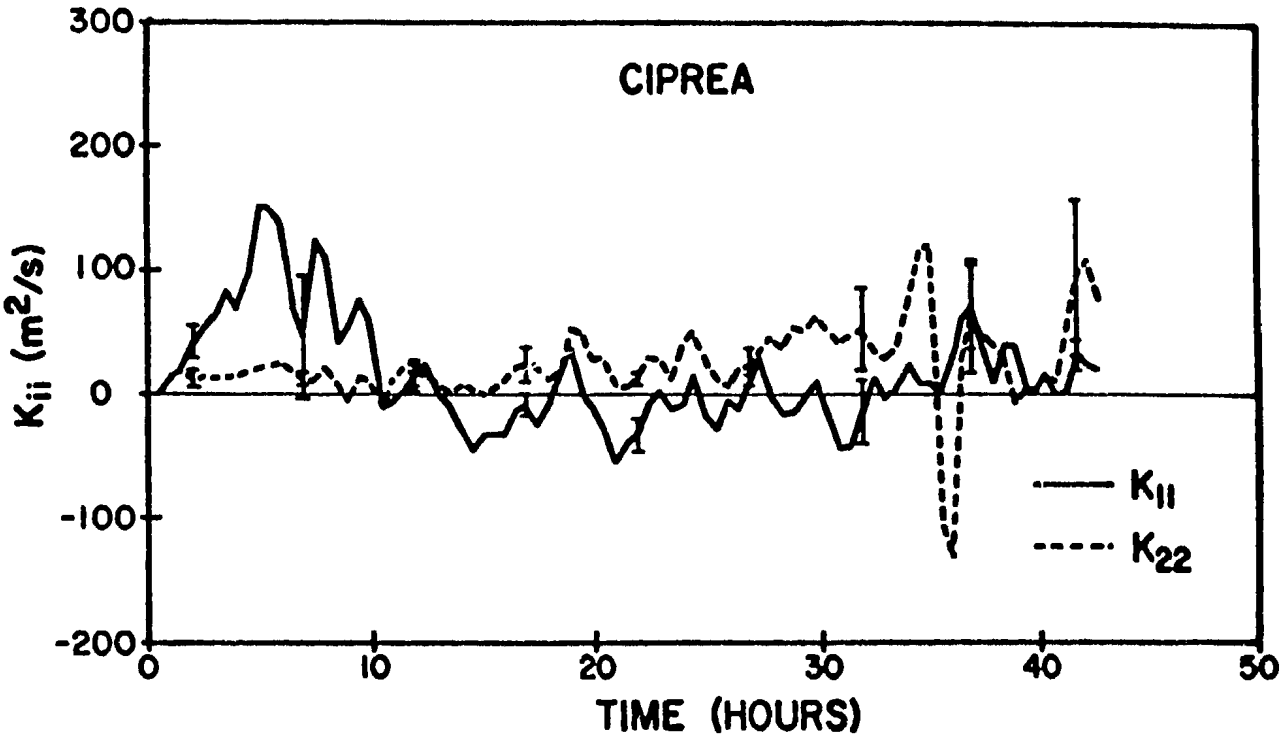

Figure 2-1: Plot of $K_{11}(t)$ and $K_{22}(t)$ for experiment CIPREA. Error bars represent plus and minus one standard deviation.

is not generally the case and, in fact, sometimes the reduced number of degrees of freedom (N-3) in (2.4) as opposed to N-1 in (2.2) leads to $\overline{K}^d_{ii} > \overline{K}_{ii}$. We conclude that for the present data the cluster dispersion is better modelled using (2.1) and (2.2) (eddy-diffusion) than (2.3) and (2.4) (spatially uniform deformation with eddy-diffusion). This contrasts with the analysis of Fahrbach et al. (1986) who removed motion due to time-averaged velocity gradients from the residuals.

Assuming that the relative velocity is statistically stationary we can use the approach of Taylor (1921) to relate patch dispersion to the Lagrangian autocorrelation of relative velocity and its integral time

scale. It is quite clear from Okubo (1971) that in general the relative velocity is not statistically stationary. Yet we might consider it quasi-stationary, if the time taken for a particle's relative velocity to become substantially auto-decorrelated is small, compared with the time taken for the statistical properties of the relative velocity to change appreciably. The quasi-stationary assumption held for other cluster data (Pal and Sanderson (submitted)). We will proceed on the assumption that quasi-stationarity holds for the present data set, and will later examine our results for consistency with this assumption. The Lagrangian autocorrelation function for velocities relative to the centroid, is

$$R_{ij}(\tau)=\frac{\frac{1}{N}\sum_{n=1}^{N}\frac{1}{T}\int_0^{T-\tau}u'_{in}(t)u'_{jn}(t+\tau)\,dt}{U'_iU'_j} \tag{2.5}$$

where $u'_{in}=\dot{x}'_{in}$ and U'_i is the root mean square value of u'_i. Division by the duration of the experiment T rather than $T-\tau$ is necessary to obtain unbiased statistics at large lags (Beauchamp and Yuen 1979). An analysis of relative diffusion that is based on (2.5) yields insight into the structure of dispersive motion, that is not immediately apparent from (2.2). The Lagrangian integral time scale τ^* gives the typical period over which a drifter velocity remains correlated with its velocity at the start of the period,

$$\tau^*_1=\int_0^{\infty}R_{11}(\tau)d\tau$$
$$\tau^*_2=\int_0^{\infty}R_{22}(\tau)d\tau \tag{2.6}$$

where for our data we are constrained to integrate between the limits 0 to T rather than 0 and ∞. Figure 2.2 shows that $R_{ii}(\tau)$ generally does

become small long before τ approaches T, indicating that truncation of the integral will still yield reasonable estimates for τ^*_1 and τ^*_2. The typical distance a drifter moves in the Lagrangian integral time scale is the Lagrangian integral length scale

$$l^*_1=\tau^*_1 U'_1$$
$$l^*_2=\tau^*_2 U'_2. \tag{2.7}$$

The relative eddy diffusivity tensor that was previously obtained by averaging (2.2) with respect to t, can also be written

$$K_{ii}=U'_i U'_i \int_0^\infty R_{ii}(\tau)\,d\tau=\frac{l^{*2}_i}{\tau_i} \tag{2.8}$$

where, again, the integration interval has to be truncated to 0 to T.

Values of eddy diffusivity are not biased by measurement error, whereas Lagrangian integral time and length scales are. Consider the measured relative velocity u' to consist of a component due to the true relative motion u'_{Tr} and an uncorrelated component due to position measurement error u'_e.

$$u'=u'_{Tr}+u'_e \tag{2.9}$$

It follows immediately that the mean square value of the true relative velocity is less than that of the measured relative velocity, as in the following equation

$$\langle u'^2_{Tr}\rangle=\langle u'^2\rangle-\langle u'^2_e\rangle \tag{2.10}$$

where < > represents averaging over drifters in a cluster as in (2.5). Using (2.9) we see that the Lagrangian autocorrelation function of the measured relative velocity is

$$R=\begin{cases}1 & \tau=0\\ \dfrac{\langle u'_{Tr}(t+\tau)u'_{Tr}(t)\rangle}{\langle u'^2_{Tr}\rangle+\langle u'^2_e\rangle} & \tau\neq 0\end{cases} \tag{2.11}$$

whereas the Lagrangian autocorrelation for the true relative velocity is

$$R_{Tr}=\frac{\langle u'_{Tr}(t+\tau)u'_{Tr}(t)\rangle}{\langle u'^2_{Tr}\rangle} \tag{2.12}$$

Using (2.10), (2.11), (2.12) we see that

$$R_{Tr}=\begin{cases}1 & \tau=0\\ \dfrac{R(\tau)\langle u'^2\rangle}{\langle u'^2\rangle-\langle u'^2_e\rangle}, & \tau\neq 0\end{cases} \tag{2.13}$$

Equation (2.13) indicates that measurement errors will bias the Lagrangian integral time scale to be smaller than its true value, since

$$\tau^*=\int R\,d\tau=[1-\frac{\langle u'^2_e\rangle}{\langle u'^2\rangle}]\int R_{Tr}d\tau. \tag{2.14}$$

Similarly, we see from (2.10) and (2.13) that the Lagrangian integral length scale is biased smaller than its true value since

$$\langle u'^2\rangle^{1/2}\int R\,d\tau=[1-\frac{\langle u'^2_e\rangle}{\langle u'^2\rangle}]^{1/2}\langle u'^2_{Tr}\rangle^{1/2}\int R_{Tr}d\tau.$$

On the other hand (2.10) and (2.13) show that eddy diffusivity is unbiased by measurement errors since

$$\langle u'^2_{Tr}\rangle\int R_{Tr}d\tau=\langle u'^2\rangle\int R\,d\tau.$$

Equation (2.13) enables us to estimate an unbiased Lagrangian autocorrelation R_{Tr} from the Lagrangian autocorrelation R that is based on measured velocities and knowledge of the mean square velocity due to position fixing errors $\langle u'^2_e\rangle$. Fahrbach et al. (1986) estimated the position fixing error to be $\pm 200m$ and the resulting velocity error to be 0.02 m/s.

Figure 2.2 shows the Lagrangian autocorrelation R_{11}, R_{22} and

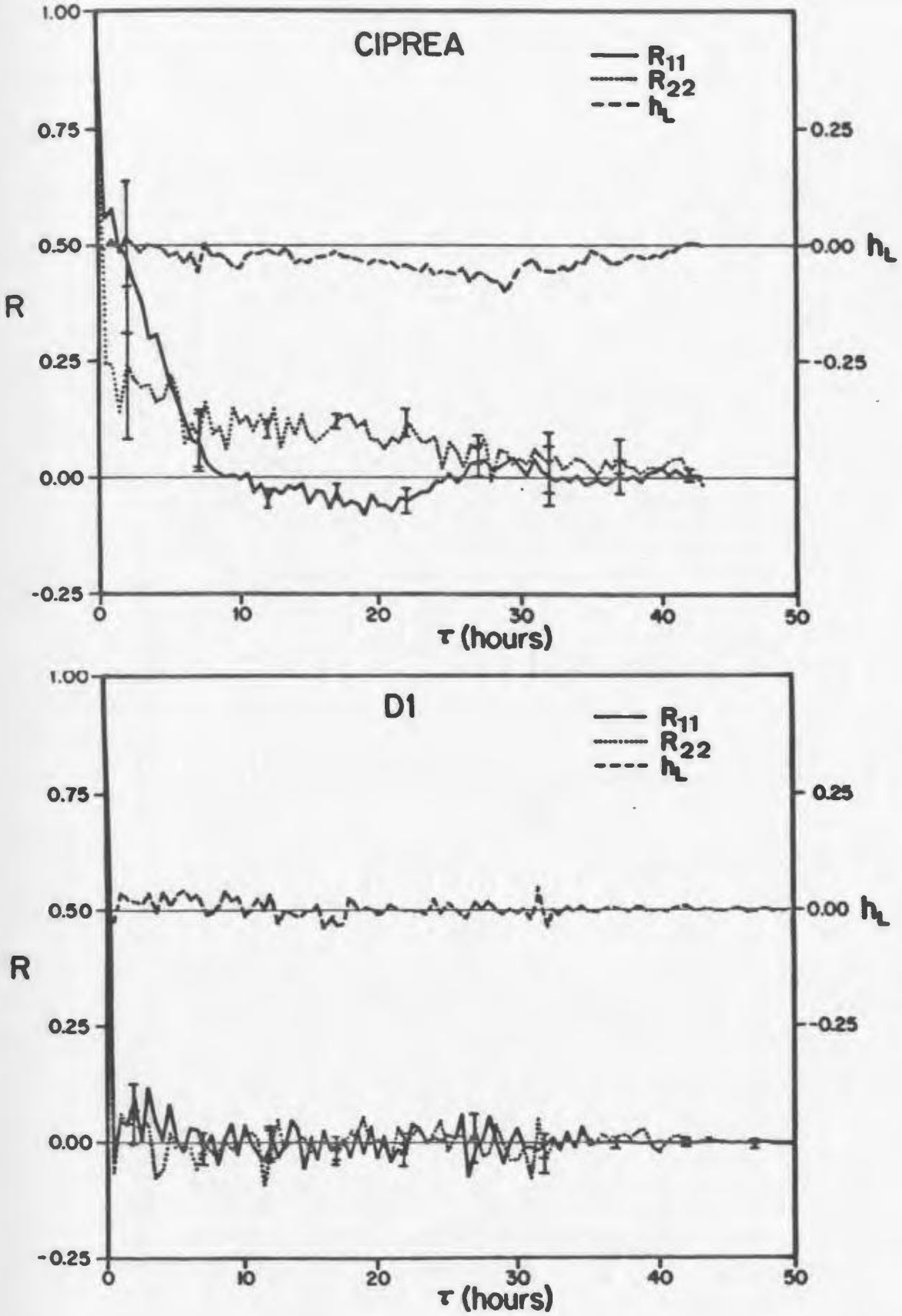

Figure 2-2: Plots of Lagrangian autocorrelation and helicity (R_{12} $-R_{21}$)/2 for velocities relative to the cluster centroid. Error bars represent plus and minus one standard deviation.

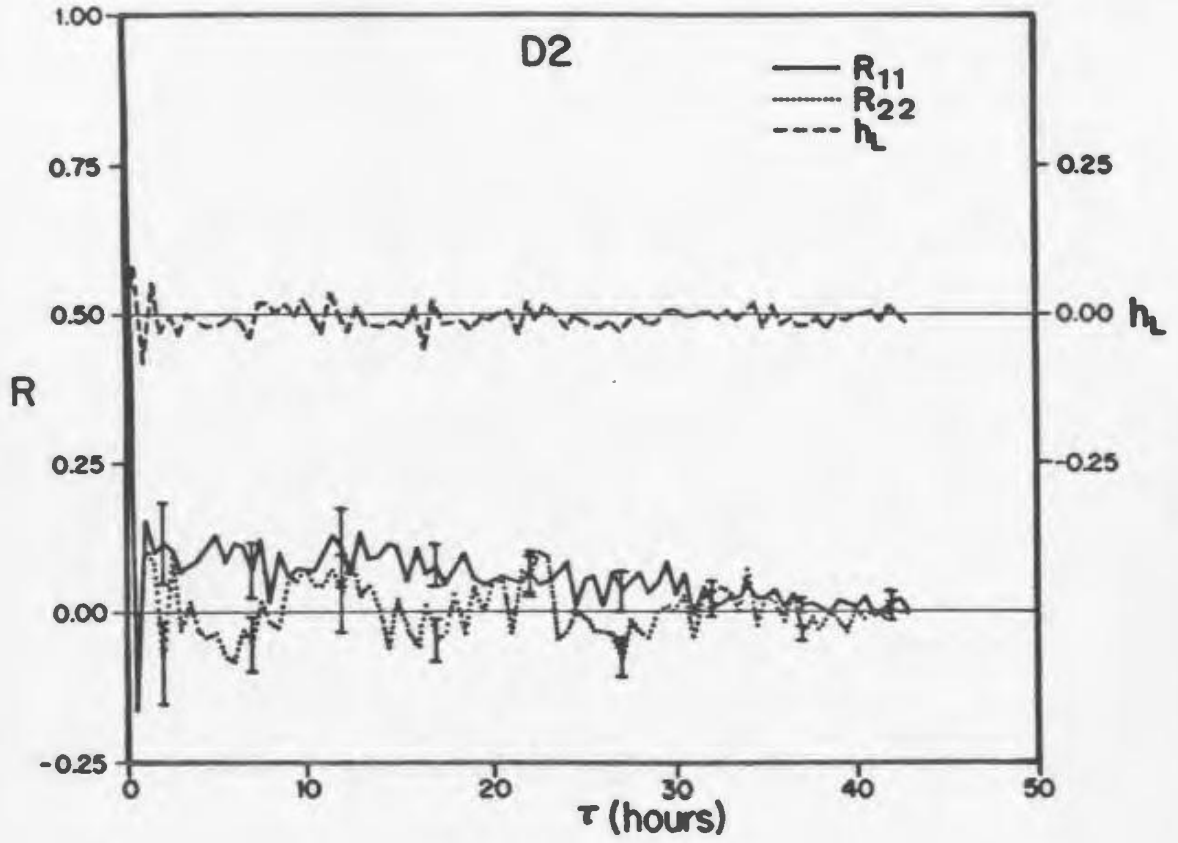

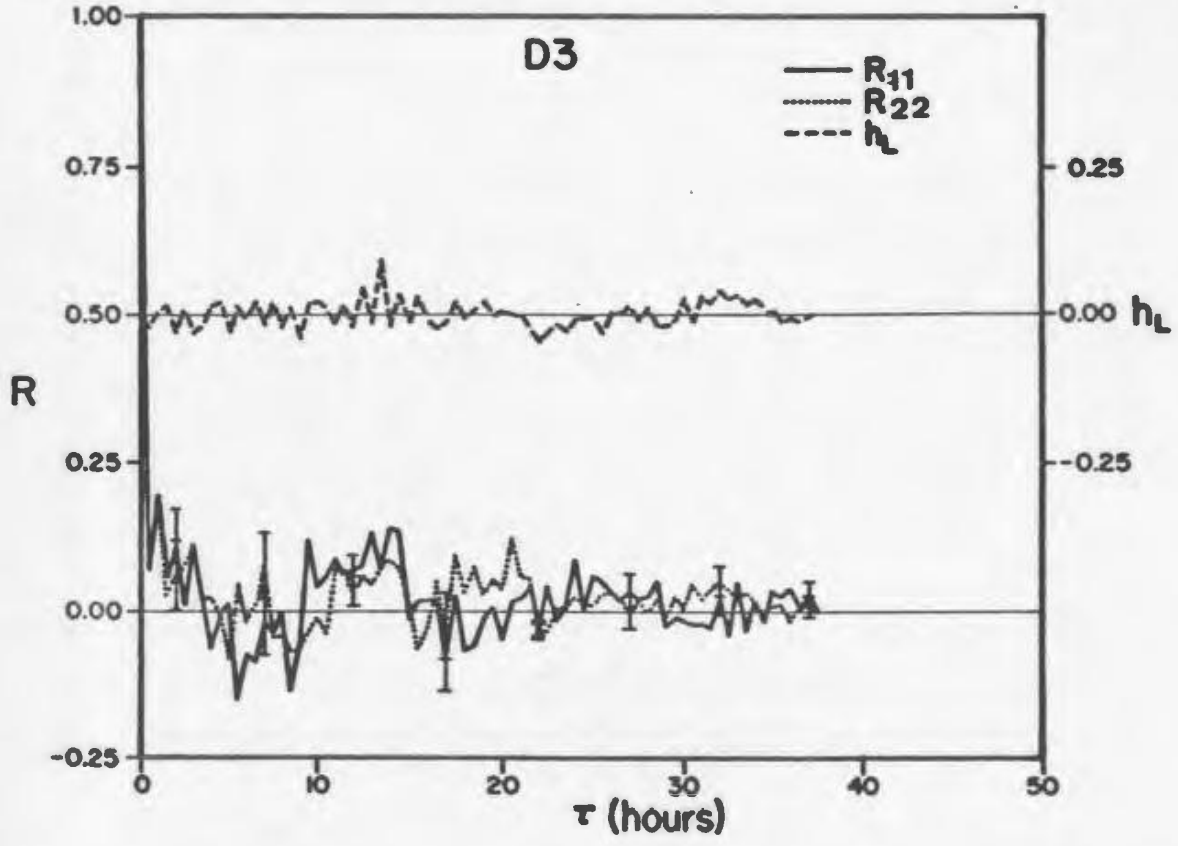

FIGURE 2-2 (CONCLUDED)

the helicity $h_L=(R_{12}-R_{21})/2$ (Middleton and Garrett 1986) plotted against lag. In general h_L is small, indicating that there is no dominant sense for rotational motion about the centroid. In all but the CIPREA experiment, the values of h_L are not significantly different from zero. In CIPREA the small negative values of h_L indicate that about 7% of the energy of relative motion can be thought of as being due to a particles relative trajectory curving in the clockwise sense. In experiments D1, D2, D3 the Lagrangian autocorrelation function drops off rapidly with increasing lag and then exhibits small amplitude ringing that is probably due to internal waves. Statistically significant (at the 50% confidence level) dominant periodicities of 12 hours were observed for the y component of motion in D2; 11 hours for the x component of motion in D3; a broad band from 40 to 12 hours for the x component of motion in CIPREA was significant at the 80% confidence level; whereas D1 had no dominant periodicity. Internal waves, propagating in a thermocline, that have periods in the range 12 to 40 hours have wavelengths much larger (50 km to 170 km) than the patch dimensions, and hence can only cause small relative velocities. Fahrbach et al. (1986) observe horizontal scales of 20 to 40 km for variations in stratification. It is possible that such large scale internal waves could indirectly cause significant relative velocities via an interaction with other components of the flow field. For example the vertical shear above the undercurrent is about 0.02 s^{-1}. Hence a 40 km internal wave of amplitude 10 m could tip this vertical shear to produce a horizontal component of shear of $2\times10^{-5}s^{-1}$ which at the scale of a patch (say 5 km) gives a relative horizontal velocity of about 0.1 m/s. Although this process seems reasonable from a scaling perspective, we lack the necessary data to test the idea.

Internal waves with periods of ~1 hour have wavelengths of 4000 m and could directly cause significant cluster distortion and could also result in the rapid drop off of R observed in experiments D1, D2, D3.

Such high frequencies are barely resolvable in our data sets due to our sampling interval and measurement errors, so this suggestion is tentative.

Experiment CIPREA was carried out further to the east than D1, D2, D3. The Lagrangian autocorrelation falls off more slowly for CIPREA. On the other hand, magnitudes of relative velocities U'_1 and U'_2 are larger for D1, D2, D3 than for CIPREA (Table 2.2). An association of larger relative velocities with shorter Lagrangian integral time scales was also observed by Pal and Sanderson (submitted). Similar associations between velocity magnitudes and integral time scales have been made by Krauss and Boning (1987) for the case of single particle statistics.

Table 2-2: Time-averaged values of the standard deviation of drifter positions σ_x and σ_y relative to the cluster centroid, magnitude of relative velocities U'_i, Lagrangian integral time-scale τ_i^*, eddy diffusivities K_{ii}, and ratio of Lagrangian integral length scale to the standard deviation of drifter positions C_{ex} and C_{ey}. The numbers enclosed in parantheses are corrected for measurement error.

Expt	σ_x	σ_y	U'_1	U'_2	τ_1^*	τ_2^*	$\bar{K}_{11}$	$\bar{K}_{22}$	C_{ex}	C_{ey}
	km	km	x 10^{-2} m/s	x 10^{-2} m/s	minutes	minutes	m^2/s	m^2/s		
CIPREA	1.76	1.94	(5.4)5.2	(4.8)4.6	(123)132	(232)254	22	32	0.23	0.36
D1	3.04	1.80	(9.6)9.4	(7.5)7.4	(30)31	(17)18	16	5.9	0.06	0.04
D2	3.81	3.68	(10.4)10.3	(8.4)8.3	(157)160	(17)17	109	7.5	0.26	0.02
D3	3.54	5.14	(6.8)6.7	(6.8)6.6	(48)50	(64)67	14	19	0.06	0.05

To understand why larger U' might be associated with smaller τ^*, let us assume that the length scales L of the eddies are constrained to be somewhat independent of U'. For relative motion within a cluster of drifters this assumption is reasonable since a continuum of eddy scales ensures that the energy-containing eddies have length scales comparable with the cluster dimensions. For single particle statistics the scales of the energy-containing eddies might be primarily determined by the internal Rossby radius. Nevertheless, if the length scale is fixed independent of U' then energy transfer rates $\overline{u'_i u'_j}\partial U'_i/\partial x_j$, the largest scale eddies (energy-containing eddies) will scale proportional to U'^3/L. This will be the rate at which the eddies change their energy U'^2/τ, which gives $\tau=L/U'$ (from $U'^2/\tau=U'^3/L$). Another approach is to consider the momentum equations where the field acceleration scales as U'^2/L, which will cause rates of velocity change that scale as U'/τ so the τ scales as $\tau=L/U'$ (from $U'/\tau=U'^2/L$).

From Table 2.2 we see that the Lagrangian integral time scale is short compared to the time taken for the cluster to change its dimensions significantly. Consequently it appears that the quasi-stationarity assumption is reasonable. This justifies our definition and use of such quantities as relative eddy diffusivities and Lagrangian integral time-/length scales.

Values of C_e are calculated for the x and y directions (C_{ex}, C_{ey}) and presented in Table 2.2. Generally C_e is 0(0.1), as assumed by Okubo and Ebbesmeyer (1976). However C_e is considerably larger than 0.1 for the CIPREA experiment and the x component of relative velocity in D2. Values of C_e in Table 2.2 are different from those in Table 2.1, because Fahrbach et al. (1986) calculated their residuals, x'_i, differently from ours. Also, Fahrbach et al. (1986) used $N-1$ as the number of degrees of freedom (following Okubo and Ebbesmeyer 1976) when they should have used $N-3$ (Sanderson et al., 1988). Both these effects would cause C_e in Table 2.1 to be bigger than the C_e in Table 2.2.

Averaging over all four experiments gives mean eddy diffusivities of 38 m^2/s, 15.5 m^2/s for the x, y directions. Corresponding values obtained from the analysis of Fahrbach et al. (1986) are 13.4 m^2/s, 12.4 m^2/s. Only the y component of eddy diffusivity is important for calculating the horizontal salt flux from the core of the equatorial undercurrent. Our analysis therefore, confirms the Fahrbach et al. (1986) estimate that only 20% of the salt loss can be due to horizontal diffusion.

2.3. EULERIAN ANALYSIS OF RELATIVE VELOCITIES

Consider a current meter deployed at position $\mathbf{x}$ at time t. At time t the current meter will measure a velocity identical to the velocity of a drifter that passes through $\mathbf{x}$ at time t. The drifter velocity could therefore be specified as a function of the Eulerian position $\mathbf{x}$ that it finds itself in at time t. Alternatively, the drifter velocity at time t could be specified as a function of its Lagrangian coordinates $\mathbf{a}=\mathbf{x}(t=0)$ and time. Thus it is the coordinate system in which we analyze drifter data that determines whether we obtain Eulerian or Lagrangian velocity statistics. In section 2.2 we used a Lagrangian coordinate system, in which each drifter's relative velocity was a function of its initial position. Thus averages over the initial drifter positions (or equivalently averages over the drifter identification number, $\sum_{n=1}^{N}$), yielded Lagrangian statistics of the relative motion. In the following work approximations to the average over all of the two-dimensional Eulerian space $\int_{\chi} d\mathbf{x}$ will be used to obtain Eulerian statistics of the relative motion. (Here the origin of the coordinate system will still be fixed to the cluster centroid, i.e. we filter out the mean patch motion.)

Often in oceanography it is easier to obtain Eulerian statistics (such as the Eulerian integral time scale τ^E) than related Lagrangian statistics (viz. τ^*). Since patch dispersion is dependent upon τ^* it is of

interest to find relationships between τ^* and τ^E. These relations also yield insight into the processes that disperse clusters. To study the space-time patterns of relative motion we will calculate joint space-time Eulerian correlations.

The joint space-time correlations of the x and y (Cartesian) components of relative velocity can be written

$$R_{ij}^{i}=\frac{\overline{u_i'(\mathbf{x},t)\,u_j'(\mathbf{x}+\mathbf{r},t+\tau)}}{(\overline{u_1'^2}\,\overline{u_2'^2})^{1/2}} \tag{2.15}$$

where the overbar represents averaging in both $\mathbf{x}$ and t. The $\mathbf{x}$, t points should be either uniformly or randomly spaced. In order to calculate unbiased estimates when averaging over data spanning a finite period T it is important to use $(1/T)\int_0^{T-\tau}(.)\,dt$ rather than $|1/(T-\tau)|\int_0^{T-\tau}(.)\,dt$. Averaging with respect to $\mathbf{x}$, t is really only appropriate for stationary and homogeneous velocities. Relative velocities are expected to be inhomogeneous and nonstationary. However we will proceed on the assumption that relative velocity is quasi-homogeneous and quasi-stationary, as discussed in the previous section.

Estimating $R_{ij}^{i}(r,\tau)$ from drifter data presents a special difficulty. Drifters follow the flow and will, therefore, preferentially sample regions of previous net convergence (Davis 1982). Fahrbach et al. (1986) observe that statistically meaningful velocity gradients could not be resolved for all experiments apart from CIPREA. Our analysis in section 2 confirms this result. Therefore we will not attempt any correction for the bias, and expect it to be small. Plots of drifter tracks for CIPREA (Fahrbach et al. 1986) indicate divergence from the cluster centroid for all drifters. It seems especially unlikely, therefore, that the R_{ij}^{i} statistics suffer from biasing by regions of previous net convergence.

Following Middleton and Garrett (1986) an estimate of $R_{ij}^{j}(\mathbf{r},\tau)$ is found by averaging over Lagrangian coordinates **a** and **b** of distinct drifters, (i.e. $\mathbf{a} \neq \mathbf{b}$)

$$\hat{R}_{ij}^{j}(\mathbf{r},\tau) = \langle u_i'(\mathbf{x}(\mathbf{a},t))\, u_j'(\mathbf{x}(\mathbf{b},t+\tau))\, \delta(\mathbf{x}(\mathbf{b},t+\tau)-\mathbf{x}(\mathbf{a},t)-\mathbf{r})\rangle (U_1' U_2')^{-1}. \quad (2.16)$$

The average < > in (2.16) also involves averaging with respect to t as well as space **x** and δ is the Dirac δ function. The position vector **x** is an Eulerian variable in both (2.15) and (2.16). In (2.15) it is assumed that the discrete values of **x** that we average over are either randomly or uniformly distributed in space. However in (2.16) the discrete values of **x** that we average over are the Eulerian coordinates that correspond to the positions of drifters. The Eulerian position **x** of a drifter depends upon the flow field, time and release position. Such positions are not necessarily, therefore, either randomly or uniformly distributed in space. Hence (2.16) is only an estimate of (2.15).

The data are not sufficiently extensive to calculate statistically meaningful values of $\hat{R}_{ij}^{j}(\mathbf{r},\tau)$, which is a function of three independent variables. However we can average over space lags to find the Eulerian time lagged correlation

$$R_{ij}^{E}(\tau) = \frac{\int \hat{R}_{ij}^{j}(\mathbf{r},\tau)\, d\mathbf{r}}{\int \hat{R}_{ij}^{j}(\mathbf{r},\tau=0)\, d\mathbf{r}}, \quad (2.17)$$

which is plotted in Figure 2.3. The Eulerian autocorrelation functions have a shape that is very similar to, but different from, the Lagrangian autocorrelations (Figure 2.2). Note that from the Eulerian perspective there is no evidence of rotation since $H = 1/2(R_{12}^{E} - R_{21}^{E})$ is essentially zero for all experiments. This contrasts with the slight amount of clockwise

rotation of Lagrangian trajectories indicated by negative values of h_L for experiment CIPREA. Integrating the Eulerian autocorrelations gives Eulerian integral time scales τ_E^* that are typically slightly larger than the corresponding Lagrangian integral time scale τ^* (Table 2.3).

We expect that Lagrangian integral time scales must be less than or equal to Eulerian integral time scales. An Eulerian velocity changes only due to the local change of the velocity field with respect to time. On the other hand, a Lagrangian velocity changes due to the drifter being advected into a region where the velocity is different, as well as due to local changes in the velocity field with respect to time. For example a frozen eddy field of relative motion could result in a finite Lagrangian integral time scale, but the corresponding Eulerian integral time scale would be infinite. Middleton and Garrett (1986) observed single particle statistics in which the Eulerian integral time scale was 42 hours while the Lagrangian integral time scale was 15 hours. This is an example where advection through the eddy field leads to a greater rate of change of particle velocity than does the change in the eddy field itself. The relative velocity field of the present data is caused by processes with time and space scales that are much smaller than those important for the single particle statistics of Middleton and Garrett (1986). For drifter clusters CIPREA, D1, D2, D3 it is clear that drifters traverse only a small portion of an eddy structure before the eddy structure has itself completely changed. This is the sort of result that might be expected, for example, in a random wave field, where particle displacements in a wave period are small compared to the wavelength (Herterich and Hasselmann 1982, Sanderson and Okubo 1988). Thus we will now calculate the time and space scales of the relative velocity field.

Although the present data are insufficient to calculate $\hat{R}_{ij}^{j}(\mathbf{r},\tau)$, we will assume isotropy and obtain useful joint correlations (of relative velocity) as a function of the magnitude of space lag $r=|\mathbf{r}|$ and τ. However

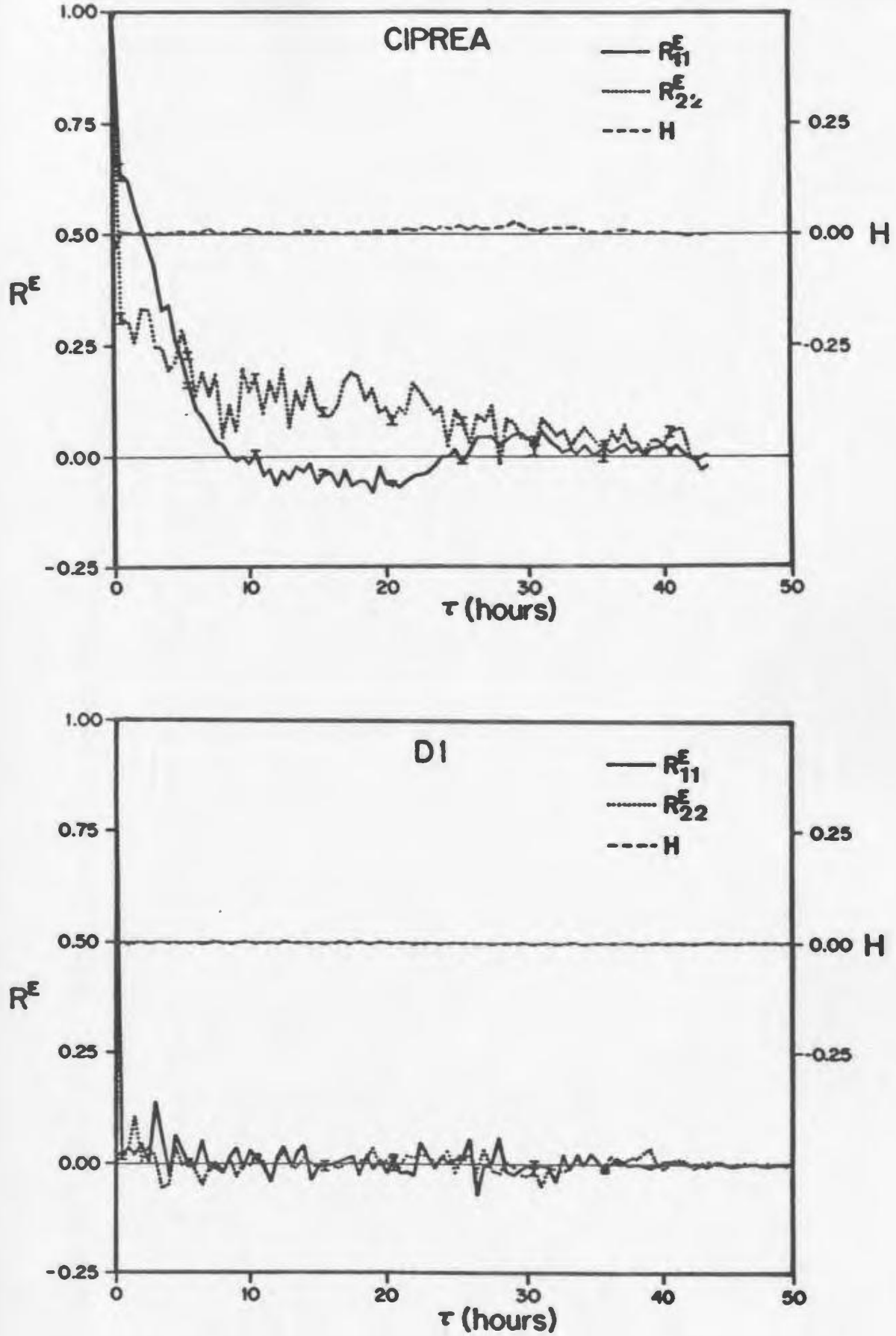

Figure 2-3: Plots of Eulerian autocorrelation coefficients of velocities relative to the centroid. Error bars represent plus and minus one standard deviation. H is $(R_{12}^E - R_{21}^E)/2$

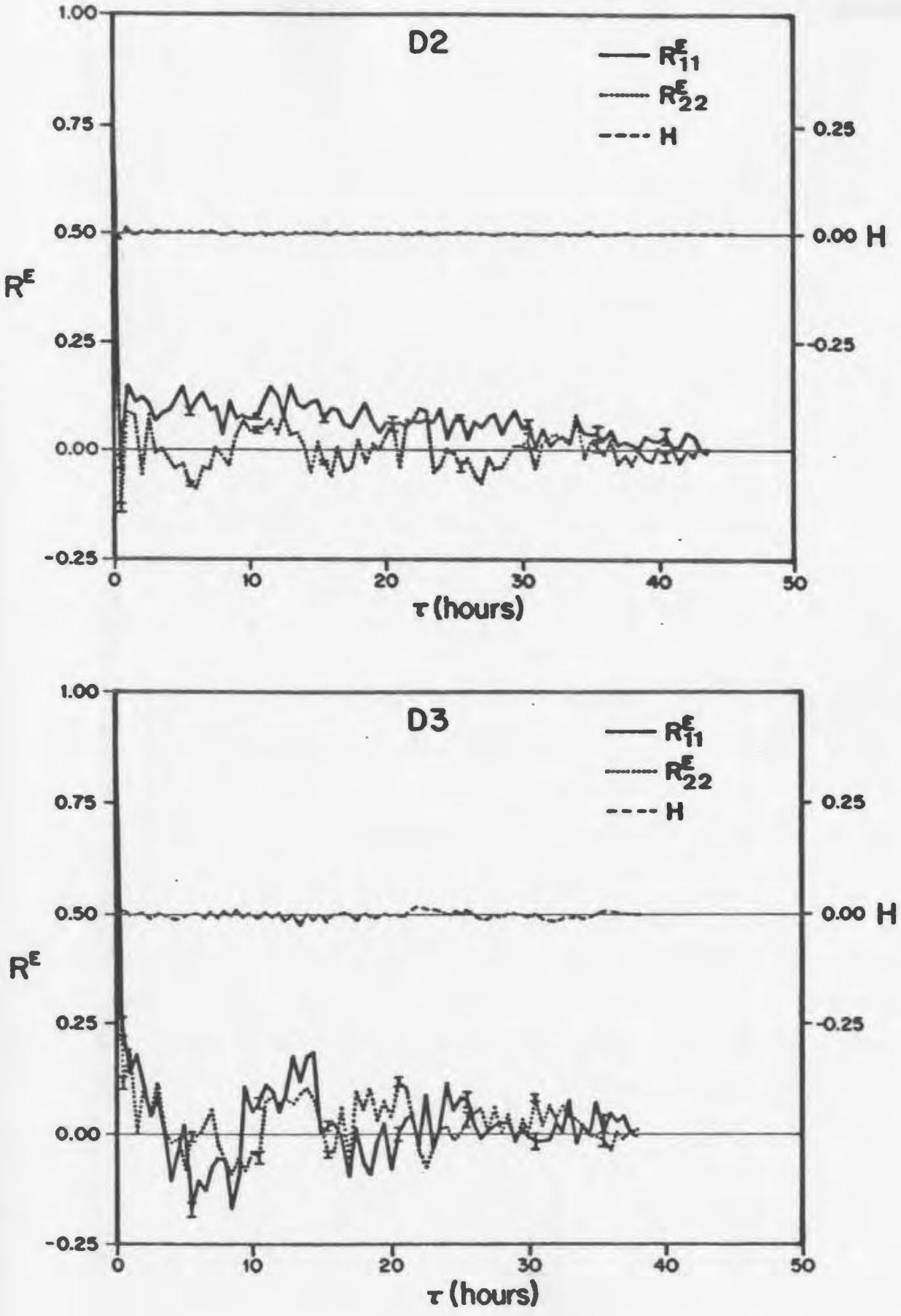

FIGURE 2-3 (CONCLUDED)

in this case it makes little sense to consider x, y components of the relative velocity since the lag vector $\mathbf{r}$ has no fixed orientation. Rather we decompose the relative velocity into components that are longitudinal u'_L and transverse u'_T to the lag vector $\mathbf{r}$ (Middleton and Garrett, 1986). This gives longitudinal f^* and transverse g^* relative velocity correlations

$$f^*(r,\tau)=\frac{\overline{u'_L(\mathbf{x},t)u'_L(\mathbf{x}+\mathbf{r},t+\tau)}}{\sqrt{\overline{u'^2_L}\,\overline{u'^2_T}}} \tag{2.18}$$

$$g^*(r,\tau)=\frac{\overline{u'_T(\mathbf{x},t)u'_T(\mathbf{x}+\mathbf{r},t+\tau)}}{\sqrt{\overline{u'^2_L}\,\overline{u'^2_T}}} \tag{2.19}$$

$$h^*(r,\tau)=\frac{\overline{u'_L(\mathbf{x},t)u'_T(\mathbf{x}+\mathbf{r},t+\tau)}-\overline{u'_T(\mathbf{x},t)u'_L(\mathbf{x}+\mathbf{r},t+\tau)}}{\sqrt{\overline{u'^2_L}\,\overline{u'^2_T}}} \tag{2.20}$$

To calculate f^*, g^*, and h^* relative velocity pairs of distinct drifters were binned for space and time lags centred on $[r_1,r_2,r_3,r_4,...]=[0.4,1.2,2.0,2.8,...]$ km and $[\tau_1,\tau_2,\tau_3,...]=[0.5,1.0,1.5,...]$ hours. Values of helicity h^* are small for all experiments, indicating that there is no preferred sense of rotation at any space or time scale. The patterns of correlations indicated by plots of f^* and g^* are complicated, and variable from one experiment to the next. Representative plots of f^* and g^* are shown for experiments CIPREA and D2 in Figure 2.4a and 2.4b respectively. In the case of CIPREA there are some clear structures in the relative velocity field correlations, although values of correlations are generally much less than 1. However it is equally clear that relative velocity is a rapidly changing function of position within the cluster. In D2 we see that the time and space scales over which correlation features persist is much less than in CIPREA. Again we speculate that the larger relative velocities in D2 (compared to CIPREA) lead to more rapid relative velocity fluctuations (in space and time).

There is a tendency for negative correlations when the space lags are large and the time lags are relatively small. This is particularly evident for the longitudinal correlation f^* in CIPREA at space lags 7 km > r > 2 km and time lags 4 hours > τ > 0 hours. In general we expect that eddy features with scales similar to the dimensions of the cluster will cause relative motion at opposing sides of the cluster to be in opposing directions for time lags corresponding to the life time of the eddy. This must be generally true for transverse motion if there is to be no net motion through a plane traversing the cluster. For longitudinal motion this will be true for singularity structures corresponding to nodes or lines of convergence/ divergence (Okubo 1970). Thus we expect g^* to be generally negative for large space lags and small time lags. We also expect f^* to be negative for large space lags and small time lags, if the dominant cluster-scale eddies have singularity structures corresponding to nodes or lines of convergence. By the same argument saddles and vortices would be expected to result in no preferred sign for f^*, whereas spirals would result in slight negative values of f^*, for large space lags and small time lags. The dominant singularity structure for CIPREA is that of an outward node, as seen from calculations of velocity gradients as well as from visual inspection of relative trajectories (Fahrbach et al. 1986). Thus it is not surprising that f^* is negative at large space lags and small time lags. Interestingly, the eddy structures apparent in Figure 2.4a,b seem to be relatively short-lived (about 3 to 4 hours for CIPREA and only 0.5 to 1.5 hours for D2). This is consistent with the eddy field evolving rapidly with time, compared to the rate at which a Lagrangian drifter sees the field change due to its advection.

Similarly wave-like motions that have wavelengths comparable to the cluster dimension will cause relative motion at opposing sides of the cluster that will be negatively correlated for short time lags, but will become positively correlated for time lags greater than half a wave period.

Table 2-3: Integral time-scales: Lagrangian τ_u^*, τ_v^*; Eulerian Cartesian components τ_{EL}^* and τ_{ET}^*. All values are in minutes and are corrected for measurement error.

Experiment	τ_u^* (minutes)	τ_v^* (minutes)	τ_{Eu}^* (minutes)	τ_{Ev}^* (minutes)	τ_{EL}^* (minutes)	τ_{ET}^* (minutes)
CIPREA	132	254	159	330	460	-839
D1	31	18	33	21	15	41
D2	160	17	194	17	88	170
D3	50	67	63	73	167	-72

The fact that Figure 2.4a does not show $f^*(r{=}3km,\tau)$ alternating between positive and negative values as τ increases indicates that the time scale for the persistence of strong negative correlations ($\tau{\approx}4$ hours) is more indicative of the lifetime of an eddy, than half the period of a wave. We also note that relative speeds were typically ~ 0.07 m/s for CIPREA. Thus in 4 hours we expect a drifter to move only about 1 km, which is a small distance compared to the scale of the eddy ($r{\approx}3$) km. This is consistent with our earlier explanation as to why Eulerian and Lagrangian integral time scales were so similar.

Eddy (or wave) features with scales (wavelengths) similar to patch dimensions will cause relative motion of particles separated by distances small compared to the cluster dimensions to be positively correlated for time lags less than the time scale of the eddy (or wave). Looking along the τ axes of plots in Figures 2.4a, b we see some tendency

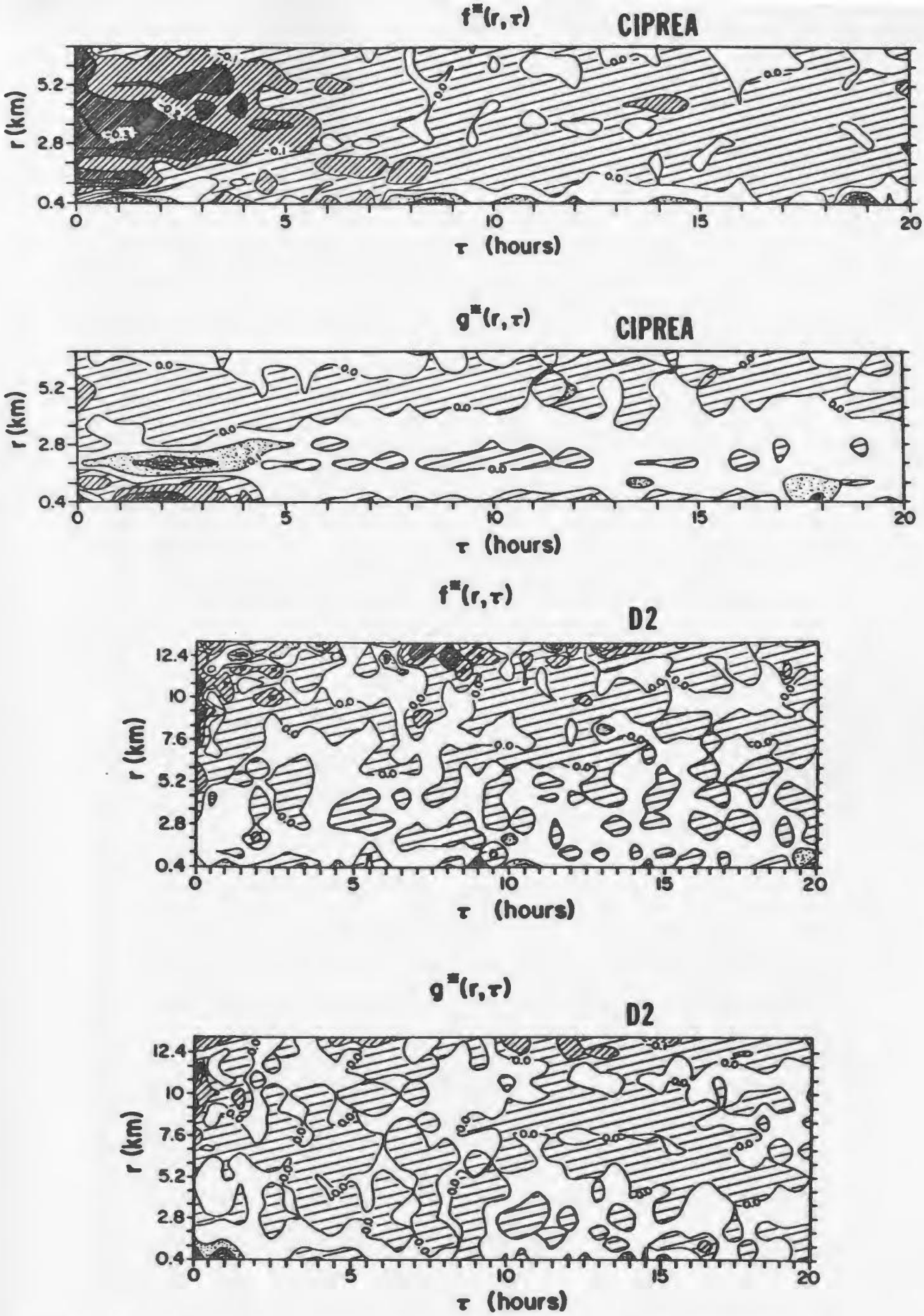

Figure 2-4: Contour plots showing f^* and g^* as functions of time and space lags, for experiments CIPREA (4a) and D2 (4b). Line shading indicates negative correlations. Unshaded areas have correlations in the range 0.0 to 0.1. Dotted shading indicates correlations greater than 0.1.

for the correlations to fluctuate between positive and negative values in a way that is indicative of relative motion due to waves. In Figure 2.4b the positive correlations of f^* at r = .4 km, τ = 11 hours are consistent with our earlier analysis that indicated dominant periodicities of about 12 hours for D2. In Figure 2.4a the positive correlations scattered along the τ axis from τ = 8 to τ = 19 hours are indicative of a broad band of periods noted earlier for CIPREA. In all cases f^* and g^* drop to zero for r in the range .4 km to 1.5 km and τ in the range 0.5 hours to 3 hours, which indicates a lot of eddy energy at small spatial scales ($r \approx$ 0.4 to 1.5 km) and small time scales ($\tau \approx$ 0.5 to 3 hours). We cannot properly resolve all of these small scales, due to the paucity of data.

There is a strong pocket of positive g^* centred at r = 2 km and τ = 2 hours in Figure 2.4a. This means that transverse motions at separations of 2 km become positively correlated after a 2 hour lag. If this feature were caused by an eddy of transverse motion propagating along **r**, then we would expect g^* to also be positive at r = 1 km and τ = 1 hour, and at all other points between (r = 0, τ = 0) and (r = 2 km, τ = 2 hours). This is not the case. Instead what we have is a packet of transverse motion that disappears for a while, and then reappears 2 hours later at a point 2 km away. This is a quite different feature from say a propagating wave. We do not know of a mechanism that might give rise to such a feature. The dimensions of the correlation pattern about the point r = 2 km, τ = 2 hours on the plot, indicate that the eddy has dimensions of about 0.8 km (about half the standard deviation of drifter positions, σ) and a lifetime of about 2 hours.

From Figure 2.4 it is clear that f^* and g^* are not separable functions of r and τ. Thus it is difficult to analyze and interpret spatial structures (of the relative velocity) independent of associated time scales. Nevertheless we define spatial correlations

$$f(r)=\frac{\int_0^T N(r=0,\tau)d\tau \int_0^T N(r,\tau)f^*(r,\tau)d\tau}{\int_0^T N(r,\tau)d\tau \int_0^T N(r=0,\tau)f^*(r=0,\tau)d\tau} \tag{2.21}$$

$$g(r)=\frac{\int_0^T N(r=0,\tau)d\tau \int_0^T N(r,\tau)g^*(r,\tau)d\tau}{\int_0^T N(r,\tau)d\tau \int_0^T N(r=0,\tau)g^*(r=0,\tau)d\tau} \tag{2.22}$$

and time lagged correlations

$$F(\tau)=\frac{\int_0^L N(r,\tau=0)dr \int_0^L N(r,\tau)f^*(r,\tau)dr}{\int_0^L N(r,\tau)dr \int_0^T N(r,\tau=0)f^*(r,\tau=0)dr} \tag{2.23}$$

$$G(\tau)=\frac{\int_0^L N(r,\tau=0)dr \int_0^L N(r,\tau)g^*(r,\tau)dr}{\int_0^L N(r,\tau)dr \int_0^L N(r,\tau=0)g^*(r,\tau=0)dr} \tag{2.24}$$

where we have normalized by the number of correlating velocity pairs $N(r,\tau)$ in the bin with space lag r and time lag τ.

We find that there is a trend for $f(r)$ and $g(r)$ to be positive for small spatial lags, and negative for larger spatial lags (Figure 2.5). This applies to both transverse and longitudinal components of motion. The resolution of space correlations is poor, due to the small number of drifters per patch. Hence the zero crossings of $f(r)$ are not well determined. However for experiment CIPREA zero crossings for $f(r)$ and

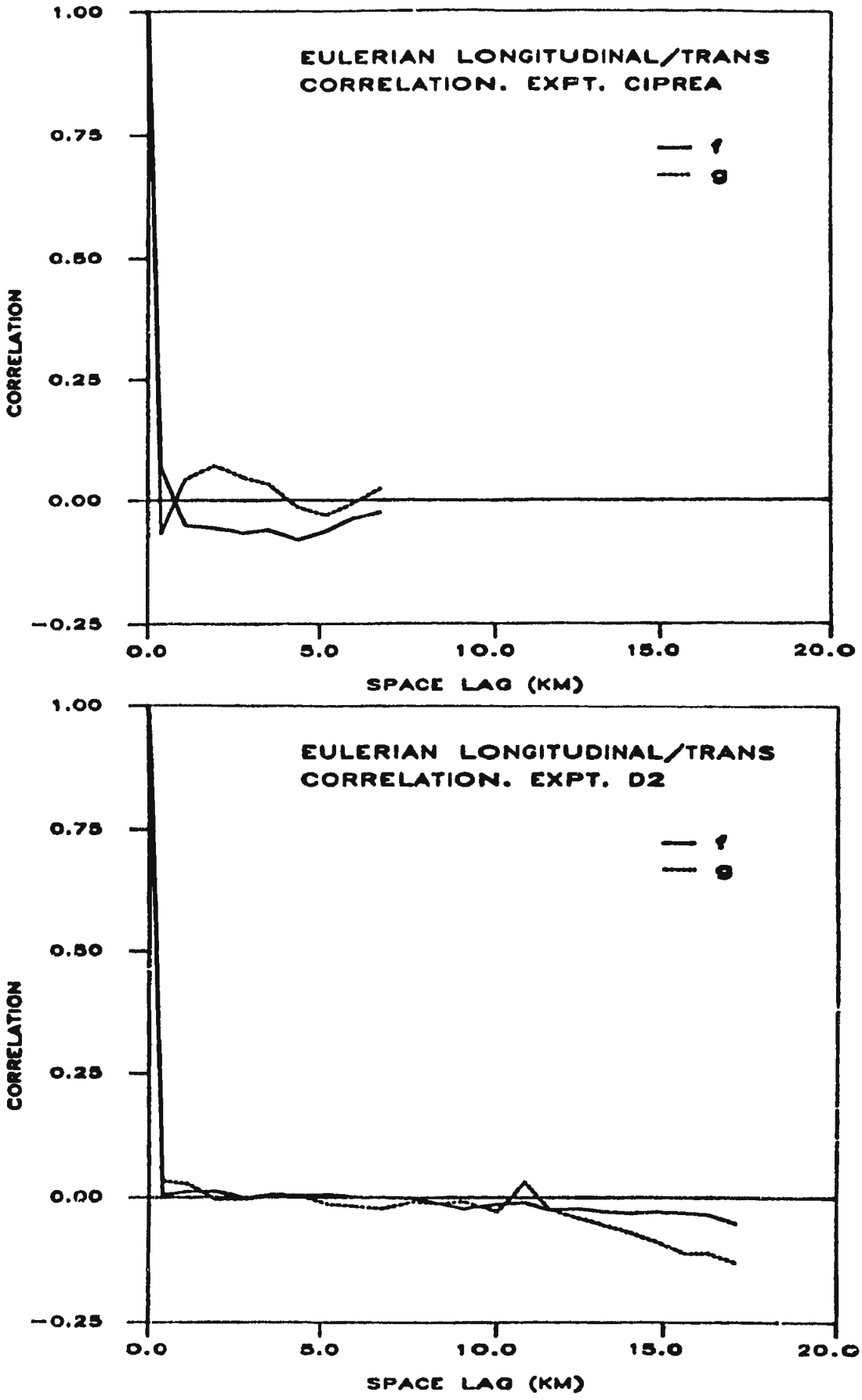

Figure 2-5: Plots of spatial correlations $f(r)$, $g(r)$ for experiments CIPREA and D2.

$g(r)$ are at space scales that are within 15% of the Lagrangian integral length scale. In the case of D2 the zero crossings are at about twice the Lagrangian integral length scale. Generally the relative velocity field becomes spatially decorrelated at scales much smaller than the patch dimensions, and negatively correlated for larger spatial lags. Negative values of $g(r)$ are expected in order to ensure that the relative velocity does not have any net transport through a plane. Negative values of $f(r)$ for large lags, are not similarly required. These, therefore, indicate an interesting structural property of the relative velocity field, that we cannot fully explain for all experiments. Although large scale eddies with nodal structures (Okubo 1970) and internal waves with scales similar to the cluster dimensions would cause negative $f(r)$ for large r.

Time-lagged correlations of the longitudinal and transverse velocities exhibit a different structure from those of the Eulerian cartesian components. In particular for CIPREA and D3 there were large negative lobes for transverse velocity correlations. Eulerian integral time scales for transverse and longitudinal velocities τ^*_{EL}, τ^*_{ET} are presented in Table 2.3. They differ greatly from τ^*_u, τ^*_v and τ^*_{Eu}, τ^*_{Ev} in that they are larger in magnitude and sometimes negative valued. It appears as though the longitudinal-transverse velocity decomposition enables us to see temporal structure that the x-y velocity decomposition misses. We might picture this as a consequence of the longitudinal-transverse coordinates being more nearly aligned with the eddy causing relative motion between particles than the x-y coordinates.

2.4. SUMMARY

Drifter cluster data of Fahrbach et al. (1986) are reanalyzed to include a detailed study of the time and space scales of relative motion. In the meridional direction the assumption $C_e = 0.1$ turns out to be reasonable, thereby confirming relative diffusivities in the meridional

direction calculated by Fahrbach et al. (1986). However the zonal diffusivity is substantially different from that of Fahrbach et al. (1986). The Lagrangian autocorrelation of relative velocity falls off on a time scale that is short compared to that for substantial changes in cluster dimension, which justifies treating relative velocity as being quasi-stationary. Of course this result can only apply approximately (i.e. on a local time and space scale), since it is well known (Okubo 1971) that cluster variance grows faster than t, indicating that the Lagrangian autocorrelation does not converge for large t.

The analysis indicated that, for the present data set, there was little to be gained by using an advection-diffusion model for cluster spreading, rather than a pure eddy-diffusion model. Measurement errors were shown to have little effect upon estimation of eddy diffusivities but biased Lagrangian integral time and space scales towards values that were smaller than they should have been.

An Eulerian analysis of the relative velocities gave integral time scales only slightly greater than the Lagrangian integral time scales. This indicates that fluctuations of the relative particle trajectories are largely temporal, rather than advective.

Joint space-time correlations of relative velocity indicate a complicated nonseparable dependence on space and time lags. In the case of CIPREA the correlations are coherent over a wider range of space and time lags than for D2. Integral time scales for transverse, longitudinal velocity components differed greatly from those for x, y velocity components.

Chapter 3

RESIDUAL MOTIONS ASSOCIATED WITH INVISCID GRAVITY WAVES

3.1. INTRODUCTION

The purpose of the following two chapters is to investigate the oceanic mixing caused by surface gravity waves. As mentioned in Chapter 1, oceanic mixing is caused by many dynamical processes. Two basic difficulties in modelling these processes are (1) the broad range of scales of the natural eddy-spectrum of the ocean and (2) the strong nonlinearity of many of the dynamical processes. There is some evidence that at smaller scale surface waves may yield an important contribution to horizontal diffusion. Diffusion measurements of Schott et al. (1978) indicate that the coefficient of horizontal diffusion depends on the surface-wave height. The relationship between surface waves and vertical diffusion is still unknown. The measurements of vertical diffusion by Kullenberg (1971, 1976, 1977) show that the coefficient of vertical diffusion is very small and inversely proportional to vertical stratification (N) and weakly dependent on wind stress. We will investigate the extent to which weak nonlinear interactions of surface waves can contribute to eddy-diffusivities. This investigation will solve the Navier Stokes equations of motion in a Lagrangian coordinate system.

One of the earliest attempts to study the diffusion due to a random field of deep water surface gravity waves was by Tamai (1972).

Tamai used a perturbation technique to solve the equations of motion. However, at a crucial stage, he chose only to consider two-dimensional motion in the vertical plane, and therefore observed no eddy-diffusion at second order in the perturbation analysis. In the third order interactions Tamai (1972) found solutions that were valid for short times and caused eddy-diffusion. By transforming the x-component of velocity into a spectral representation of two wave groups, he estimated coefficients of surface diffusivities which turned out to be too small to account for experimentally measured values. Herterich and Hasselmann (1982) considered the horizontal diffusion of tracers in the presence of a random field of ocean surface gravity waves. Instead of finding solutions to the Lagrangian equations of motion, they constructed Eulerian velocities for second order interactions following the procedure of Hasselmann (1961) and others. The second order Eulerian solutions could not cause eddy-diffusion at zero-frequency interaction. Second order Lagrangian solutions were obtained from the sum of the second order Eulerian solutions and a Stokes drift due to Euler-Lagrange transformation of the first order Eulerian solutions. The Stokes-drift-part of their second order Lagrangian solution exhibited horizontal diffusion as a particular case of zero-frequency interactions but no vertical diffusion. Recently, Sanderson and Okubo (1988) solved the inviscid, nonrotating equations of motion in Lagrangian coordinates for an internal wave field. They found solutions which gave horizontal eddy-diffusion.

The present approach solves the 3-D Navier Stokes' equations of motion in a Lagrangian coordinate system by applying a perturbation technique. In this manner we solve for particle motion directly. The Eulerian analysis, on the other hand, requires a nonlinear transformation to obtain particle motion. At second order we obtain solutions that result from zero-frequency wave interaction, that disperse material.

The motivation for the present work is to solve the 3-D Lagrangian equations of motion for a spectrum of surface waves in an inviscid irrotational ocean. We will consider the zero-frequency motion resulting from interactions of statistically independent random wave packets. The zero-frequency second-order Lagrangian particle velocity will therefore be a random function of position and will fluctuate as wave packets propagate by (Herterich and Hasselmann, 1982). It will be shown that this second order velocity field is horizontally nondivergent. This implies that the solutions can cause only horizontal dispersion but no vertical dispersion. This character of the solutions is changed when we introduce viscosity in the equations of motion as discussed in the next chapter.

This chapter is organized as follows. The mathematical formulation of the problem is given in section 3.2. Section 3.3 deals with the solution of the first order Lagrangian equations of motion. In section 3.4, the second order equations are solved by considering zero-frequency interaction of two groups of primary waves. The chapter is concluded with a summary in section 3.5.

3.2. MATHEMATICAL FORMULATION

Consider an homogeneous incompressible ocean of infinite depth and horizontal extent. A right-handed Cartesian coordinate system is chosen with the x- and y- axes along the undisturbed sea surface and the z-axis pointing vertically upwards. The motion is described by using a Lagrangian coordinate system. Let a fluid particle has Lagrangian coordinates (a,b,c), the undisturbed state being

$$x=a,\ y=b,\ z=c,\ p=p_0-\rho gc$$

where p is the fluid pressure, p_0 the atmospheric pressure, ρ the water

density and g the acceleration due to gravity. The Lagrangian equations of motion for inviscid fluid are given by

$$x_{tt}x_a+y_{tt}y_a+(g+z_{tt})z_a+\frac{p_a}{\rho}=0 \tag{3.1}$$

$$x_{tt}x_b+y_{tt}y_b+(g+z_{tt})z_b+\frac{p_b}{\rho}=0 \tag{3.2}$$

$$x_{tt}x_c+y_{tt}y_c+(g+z_{tt})z_c+\frac{p_c}{\rho}=0 \tag{3.3}$$

Here the subscripts a, b, c, t indicate differentiation. The equation of mass conservation is

$$\rho(a,b,c,t)\frac{\partial(x,y,z)}{\partial(a,b,c)}=\rho(a,b,c,0) \tag{3.4}$$

where $\frac{\partial(x,y,z)}{\partial(a,b,c)}$ is the Jacobian. Assuming that the fluid is incompressible,

$$\rho(a,b,c,t)=\rho(a,b,c,0) \tag{3.5}$$

then (3.4) reduces to

$$\frac{\partial(x,y,z)}{\partial(a,b,c)}=1 \tag{3.6}$$

which becomes

$$x_ay_bz_c+x_cy_az_b+x_by_cz_a-x_by_az_c-x_ay_cz_b-x_cy_bz_a=1 \tag{3.7}$$

when the Jacobian is expanded.

Now assume that x, y, z and p can be expressed as a power series

$$x=a+\varepsilon x_1+\varepsilon^2 x_2+\varepsilon^3 x_3 \tag{3.8}$$

$$y=b+\varepsilon y_1+\varepsilon^2 y_2+\varepsilon^3 y_3 \tag{3.9}$$

$$z=c+\varepsilon z_1+\varepsilon^2 z_2+\varepsilon^3 z_3 \tag{3.10}$$

$$p=p_0-\rho g c+\varepsilon p_1+\varepsilon^2 p_2+\varepsilon^3 p_3. \tag{3.11}$$

The parameter ε is the wave steepness and will be small providing wave amplitude is small compared to wavelength. Substituting the above power series into the equations of motion (3.1) - (3.3) and continuity equation (3.7) we find that the zero order equations are satisfied identically. Equating the coefficients of ε and ε^2 one obtains the first order equations

$$x_{1tt}+gz_{1a}+\frac{p_{1a}}{\rho}=0 \tag{3.12}$$

$$y_{1tt}+gz_{1b}+\frac{p_{1b}}{\rho}=0 \tag{3.13}$$

$$z_{1tt}+gz_{1c}+\frac{p_{1c}}{\rho}=0 \tag{3.14}$$

$$x_{1a}+y_{1b}+z_{1c}=0 \tag{3.15}$$

and second order equations

$$x_{2tt}+gz_{2a}+\frac{p_{2a}}{\rho}+z_{1a}z_{1tt}+y_{1a}y_{1tt}+x_{1a}x_{1tt}=0 \tag{3.16}$$

$$y_{2tt}+gz_{2b}+\frac{p_{2b}}{\rho}+z_{1b}z_{1tt}+y_{1b}y_{1tt}+x_{1b}x_{1tt}=0 \tag{3.17}$$

$$z_{2tt}+gz_{2c}+\frac{p_{2c}}{\rho}+z_{1c}z_{1tt}+y_{1c}y_{1tt}+x_{1c}x_{1tt}=0 \tag{3.18}$$

$$x_{2a}+y_{2b}+z_{2c}+y_{1b}z_{1c}+x_{1a}z_{1c}+x_{1a}y_{1b}-y_{1c}z_{1b}-x_{1c}z_{1a}-x_{1b}y_{1a}=0 \tag{3.19}$$

respectively.

The surface boundary condition is that the pressure at the surface is zero

$$p_0 = p(a,b,c=0,t) = 0 \tag{3.20}$$

and the perturbation particle displacements tend to zero as the depth tends to infinity

$$\begin{aligned} x_1(a,b,c=-\infty,t) &= x_2(a,b,c=-\infty,t) = 0 \\ y_1(a,b,c=-\infty,t) &= y_2(a,b,c=-\infty,t) = 0 \\ z_1(a,b,c=-\infty,t) &= z_2(a,b,c=-\infty,t) = 0. \end{aligned} \tag{3.21}$$

3.3. SOLUTION OF THE FIRST ORDER EQUATIONS

Under the assumption that x_1, y_1, z_1, p_1 are stationary random processes with respect to a,b,c,t, let the spectral representations of the first order solutions be

$$x_1 = \int_{-\pi}^{+\pi}\int_{-\infty}^{+\infty}\int_{-\infty}^{+\infty} e^{i(k\cos\theta a + k\sin\theta b - \omega t)} d\xi_x(k,\omega,\theta,c) \tag{3.22}$$

$$y_1 = \int_{-\pi}^{+\pi}\int_{-\infty}^{+\infty}\int_{-\infty}^{+\infty} e^{i(k\cos\theta a + k\sin\theta b - \omega t)} d\xi_y(k,\omega,\theta,c) \tag{3.23}$$

$$z_1 = \int_{-\pi}^{+\pi}\int_{-\infty}^{+\infty}\int_{-\infty}^{+\infty} e^{i(k\cos\theta a + k\sin\theta b - \omega t)} d\xi_z(k,\omega,\theta,c) \tag{3.24}$$

$$p_1 = \int_{-\pi}^{+\pi}\int_{-\infty}^{+\infty}\int_{-\infty}^{+\infty} e^{i(k\cos\theta a + k\sin\theta b - \omega t)} d\xi_p(k,\omega,\theta,c) \tag{3.25}$$

where $d\xi_x, d\xi_y, d\xi_z$ and $d\xi_p$ are spectral density functions of the first order components of the displacement and pressure. They have a functional dependence on the independent variable c, and depend on the frequency ω, wave number k and direction of wave propagation θ.

Eliminating p from (3.12) and (3.14) gives

$$x_{1tt}-z_{1tta}=0 \tag{3.26}$$

Similarly, eliminating p from (3.13) and (3.14)

$$y_{1tt}-z_{1ttb}=0. \tag{3.27}$$

Using (3.26) and (3.27) to eliminate x_1 and y_1 from (3.15) we obtain

$$z_{1ttc}+z_{1ttbb}+z_{1ttaa}=0. \tag{3.28}$$

Substituting (3.24) into (3.28) gives

$$d\xi_{zcc}-k^2 d\xi_z=0. \tag{3.29}$$

The solution of (3.29) that satisfies the boundary condition (3.21) is

$$d\xi_z=-i\frac{|k|}{k}e^{|k|c}d\xi_1(\omega,\theta). \tag{3.30}$$

Substituting (3.22) and (3.24) into (3.26) and using (3.30) gives

$$d\xi_x=cos\theta\, e^{|k|c}d\xi_1(\omega,\theta). \tag{3.31}$$

Similarly, substituting (3.23) and (3.24) into (3.27) and using (3.30) gives

$$d\xi_y=sin\theta\, e^{|k|c}d\xi_1(\omega,\theta). \tag{3.32}$$

Substituting (3.22), (3.24) and (3.25) into (3.12) and applying the boundary condition (3.20)

$$d\xi_p=\frac{-i}{k}\rho\, e^{|k|c}(\omega^2-g|k|)\,d\xi_1(\omega,\theta) \tag{3.33}$$

and

$$k=\frac{\omega|\omega|}{g}. \tag{3.34}$$

Hence the solutions for the first order equations can be written as

$$x_1^{IN}=\int_{-\pi}^{+\pi}\int_{-\infty}^{+\infty} cos\theta\, e^{i(kcos\theta a+ksin\theta b-\omega t)}\, e^{\omega^2 c/g}\, d\xi_1(\omega,\theta) \tag{3.35}$$

$$y_1^{IN}=\int_{-\pi}^{+\pi}\int_{-\infty}^{+\infty} sin\theta\, e^{i(kcos\theta a+ksin\theta b-\omega t)}\, e^{\omega^2 c/g}\, d\xi_1(\omega,\theta) \tag{3.36}$$

$$z_1^{IN}=\int_{-\pi}^{+\pi}\int_{-\infty}^{+\infty} -i\frac{|k|}{k}\, e^{i(kcos\theta a+ksin\theta b-\omega t)}\, e^{\omega^2 c/g}\, d\xi_1(\omega,\theta) \tag{3.37}$$

$$P_1^{IN}=0 \tag{3.38}$$

where the superscript *IN* denotes inviscid wave dynamics. The spectral density function for the horizontal displacements ξ_1 is a random complex valued function such that

$$<d\xi_1(\omega,\theta)\, d\xi_1{}^*(\omega'',\theta'')>=S_1(\omega,\theta)d\omega\, d\theta;\ \omega=\omega'',\ \theta=\theta''$$

$$=0\ \ otherwise.$$

where S_1 is the wave spectrum, <.> represents ensemble average and the superscript * denotes the complex conjugate.

3.4. SOLUTION OF THE SECOND ORDER EQUATIONS

Pierson (1962) demonstrated that substitution of the solutions of the first order differential equations (3.35) to (3.38) into the second order equations (3.16) to (3.19) gives inhomogeneous linear second order equations which are solveable. Herterich and Hasselmann (1982) and Sanderson and Okubo (1988) showed that it is possible for two waves of frequencies ω and ω′ to give a zero-frequency interaction if ω′=−ω. It is

also possible to have interactions with $\omega \neq \omega'$. The latter type of interactions give solutions that are oscillatory in time and do not cause any diffusion. So the interactions with $\omega \neq \omega'$ will not be considered in this thesis. Therefore, considering zero-frequency interaction equations (3.16) - (3.19) reduce to

$$x_{2tt}+gz_{2a}+\frac{p_{2a}}{\rho}=\int_{-\pi}^{+\pi}\int_{-\pi}^{+\pi}\int_{-\infty}^{+\infty}\Theta_a d\xi_1(\omega,\theta)d\xi_1(-\omega,\theta') \tag{3.39}$$

$$y_{2tt}+gz_{2b}+\frac{p_{2b}}{\rho}=\int_{-\pi}^{+\pi}\int_{-\pi}^{+\pi}\int_{-\infty}^{+\infty}\Theta_b d\xi_1(\omega,\theta)d\xi_1(-\omega,\theta') \tag{3.40}$$

$$z_{2tt}+gz_{2c}+\frac{p_{2c}}{\rho}=\int_{-\pi}^{+\pi}\int_{-\pi}^{+\pi}\int_{-\infty}^{+\infty}\Theta_c d\xi_1(\omega,\theta)d\xi_1(-\omega,\theta') \tag{3.41}$$

$$x_{2a}+y_{2b}+z_{2c}=\int_{-\pi}^{+\pi}\int_{-\pi}^{+\pi}\int_{-\infty}^{+\infty}\Phi d\xi_1(\omega,\theta)\,d\xi_1(-\omega,\theta') \tag{3.42}$$

where

$$\Theta=\frac{\omega^2}{2}[1+cos(\theta-\theta')]e^{ik(\gamma_1 a+\gamma_2 b)}e^{2\omega^2 c/g} \tag{3.43}$$

$$\Phi=\frac{\omega^4}{2g^2}[1+cos(\theta-\theta')]^2 e^{ik(\gamma_1 a+\gamma_2 b)}e^{2\omega^2 c/g} \tag{3.44}$$

$$\gamma_1=cos\theta-cos\theta'$$

$$\gamma_2=sin\theta-sin\theta'.$$

The terms on the right hand side of (3.39)-(3.42) come from the nonlinear quadratic in first order solution terms in equations (3.16)-(3.19).

It is clear from (3.39) - (3.44) that x_2, y_2, z_2 cannot be periodic in time since none of the inhomogeneous terms on the right hand side of (3.39), (3.40), (3.41) and (3.42) show time dependence. Excluding the

possibility of accelerated motion (i.e., steady state), the equations (3.39) - (3.41) are not independent.

This system of equations can be solved by considering the vorticity equations in a manner similar to that first used by Pierson (1962). Sanderson and Okubo (1988) also followed a similar technique to solve the diffusion due to random internal wave motions. Differentiating (3.2) with respect to c and (3.3) with respect to b and subtracting gives

$$(x_{tt}x_b+y_{tt}y_b+z_{tt}z_b)_c-(x_{tt}x_c+y_{tt}y_c+z_{tt}z_c)_b=0 \tag{3.45}$$

Differentiating (3.1) with respect to b and (3.2) with respect to a and subtracting gives

$$(x_{tt}x_a+y_{tt}y_a+z_{tt}z_a)_b-(x_{tt}x_b+y_{tt}y_b+z_{tt}z_b)_a=0 \tag{3.46}$$

Noting the following identities

$$(x_{tt}x_a+y_{tt}y_a+z_{tt}z_a)_b=(x_tx_a+y_ty_a+z_tz_a)_{bt}-(x_t^2+y_t^2+z_t^2)_{ab}/2 \tag{3.47}$$

$$(x_{tt}x_b+y_{tt}y_b+z_{tt}z_b)_a=(x_tx_b+y_ty_b+z_tz_b)_{at}-(x_t^2+y_t^2+z_t^2)_{ab}/2 \tag{3.48}$$

$$(x_{tt}x_b+y_{tt}y_b+z_{tt}z_b)_c=(x_tx_b+y_ty_b+z_tz_b)_{ct}-(x_t^2+y_t^2+z_t^2)_{bc}/2 \tag{3.49}$$

$$(x_{tt}x_c+y_{tt}y_c+z_{tt}z_c)_b=(x_tx_c+y_ty_c+z_tz_c)_{bt}-(x_t^2+y_t^2+z_t^2)_{bc}/2 \tag{3.50}$$

it is clear that equations (3.45) and (3.46) may be written as

$$(x_tx_b+y_ty_b+z_tz_b)_{ct}-(x_tx_c+y_ty_c+z_tz_c)_{bt}=0 \tag{3.51}$$

$$(x_tx_a+y_ty_a+z_tz_a)_{bt}-(x_tx_b+y_ty_b+z_tz_b)_{at}=0. \tag{3.52}$$

Considering the case where unperturbed fluid has no vorticity, we can integrate the above equations to give

$$(x_t x_b + y_t y_b + z_t z_b)_c - (x_t x_c + y_t y_c + z_t z_c)_b = 0 \tag{3.53}$$

$$(x_t x_a + y_t y_a + z_t z_a)_b - (x_t x_b + y_t y_b + z_t z_b)_a = 0. \tag{3.54}$$

The vorticity equations (3.53) and (3.54) give

$$(y_{2t} + x_{1t}x_{1b} + y_{1t}y_{1b} + z_{1t}z_{1b})_c - (z_{2t} + x_{1t}x_{1c} + y_{1t}y_{1c} + z_{1t}z_{1c})_b = 0 \tag{3.55}$$

$$(x_{2t} + x_{1t}x_{1a} + y_{1t}y_{1a} + z_{1t}z_{1a})_b - (y_{2t} + x_{1t}x_{1b} + y_{1t}y_{1b} + z_{1t}z_{1b})_a = 0 \tag{3.56}$$

at second order in ε. (The first order vorticity equations are satisfied by the first order solutions (3.35-3.38)). Substituting the first order solutions (3.35), (3.36), (3.37) into (3.55), (3.56) and considering zero-frequency interactions, one obtains

$$y_{2tc} - z_{2tb} = \int_{-\pi}^{+\pi}\int_{-\pi}^{+\pi}\int_{-\infty}^{+\infty} k\omega^3(\sin\theta + \sin\theta')\,|1+\cos(\theta-\theta')|/g\, e^{2|k|c}\, e^{ik(\gamma_1 a + \gamma_2 b)} \, d\xi_1(\omega,\theta)\, d\xi_1(-\omega,\theta') \tag{3.57}$$

$$x_{2tb} - y_{2ta} = -i\int_{-\pi}^{+\pi}\int_{-\pi}^{+\pi}\int_{-\infty}^{+\infty} \omega k^2 \sin(\theta'-\theta)\,|1+\cos(\theta-\theta')|\, e^{2|k|c}\, e^{ik(\gamma_1 a + \gamma_2 b)} \, d\xi_1(\omega,\theta)\, d\xi_1(-\omega,\theta') \tag{3.58}$$

where

$$|k| = \omega^2/g. \tag{3.59}$$

Equations (3.57), (3.58) and the continuity equation (3.42) may be used to solve for u_2^{IN}, v_2^{IN} and w_2^{IN} where u_2^{IN}, v_2^{IN} and w_2^{IN} denote the inviscid Lagrangian velocities x_{2t}, y_{2t} and z_{2t} respectively. Differentiating (3.42) with respect to t and b and using (3.57) and (3.58) to eliminate u_2^{IN}, w_2^{IN} we have

$$v_{2aa}{}^{IN}+v_{2bb}{}^{IN}+v_{2cc}{}^{IN}=\int_{-\pi}^{+\pi}\int_{-\pi}^{+\pi}\int_{-\infty}^{+\infty}\omega k^3[2(sin\theta+sin\theta')-(cos\theta-cos\theta')$$

$$sin(\theta'-\theta)||1+cos(\theta-\theta')]e^{2|k|c}e^{ik(\gamma_1 a+\gamma_2 b)}d\xi_1(\omega,\theta)d\xi_1(-\omega,\theta'). \tag{3.60}$$

Equation (3.60) has a particular solution of the form

$$v_2{}^{IN}=\int_{-\pi}^{+\pi}\int_{-\pi}^{+\pi}\int_{-\infty}^{+\infty}(sin\theta+sin\theta')A^{IN}e^{2|k|c}e^{ik(\gamma_1 a+\gamma_2 b)}d\xi_1(\omega,\theta)d\xi_1(-\omega,\theta') \tag{3.61}$$

where

$$A^{IN}=\omega k|1+cos(\theta-\theta')]/2 \tag{3.62}$$

Using (3.61) in (3.58), the solution for the inviscid Lagrangian velocity $u_2{}^{IN}$ is given by

$$u_2{}^{IN}=\int_{-\pi}^{+\pi}\int_{-\pi}^{+\pi}\int_{-\infty}^{+\infty}(cos\theta+cos\theta')A^{IN}e^{2|k|c}e^{ik(\gamma_1 a+\gamma_2 b)}d\xi_1(\omega,\theta)d\xi_1(-\omega,\theta'). \tag{3.63}$$

The solutions (3.61) and (3.63) satisfy the boundary conditions (3.20) and (3.21). Therefore, it is not necessary to consider homogeneous solutions.

Equations (3.61) and (3.63) are zero-frequency horizontal Lagrangian velocities. They are the zero-frequency particle motion resulting from superpositions of deep water surface gravity waves that have wavenumber components represented by $k\gamma_1$ and $k\gamma_2$ in the a and b axis directions respectively. The resultant wave number is

$$K=k[\gamma_1{}^2+\gamma_2{}^2]^{1/2}$$

along a direction at

$$\Theta_r = tan^{-1}\gamma_2/\gamma_1$$

measured counterclockwise relative to the a axis. Figure (3.1) shows the schematic of two primary waves interacting to produce zero-frequency second order motion. The zero-frequency component of the horizontal velocity (u_2^{IN}, v_2^{IN}) fluctuates as a function of space as indicated by the dashed lines oriented along the K vector in Figure 3.1. Note that

$$u_{2a}^{IN} + v_{2b}^{IN} = 0, \tag{3.64}$$

therefore the motion is horizontally nondivergent. This type of motion cannot cause any vertical motion. The solutions of Herterich and Hasselmann (1982) and Sanderson and Okubo (1988) are also horizontally nondivergent. Therefore their inviscid solutions did not give any vertical motion. In the following chapter it will be shown that introduction of viscosity into the equations of motion makes the flow field horizontally divergent. This, in turn, causes vertical motion.

The solutions (3.61) and (3.63) are identical to solutions of Herterich and Hasselmann (1982). For $\theta = \theta' = 0$, (3.63) gives

$$u_2^{IN} = \int_{-\infty}^{+\infty} 2\omega k e^{2|k|c} d\xi_1(\omega)\, d\xi_1(-\omega). \tag{3.65}$$

Invoking the difinition for the wave amplitude, A_0,

$$A_0^2 = \int_{-\infty}^{+\infty} 2\, d\xi_1(\omega)\, d\xi_1(-\omega), \tag{3.66}$$

the equation (3.65) reduces to

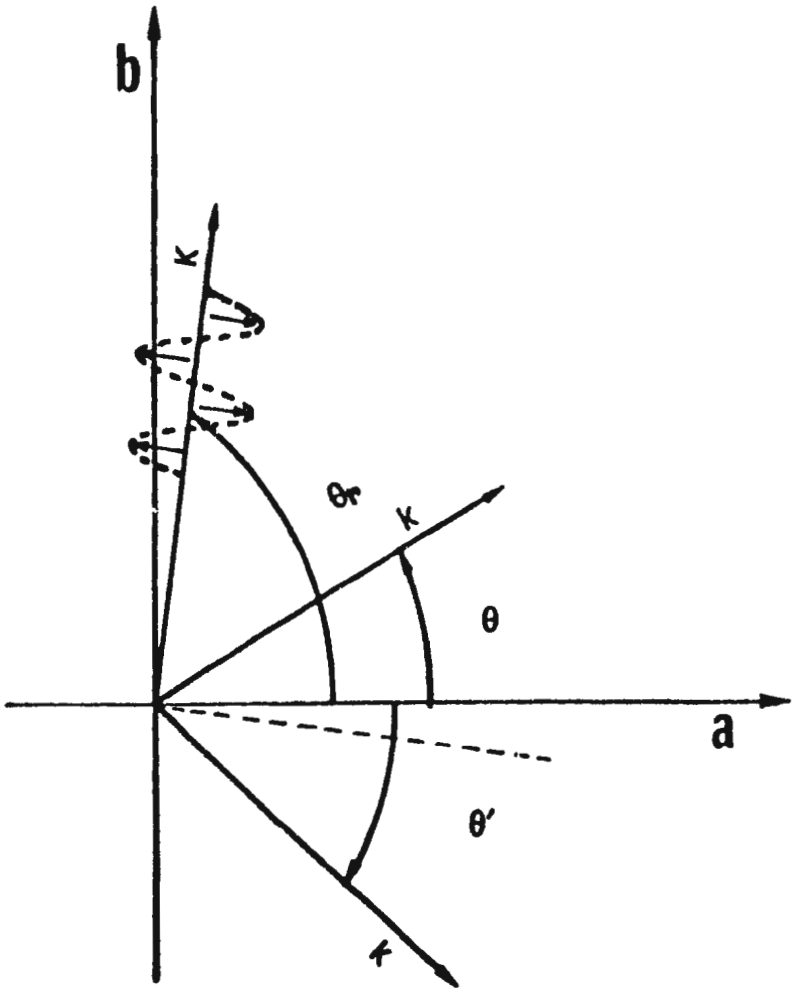

Figure 3-1: Surface waves with wavenumbers k and k travel in the θ and θ' directions respectively. The resulting zero-frequency second-order interaction causes motion with wave number components $k\gamma_1$, $k\gamma_2$, which have a resultant in the Θ_r direction. The zero-frequency velocity is in the horizontal plane and is parallel to the angle bisector (dashed line). It is also sheared in the horizontal plane as indicated by the sinusoidally varying flow pattern.

$$u_2^{IN} = A_0^2 \omega k e^{2|k|z}$$

which is the Stokes' (1847) classical result.

3.5. SUMMARY

Navier-Stokes' equations of motion are solved for deep water surface gravity waves in an inviscid, irrotational, homogeneous ocean. The analysis is in the Lagrangian coordinate system. We consider zero-frequency interaction between pairs of primary waves interacting at any arbitrary angles. The solutions agree with those of Herterich and Hasselmann (1982) who solved the same problem by using an Eulerian frame of reference.

We obtain solutions that are nondivergent in the horizontal plane. For $\theta = \theta' = 0$, the above solutions reduce to Stoke's (1847) classical result.

The solutions (3.61, 3.63) cause random shearing motion in the horizontal plane. Such a velocity field cannot change the area of a patch of tracer. However, its shape can be greately distorted, thereby changing the moments of its distribution. Sanderson and Okubo (1988) and Herterich and Hasselmann (1982) showed how to calculate eddy-diffusivities from the random waves. These will be discussed in detail in Chapter 5.

The above solutions show that for inviscid fluid the zero-frequency interactions of random gravity waves can cause horizontal eddy-diffusion, but no vertical eddy-diffusion. However, water is not a perfectly inviscid liquid. It has some small but finite viscosity. In the next chapter, we solve the viscous equations. It will be shown that the introduction of viscosity changes the solutions in a manner that leads to both vertical and horizontal diffusion.

Chapter 4

RESIDUAL MOTIONS ASSOCIATED WITH VISCOUS GRAVITY WAVES

4.1. INTRODUCTION

It was demonstrated in the last chapter that small-amplitude surface gravity waves induce a flow that disperse material in the horizontal plane. The analysis was based on the assumption of irrotational flow originally suggested by Stokes' in 1847. Longuet-Higgins (1953, 1960) introduced viscosity and showed that the presence of small viscosity produces significant changes in the mass transport not only in the thin boundary layers near the surface, but also in the interior of the fluid. His analysis was based on solving the equations of motion in an Eulerian curvilinear coordinate system attached to the moving surface boundary. By dropping the temporal wave decay terms he implicitly assumed that the wavefield is maintained by an external device.

Russel and Osorio (1957) found that the mass transport observed in a laboratory simulation agrees best with the Stokes' inviscid theory when the water depth is large (compared to wavelength) while for shallower water depth Longuet-Higgins solutions were then the best available comparison. They concluded, however, that except for the velocity profile at the bottom of the channel, no theory satisfactorily predicts mass transport. Swan and Sleath (1990) extended the work of Longuet-Higgins (1953) by deriving a fourth order solution for the mean

drift induced by the steady train of waves in water of constant depth and conducted an experiment to measure mass transport velocity in the wave tank. They found that the fourth order viscous theory shows better agreement with the experiment than the second order viscous theory.

Chang (1969) and Unluta and Mei (1970) calculated the mass transport using a Lagrangian coordinate system for the two dimensional case of one horizontal and one vertical dimension. Chang (1969) considered a random wavefield and obtained a solution for the second order horizontal mass transport velocity that does not decay with depth. Unluta and Mei (1970) incorporated the boundary layer concepts into the Lagrangian equations. At second order, they considered only one horizontal dimension and therefore, the solution of Unluta and Mei did not show any diffusion. In addition, their solution remains unbounded as the depth approaches infinity. Huang (1970) also pointed out deficiencies in the Longuet-Higgins analysis, in particular that the mass transport velocity becomes unbounded as the depth approaches infinity.

Weber (1983a) used perturbation analysis in a Lagrangian coordinate system to derive time dependent results for mass transport due to swell in the deep rotating ocean with viscosity. In a subsequent paper Weber (1983b) investigated the zero-frequency wave induced currents due to a variable wind stress. In both papers, he considered solutions for single frequency sine waves in the horizontal plane with waves interacting at zero angle. Therefore his solutions did not show any diffusion. Later, Weber (1985) extended his computations from a single wave to a pair of crossing waves. One of these waves travelled at an angle θ relative to the a-direction and the other at an angle $-\theta$. The solution indicated that nondecaying deep water surface gravity waves induced roll motion in a viscous fluid. He reduced the three dimensional problem to a two dimensional problem by averaging the second order equations over one wave-length in the a-direction. Therefore, his solutions are

nondivergent in the vertical (a–c) plane. He also showed that the solutions are capable of producing roll motion similar to Langmuir circulation (Leibovich 1983). Jenkins (1986, 1987) generalized Weber's (1983a, b) solutions by including spatially varying windstress and depth varying viscosity.

The objective of the present work is to solve the 3-D Lagrangian equations of motion for a spectrum of nondecaying surface waves in a viscous nonrotating ocean. We will search for zero-frequency motion resulting from wave-wave interactions through the nonlinear terms. In particular we search for such solutions that can diffuse material vertically and / or horizontally in the ocean. The problem is solved by using two approaches. First, following the technique of Longuet-Higgins (1953), Unluta and Mei (1970) and Weber (1983b, 1985), it will be assumed that the waves are nondecaying waves. This implies that the primary waves are maintained by a suitably adjusted stress. The second approach is to consider decaying waves (Chang 1969, Weber 1983a). It will be shown later in this section that, unlike the nondecaying case, the space and time coordinates of the homogeneous solutions are not separable. The homogeneous equations are solved subject to an initial condition.

The mathematical formulation of the problem is given in section 4.2. Section 4.3 derives the surface boundary conditions. The nondecaying wave problem is formulated and solved in section 4.4. In section 4.5, we solve the decaying wave problem. Difficulties encountered in solving the second order momentum equations, for the latter problem, by using a separation of variables are also discussed.

4.2. MATHEMATICAL FORMULATION

To describe the model, we consider an ocean with a viscous incompressible homogeneous fluid of infinite depth and unlimited horizontal extent. When undisturbed, the surface is horizontal. A cartesian coordinate system is chosen such that the (x, y)-axes are situated at the undisturbed surface and the z-axis is positive upwards. The motion is described by formulating the equations of motion in a Lagrangian coordinate system. Let a fluid particle initially have coordinates (a, b, c). Its position (x, y, z) and pressure p at later times will then be functions of a, b, c and time t. The Lagrangian equations of motion for viscous fluid are given by Pierson (1962)

$$x_{tt} = -\frac{1}{\rho}\frac{\partial(p,y,z)}{\partial(a,b,c)} + \nu\nabla_L^2 x_t \tag{4.1}$$

$$y_{tt} = -\frac{1}{\rho}\frac{\partial(x,p,z)}{\partial(a,b,c)} + \nu\nabla_L^2 y_t \tag{4.2}$$

$$z_{tt} + g = -\frac{1}{\rho}\frac{\partial(x,y,p)}{\partial(a,b,c)} + \nu\nabla_L^2 z_t \tag{4.3}$$

where $\partial(.....)/\partial(a,b,c)$ is the Jacobian and the Laplacian operator ∇_L^2 in Lagrangian form is given by

$$\nabla_L^2 x_t = \frac{\partial\left(\frac{\partial(x_t,y,z)}{\partial(a,b,c)},y,z\right)}{\partial(a,b,c)} + \frac{\partial\left(x,\frac{\partial(x,x_t,z)}{\partial(a,b,c)},z\right)}{\partial(a,b,c)} + \frac{\partial\left(x,y,\frac{\partial(x,y,x_t)}{\partial(a,b,c)}\right)}{\partial(a,b,c)} \tag{4.4}$$

Similar expressions will result for $\nabla_L^2 y_t$ and $\nabla_L^2 z_t$. The equation of continuity does not change by inclusion of the viscous term and is given by (3.6). Again we assume that x, y, z and p can be expressed as a power series. Substituting (3.8) - (3.11) into (4.1) to (4.3) and equating the equal powers of ε, one obtains

$$x_{1tt}+gz_{1a}+\frac{p_{1a}}{\rho}=\nu\nabla^2 x_{1t} \tag{4.5}$$

$$y_{1tt}+gz_{1b}+\frac{p_{1b}}{\rho}=\nu\nabla^2 y_{1t} \tag{4.6}$$

$$z_{1tt}+gz_{1c}+\frac{p_{1c}}{\rho}=\nu\nabla^2 z_{1t} \tag{4.7}$$

$$x_{1a}+y_{1b}+z_{1c}=0 \tag{4.8}$$

at first order in ε, and

$$x_{2tt}+gz_{2a}+\frac{p_{2a}}{\rho}-\nu\nabla^2 x_{2t}=-z_{1a}z_{1tt}-y_{1a}y_{1tt}-x_{1a}x_{1tt}+$$
$$\nu[x_{1a}\nabla^2 x_{1t}+y_{1a}\nabla^2 y_{1t}+z_{1a}\nabla^2 z_{1t}-2(x_{1taa}x_{1a}+x_{1tbb}y_{1b}+x_{1tcc}z_{1c}$$
$$+x_{1tab}(y_{1a}+x_{1b})+x_{1tac}(z_{1a}+x_{1c})+x_{1tbc}(y_{1c}+z_{1b}))-x_{1ta}\nabla^2 x_1-$$
$$x_{1tb}\nabla^2 y_1-x_{1tc}\nabla^2 z_1] \tag{4.9}$$

$$y_{2tt}+gz_{2b}+\frac{p_{2b}}{\rho}-\nu\nabla^2 y_{2t}=-z_{1b}z_{1tt}-y_{1b}y_{1tt}-x_{1b}x_{1tt}+$$
$$\nu[x_{1b}\nabla^2 x_{1t}+y_{1b}\nabla^2 y_{1t}+z_{1b}\nabla^2 z_{1t}-2(y_{1taa}x_{1a}+y_{1tbb}y_{1b}+y_{1tcc}z_{1c}$$
$$+y_{1tab}(y_{1a}+x_{1b})+y_{1tac}(z_{1a}+x_{1c})+y_{1tbc}(y_{1c}+z_{1b}))-y_{1ta}\nabla^2 x_1-$$
$$y_{1tb}\nabla^2 y_1-y_{1tc}\nabla^2 z_1] \tag{4.10}$$

$$z_{2t}+gz_{2c}+\frac{p_{2c}}{\rho}-\nu\nabla^2 z_{2t}=-z_{1c}z_{1t}-y_{1c}y_{1t}-x_{1c}x_{1t}+$$

$$\nu[x_{1c}\nabla^2 x_{1t}+y_{1c}\nabla^2 y_{1t}+z_{1c}\nabla^2 z_{1t}-2(z_{1taa}x_{1a}+z_{1tbb}y_{1b}+z_{1tcc}z_{1c}$$

$$+z_{1tab}(y_{1a}+x_{1b})+z_{1tac}(z_{1a}+x_{1c})+z_{1tbc}(y_{1c}+z_{1b}))-z_{1ta}\nabla^2 x_1-$$

$$z_{1tb}\nabla^2 y_1-z_{1tc}\nabla^2 z_1] \qquad (4.11)$$

$$x_{2a}+y_{2b}+z_{2c}+y_{1b}z_{1c}+x_{1a}z_{1c}+x_{1a}y_{1b}-y_{1c}z_{1b}-x_{1c}z_{1a}-x_{1b}y_{1a}=0 \qquad (4.12)$$

at second order in ε. Here

$$\nabla^2=\frac{\partial^2}{\partial a^2}+\frac{\partial^2}{\partial b^2}+\frac{\partial^2}{\partial c^2}$$

is the usual Laplacian operator. The equations reduce to an identity at zeroth order in ε. The continuity equations (4.8) and (4.12) are same as (3.15) and (3.41) respectively for the inviscid case.

The perturbation parameter ε (which is the maximum wave slope) is not the only small parameter for surface gravity waves in a viscous ocean. Another small parameter that is imposed by the presence of the small viscous terms is $\varepsilon_1 \sim 1/R_w^{1/2}$ where $R_w(=\omega/(\nu k^2))$ is the wave Reynold's number. The wave Reynold's number is the ratio of the acceleration term to the viscous term. The surface viscous boundary layer has a thickness $l=\sqrt{2\nu/\omega}$, thus ε_1 can also be thought of as a ratio of the viscous boundary layer thickness to the wave length, $\varepsilon_1 \sim kl$. The magnitude of ε_1 is much smaller than the wave slope ε except when wave slope is very small and viscosity is large (see discussion at the end of section 4.4). The presence of two small parameters give one a choice whether to use a boundary-layer approach by introducing separate equations for different regimes (e.g., Longuett-Higgins, 1953; Unluta and Mei, 1970) or to consider a single equation governing the entire fluid column (e.g., Chang, 1969; Weber, 1983a, b, 1985). In this dissertation, we will follow the later approach.

4.3. BOUNDARY CONDITIONS

The boundary conditions at a free surface are obtained by the vertical and horizontal balance of forces. A two dimensional derivation of these equations in the vertical plane is given by Kinsman (1984). Chang (1969) used Kinsman's boundary conditions for her calculations but the equation for the vertical component (equations 89 and 91 of Chang 1969) is wrong. Kinsman (1984) used a geometrical approach to derive the boundary conditions at the surface. In this section, we apply a generalized technique to derive the surface boundary conditions for the three dimensional motion of a viscous, incompressible liquid.

Consider an element ds of sloping free surface of a viscous incompressible Newtonian fluid. Let the equation of the free surface be

$$z=\eta(x,y,t). \tag{4.13}$$

Let $\hat{t}$ be a unit vector tangential to this surface whose equation is given by (fig. 4.1)

$$\hat{t} = cos\phi cos\theta\hat{i} + sin\phi cos\theta\hat{j} + sin\theta\hat{k} \tag{4.14}$$

where $\hat{i}$, $\hat{j}$, $\hat{k}$ are the unit vectors along the (x,y,z) directions. The unit vector normal to this free surface is given by

$$\hat{n} = -cos\phi sin\theta\hat{i} - sin\phi sin\theta\hat{j} + cos\theta\hat{k}. \tag{4.15}$$

Let p_o be the atmospheric pressure at the surface and τ be the external tangential wind stress parallel to the $\hat{t}$ direction. The fluid motion will give rise to stresses in the interior of the fluid that balance the external stresses at the surface. We have neglected surface tension. The equilibrium condition requires that the vector sum of the external

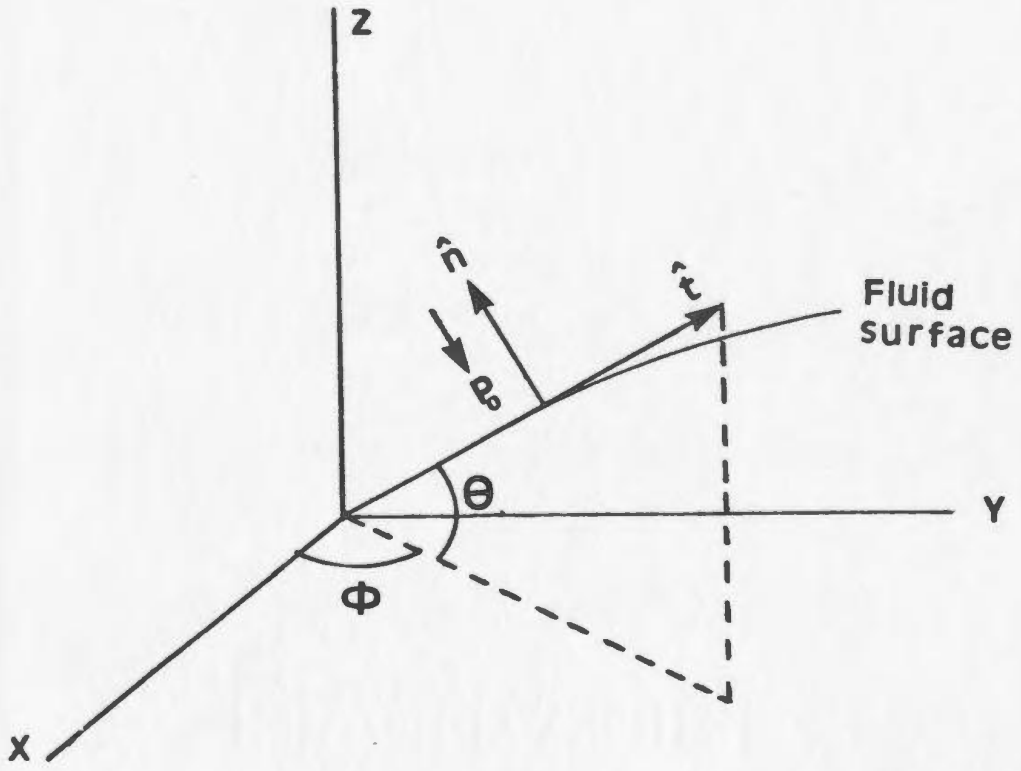

Figure 4-1: Balance of forces on an elevated fluid surface.

forces must balance the internal forces at the surface. In tensor notation, this is given by (neglecting forces due to surface tension)

$$-p_o n_i ds + \tau t_i ds = \sigma_{ij} n_j ds \tag{4.16}$$

where σ_{ij} is the internal stress tensor. Water is a Newtonian fluid so, σ_{ij} is given by

$$\sigma_{ij} = -p\delta_{ij} + \rho\nu\left(\frac{\partial u_j}{\partial x_i} + \frac{\partial u_i}{\partial x_j}\right). \tag{4.17}$$

Substituting t_i and n_i from (4.14) and (4.15) into (4.16) one obtains the following equations

$$p_o \cos\phi \sin\theta + \tau \cos\phi \cos\theta = -\sigma_{11} \cos\phi \sin\theta - \sigma_{12} \sin\phi \sin\theta + \sigma_{13} \cos\theta \tag{4.18}$$

$$p_o \sin\phi \sin\theta + \tau \sin\phi \cos\theta = -\sigma_{21} \cos\phi \sin\theta - \sigma_{22} \sin\phi \sin\theta + \sigma_{23} \cos\theta \tag{4.19}$$

$$-p_o \cos\theta + \tau \sin\theta = -\sigma_{31} \cos\phi \sin\theta - \sigma_{32} \sin\phi \sin\theta + \sigma_{33} \cos\theta \tag{4.20}$$

which are respectively the balance of the x, y, z components of force at the surface.

If we assume that $p_o = 0$ at the free surface, the above equations reduce to

$$-\sigma_{11} \cos\phi \sin\theta - \sigma_{12} \sin\phi \sin\theta + \sigma_{13} \cos\theta = \tau_1 \tag{4.21}$$

$$-\sigma_{21} \cos\phi \sin\theta - \sigma_{22} \sin\phi \sin\theta + \sigma_{23} \cos\theta = \tau_2 \tag{4.22}$$

$$-\sigma_{31} \cos\phi \sin\theta - \sigma_{32} \sin\phi \sin\theta + \sigma_{33} \cos\theta = \tau_3 \tag{4.23}$$

where τ_1, τ_2 and τ_3 are x, y and z components of surface stress respectively.

The angles θ and ϕ in the above equations can be related to the derivatives of $\eta(x,y)$ through the relation

$$\nabla (z - \eta(x,y,t)) = c' \hat{n} \tag{4.24}$$

where c' is an arbitrary constant and $\nabla = \hat{i} \frac{\partial}{\partial x} + \hat{j} \frac{\partial}{\partial y} + \hat{k} \frac{\partial}{\partial z}$. Substituting (4.15) in (4.24) and equating the coefficients of unit vectors $\hat{i}$, $\hat{j}$ and $\hat{k}$ from both sides of (4.24), one obtains

$$c' = \frac{1}{\cos\theta} \tag{4.25a}$$

$$\frac{\partial \eta}{\partial x} = \cos\phi \tan\theta \tag{4.25b}$$

$$\frac{\partial \eta}{\partial y} = \sin\phi \tan\theta \tag{4.25c}$$

Using (4.25a,b) to eliminate θ and ϕ in (4.21) through (4.23) gives

$$-\sigma_{11}\frac{\partial \eta}{\partial x} - \sigma_{12}\frac{\partial \eta}{\partial y} + \sigma_{13} = \tau_1 \tag{4.26}$$

$$-\sigma_{21}\frac{\partial \eta}{\partial x} - \sigma_{22}\frac{\partial \eta}{\partial y} + \sigma_{23} = \tau_2 \tag{4.27}$$

$$-\sigma_{31}\frac{\partial \eta}{\partial x} - \sigma_{32}\frac{\partial \eta}{\partial y} + \sigma_{33} = \tau_3. \tag{4.28}$$

We must now transform the Eulerian surface $\eta(x,y,t)$ to its Lagrangian equivalent $z(a,b,c=0,t)$. At the free surface (i.e., $c=0$) x, y and z are all functions of (a,b,t). In Lagrangian coordinates, the differential operators $\frac{\partial}{\partial x}$, $\frac{\partial}{\partial y}$ transform to

$$\frac{\partial}{\partial x} = \frac{y_b \frac{\partial}{\partial a} - y_a \frac{\partial}{\partial b}}{x_a y_b - y_a x_b}$$

$$\frac{\partial}{\partial y} = \frac{x_a \frac{\partial}{\partial b} - x_b \frac{\partial}{\partial a}}{x_a y_b - y_a x_b}. \tag{4.29}$$

Using (4.29) to transform (4.17) into Lagrangian coordinate system and writing $u = x_t$, $v = y_t$, $w = z_t$, the components of the stress tensor σ_{ij} (4.17) are given by

$$\sigma_{11}=-p+2\rho\nu\frac{\partial(x_t,y,z)}{\partial(a,b,c)}$$

$$\sigma_{22}=-p+2\rho\nu\frac{\partial(x,y_t,z)}{\partial(a,b,c)}$$

$$\sigma_{33}=-p+2\rho\nu\frac{\partial(x,y,z_t)}{\partial(a,b,c)}$$

$$\sigma_{12}=\sigma_{21}=\rho\nu\left[\frac{\partial(y_t,y,z)}{\partial(a,b,c)}+\frac{\partial(x,x_t,z)}{\partial(a,b,c)}\right]$$

$$\sigma_{13}=\sigma_{31}=\rho\nu\left[\frac{\partial(z_t,y,z)}{\partial(a,b,c)}+\frac{\partial(x,y,x_t)}{\partial(a,b,c)}\right]$$

$$\sigma_{23}=\sigma_{32}=\rho\nu\left[\frac{\partial(x,z_t,z)}{\partial(a,b,c)}+\frac{\partial(x,y,y_t)}{\partial(a,b,c)}\right] \qquad (4.30)$$

where $\frac{\partial(.....)}{\partial(a,b,c)}$ is the Jacobian. Equations (4.26)-(4.28) can also be transformed into a Lagrangian system using (4.29). Substituting (4.30) into the resulting equations gives

$$\left[p-2\rho\nu\frac{\partial(x_t,y,z)}{\partial(a,b,c)}\right](y_b z_a-y_a z_b)-\rho\nu\left[\frac{\partial(y_t,y,z)}{\partial(a,b,c)}+\frac{\partial(x,x_t,z)}{\partial(a,b,c)}\right]$$

$$(x_a z_b-x_b z_a)+\rho\nu\left[\frac{\partial(z_t,y,z)}{\partial(a,b,c)}+\frac{\partial(x,y,x_t)}{\partial(a,b,c)}\right](x_a y_b-y_a x_b)=\tau_1 \qquad (4.31)$$

$$at\ c=0,$$

$$-\rho\nu\left[\frac{\partial(y_t,y,z)}{\partial(a,b,c)}+\frac{\partial(x,x_t,z)}{\partial(a,b,c)}\right](y_b z_a-y_a z_b)+\left[p-2\rho\nu\frac{\partial(x,y_t,z)}{\partial(a,b,c)}\right](x_a z_b-x_b z_a)$$

$$+\rho\nu\left[\frac{\partial(x,z_t,z)}{\partial(a,b,c)}+\frac{\partial(x,y,y_t)}{\partial(a,b,c)}\right](x_a y_b-y_a x_b)=\tau_2 \qquad (4.32)$$

$$at\ c=0,$$

$$-\rho\nu\left|\frac{\partial(z_t,y,z)}{\partial(a,b,c)}+\frac{\partial(x,y,x_t)}{\partial(a,b,c)}\right|(y_b z_a-y_a z_b)-\rho\nu\left|\frac{\partial(x,z_t,z)}{\partial(a,b,c)}+\frac{\partial(x,y,y_t)}{\partial(a,b,c)}\right|$$
$$(x_a z_b-x_b z_a)-\left|p-2\rho\nu\frac{\partial(x,y,z_t)}{\partial(a,b,c)}\right|(x_a y_b-y_a x_b)=\tau_3 \qquad (4.33)$$

$$at\ c=0,$$

for the x, y, z components respectively of the force balance at the surface. Equations (4.31) - (4.33) represent the Lagrangian form of the boundary conditions at the free surface $c=0$.

Applying a perturbation expansion by substituting (3.8) - (3.11) and $\tau_i=\varepsilon\tau_i'+\varepsilon^2\tau_i''+O(\varepsilon^3)$ into (4.31)-(4.33) and equating coefficients of ε and ε^2 one obtains first order surface ($c=0$) boundary conditions

$$\rho\nu\left|z_{1ta}+x_{1tc}\right|=\tau_1' \qquad (4.34)$$

$$\rho\nu\left|y_{1tc}+z_{1tb}\right|=\tau_2' \qquad (4.35)$$

$$-p_1+2\rho\nu z_{1tc}=\tau_3' \qquad (4.36)$$

and second order surface ($c=0$) boundary conditions:

$$\rho\nu[x_{2tc}+z_{2ta}+x_{1tc}x_{1a}-x_{1ta}x_{1c}+x_{1tc}y_{1b}-x_{1tb}y_{1c}+z_{1ta}z_{1c}-z_{1tc}z_{1a}+$$
$$z_{1ta}y_{1b}-z_{1tb}y_{1a}-x_{1tb}z_{1b}-y_{1ta}z_{1b}-2x_{1ta}z_{1a}|+p_1z_{1a}=\tau_1'' \qquad (4.37)$$

$$\rho\nu|y_{2tc}+z_{2tb}+y_{1tc}y_{1b}-y_{1tb}x_{1c}+y_{1tc}x_{1a}-y_{1ta}x_{1c}+z_{1tb}z_{1c}-z_{1tc}z_{1b}+$$
$$z_{1tb}x_{1a}-z_{1ta}x_{1b}-x_{1tb}z_{1a}-y_{1ta}z_{1a}-2y_{1tb}z_{1b}|+p_1z_{1b}=\tau_2'' \qquad (4.38)$$

$$-p_2+\rho\nu[2z_{2tc}+2z_{1tc}x_{1a}+2z_{1tc}y_{1b}-2z_{1tb}y_{1c}-2z_{1ta}x_{1c}-x_{1tc}z_{1a}-z_{1ta}z_{1a}-$$
$$y_{1tc}z_{1b}-z_{1tb}z_{1b}|=\tau_3''. \qquad (4.39)$$

The surface boundary conditions given by (4.34) to (4.39) are identical to

Weber's (1985) surface boundary conditions. The lower boundary conditions are simply that perturbation pressures and displacements tend to zero as $c \to -\infty$.

4.4. SOLUTION FOR NONDECAYING VISCOUS GRAVITY WAVES

The approach adopted here is similar to those of Weber (1985) but it differs in two respects. First, Weber (1985) started by constructing first order solutions by considering two single frequency primary waves propagating at oblique angles, as opposed to a continuous spectrum. Second, he averaged the equations of motion over one wave-length along x-direction. Thus his solutions are non-divergent in the vertical plane. The following work considers a continuous spectrum of random waves interacting at any arbitrary angle and presents the full three dimensional solution. This enables calculation of the eddy-diffusivities resulting from the spectrum of deep water viscous gravity waves by using the technique of Herterich and Hasselmann (1982). Chapter 5 investigates analytically and numerically the horizontal and vertical eddy-diffusivities calculated from deep water surface gravity waves with viscosity.

4.4.1. THE FIRST ORDER SOLUTION

In this section we solve the first order equations (4.5) - (4.8) subject to the boundary conditions (4.34) - (4.36) to find nondecaying waves. Under the assumption that x_1, y_1, z_1, p_1 are stationary random processes with respect to a, b, c, t, the spectral representations of the first order solutions are

$$x_1=\int_{-\pi}^{+\pi}\int_{-\infty}^{+\infty}\int_{-\infty}^{+\infty}e^{i(k\cos\theta a+k\sin\theta b-\omega t)}d\xi_{(x)}(k,\omega,\theta\cdot c) \tag{4.40}$$

$$y_1=\int_{-\pi}^{+\pi}\int_{-\infty}^{+\infty}\int_{-\infty}^{+\infty}e^{i(k\cos\theta a+k\sin\theta b-\omega t)}d\xi_{(y)}(k,\omega,\theta\cdot c) \tag{4.41}$$

$$z_1=\int_{-\pi}^{+\pi}\int_{-\infty}^{+\infty}\int_{-\infty}^{+\infty}e^{i(k\cos\theta a+k\sin\theta b-\omega t)}d\xi_{(z)}(k,\omega,\theta\cdot c) \tag{4.42}$$

$$p_1=\int_{-\pi}^{+\pi}\int_{-\infty}^{+\infty}\int_{-\infty}^{+\infty}e^{i(k\cos\theta a+k\sin\theta b-\omega t)}d\xi_{(p)}(k,\omega,\theta\cdot c) \tag{4.43}$$

where $d\xi_{(x)}$, $d\xi_{(y)}$, $d\xi_{(z)}$ and $d\xi_{(p)}$ are spectral density functions of the first order components of the displacement and pressure. Eliminating p_1 from (4.5) and (4.7) by cross differentiation and subtracting gives

$$x_{1tcc}-z_{1tta}=\nu\nabla^2(x_{1tc}-z_{1ta}). \tag{4.44}$$

Similarly, eliminating p_1 from (4.6) and (4.7) yields

$$y_{1tcc}-z_{1ttb}=\nu\nabla^2(y_{1tc}-z_{1tb}). \tag{4.45}$$

Differentiating (4.44) with respect to a, (4.45) with respect to b and adding and using the continuity equation (4.8) gives the following equation for z_1:

$$z_{1ttaa}+z_{1ttbb}+z_{1tcc}=\nu\nabla^2(z_{1taa}+z_{1tbb}+z_{1tc}). \tag{4.46}$$

Similarly, one can also obtain the equation for x_1

$$x_{1ttaa}+x_{1ttbb}+x_{1tcc}=\nu\nabla^2(x_{1taa}+x_{1tbb}+x_{1tc}). \tag{4.47}$$

Substituting (4.42) into (4.46) gives the following fourth order homogenous equation in $d\xi_{(z)}$

$$d\xi_{(z)cccc}-(2k^2-i\omega/\nu)d\xi_{(z)cc}+(k^4-i\omega k^2/\nu)d\xi_{(z)}=0\ . \tag{4.48}$$

The solution of (4.48) that satisfies the lower boundary condition for deep-water gravity waves, i.e., displacement tends to zero as depth $c \to -\infty$, is

$$d\xi_{(z)}=e^{|k|c}d\xi_1(\omega,\theta)+e^{\beta c}d\xi'_1(\omega,\theta) \tag{4.49}$$

where

$$\beta=(k^2-i\omega/\nu)^{1/2}\ . \tag{4.50}$$

Similarly, the solution of equation (4.47) may be written as

$$d\xi_{(x)}=e^{|k|c}d\xi_x(\omega,\theta)+e^{\beta c}d\xi'_x(\omega,\theta) \tag{4.51}$$

where subscript x on $d\xi_x$ and $d\xi_x'$ does not denote differentiation with respect to x. Substituting equations (4.40), (4.41) and (4.42) for x_1, y_1 and z_1 respectively in the first order continuity equation (4.8) and using (4.49) and (4.51) to replace $d\xi_{(z)}$ and $d\xi_{(x)}$ one obtains the following relation for $d\xi_{(y)}$ in terms of $d\xi_x$, $d\xi'_x$, $d\xi_1$, $d\xi'_1$

$$\begin{aligned} d\xi_{(y)}=&-\cot\theta\ \{\ e^{|k|c}d\xi_x(\omega,\theta)+e^{\beta c}d\xi'_x(\omega,\theta)\ \} \\ &-\frac{1}{ik\sin\theta}\{\ |k|e^{|k|c}d\xi_1(\omega,\theta)+\beta e^{\beta c}d\xi'_1(\omega,\theta)\ \}. \end{aligned} \tag{4.52}$$

We substitute (4.40) and (4.42) into the vorticity equation (4.44) and use (4.49) and (4.51) to obtain

$$d\xi_{3'} = \frac{ik\cos\theta}{|k|} d\xi_1. \tag{4.53}$$

Two of the three boundary conditions given by (4.34) - (4.36) are now used to relate the unknown spectral density functions $d\xi'_1$, $d\xi'_1$ to $d\xi_1$. The other boundary condition will determine the magnitude of the applied external stress required in order to maintain the wave against decay.

The general forms of the boundary conditions were derived in section 4.3. Since the ocean is viscous, the surface gravity waves will attenuate in time if no surface stress is applied. (This will be called the decaying wave problem and is treated in the next section.) The frequency of decaying waves is complex and the imaginary part of the frequency is responsible for the decay of the waves. In this section, we will consider nondecaying waves that are maintained by applying a suitable stress at the surface. Naturally the frequency of such waves will be real. Lamb (1932) demonstrated that nondecaying waves could be achieved either by choosing a suitable tangential stress or by applying a vertical stress at the surface. Weber (1983b) showed that the choice of horizontal stress as a means of maintaining the permanent wave leads to an unbounded solution. By choosing a vertical stress he obtained a solution that decays with depth. Following Weber (1983b, 1985), we consider a vertical surface stress τ'_3 that transfers exactly enough energy to the wave motion to compensate for the loss due to viscous dissipation. Accordingly at $c = 0$, the first order surface boundary conditions (4.34 - 4.36) reduce to

$$z_{1ta}+x_{1tc}=0 \tag{4.54}$$

$$y_{1tc}+z_{1tb}=0 \tag{4.55}$$

$$-p_1+2\rho\nu z_{1tc}=\tau_3' \tag{4.56}$$

where τ_3' is determined later.

Substituting (4.40) and (4.42) in the x_1-boundary condition (4.54) and using (4.49), (4.51) and (4.53) yields

$$2d\xi_1+d\xi'_1=-\frac{\beta}{ik\cos\theta}d\xi'_x \ . \tag{4.57}$$

Similarly, substituting (4.41) and (4.42) into y_1-boundary condition (4.55) and using (4.49), (4.52) and (4.53) one obtains

$$d\xi'_x=\frac{i\beta}{k}\cos\theta\, d\xi'_1 \ . \tag{4.58}$$

Now substituting (4.58) into (4.57) gives

$$d\xi'_1=-\frac{2k^2}{\beta^2+k^2}d\xi_1 \tag{4.59}$$

and (4.59) substituted into (4.58) gives

$$d\xi'_x=-\frac{2ik\beta\cos\theta}{\beta^2+k^2}d\xi_1 \ . \tag{4.60}$$

Finally, substituting equations (4.53), (4.59) and (4.60) in equations (4.49), (4.51) and (4.52), $d\xi_{(x)}$, $d\xi_{(y)}$, $d\xi_{(z)}$ may be written as

$$d\xi_{(x)}=\frac{ik\cos\theta}{|k|}\left(e^{|k|c}-\frac{2\beta|k|}{\beta^2+k^2}e^{\beta c}\right)d\xi_1(\omega,\theta), \tag{4.61}$$

$$d\xi_{(y)}=\frac{ik\sin\theta}{|k|}\left(e^{|k|c}-\frac{2\beta|k|}{\beta^2+k^2}e^{\beta c}\right)d\xi_1(\omega,\theta), \tag{4.62}$$

$$d\xi_{(z)}=\left(e^{|k|c}-\frac{2k^2}{\beta^2+k^2}e^{\beta c}\right)d\xi_1(\omega,\theta). \tag{4.63}$$

To express $d\xi_{(p)}$ in terms of $d\xi_1$, substitute (4.40), (4.42) and (4.43) into x_1-momentum equation (4.5) and use (4.61) and (4.63) to give

$$d\xi_{(p)}=\left(\frac{\rho}{|k|}(\omega^2-|k|g)e^{|k|c}+\frac{2\rho gk^2}{\beta^2+k^2}e^{\beta c}\right)d\xi_1(\omega,\theta)\ . \tag{4.64}$$

Now, we apply the third boundary condition (4.56) to determine the necessary vertical stress τ_3' at the surface to maintain the wave against decay. Assume that τ_3' has spectral form

$$\tau_3'=\int_{-\pi}^{+\pi}\int_{-\infty}^{+\infty}\int_{-\infty}^{+\infty}e^{i(k\cos\theta a+k\sin\theta b-\omega t)}d\xi_\tau\ . \tag{4.65}$$

Substituting (4.42), (4.43), (4.63), (4.64) and (4.65) into the remaining boundary condition (4.56) and evaluating at $c=0$ gives

$$d\xi_\tau = \left| -\frac{\rho}{|k|}(\omega^2 - |k|g) - \frac{2\rho g k^2}{\beta^2 + k^2} - 2i\rho\nu\omega\left\{|k| - \frac{2k^2\beta}{\beta^2 + k^2}\right\}\right| d\xi_1 . \tag{4.66}$$

For surface waves on water, the ratio $\omega/(\nu k^2)$ (wave Reynold's number, R_w) is very large (Chang, 1969). Therefore, it is always safe to make the following approximation

$$\frac{\beta}{k} = \left| 1 + (1-i)^2 \frac{\omega}{2\nu k^2}\right|^{1/2} \approx (1-i)\left(\frac{\omega}{2\nu k^2}\right)^{1/2} \gg 1 \tag{4.67a}$$

hence

$$\frac{k}{\beta} \ll 1 \tag{4.67b}$$

where β is given by (4.50). Equation (4.66) reduces to

$$d\xi_\tau = \left| -\frac{\rho}{|k|}(\omega^2 - |k|g) - 2i\rho\nu|k|\left(\frac{g|k|}{\omega} + \omega\right)\right| d\xi_1 \tag{4.68}$$

where we use (4.67) to eliminate the small terms. Since the wave does not decay, the frequency must be real. If we choose $d\xi_\tau$ to be imaginary then the real part of (4.68) gives the dispersion relation

$$\omega^2 = \omega_o^2 = g|k| \tag{4.69a}$$

where ω_0 is the real frequency. The imaginary part of (4.68) gives the surface stress required to maintain a nondecaying wave

$$d\xi_\tau = -4i\rho\nu\omega|k|d\xi_1. \tag{4.69b}$$

Equation (4.69b) is equivalent to

$$\tau_3' = 4\rho\nu z_{1a} \quad \text{at} \quad z=0 \tag{4.70}$$

which is identical to Weber's (1985) equation (A6).

The viscous length scale l is related to ω_0 and β as follows

$$l^2 = 2\nu/|\omega_0|$$

$$\beta = \frac{1-i}{l} \quad \omega > 0$$

$$\beta = \frac{1+i}{l} \quad \omega < 0. \tag{4.71}$$

It is the distance over which the molecular- or eddy- viscosity will diffuse momentum in one wave period. The viscous length scale grows with increasing viscosity and decreases with increasing frequency. As an example, consider the typical frequency range (0.3 - 1.0) s^{-1} of the deep water surface gravity waves. For $\omega = 1\ s^{-1}$, and eddy-viscosity $\nu = 0.01\ m^2 s^{-1}$ equation (4.71) gives $l \sim 0.06$ m, and for $\omega = 0.3\ s^{-1}$ the viscous length scale is $l \sim 0.26$ m. Thus the viscous length scale is very small compared to the scale of the wave (63 - 600 m). For molecular diffusion, the viscous length scale is even smaller. Nevertheless, Longuet-Higgins (1953) has demonstrated that the inclusion of viscosity changes the solutions.

The first order solutions are therefore obtained by substituting (4.61) to (4.64) into (4.40) to (4.43) with ω replaced by ω_0.

$$x_1^{VF} = \int_0^{+\pi}\int_{-\infty}^{+\infty} \cos\theta \left| e^{|k|z} - \frac{2|k|}{\beta} e^{\beta z} \right| e^{i(k\cos\theta a + k\sin\theta b - \omega_0 t)} d\xi_1(\omega,\theta) \tag{4.72a}$$

$$y_1^{VF} = \int_0^{+\pi}\int_{-\infty}^{+\infty} \sin\theta \left| e^{|k|c} - \frac{2|k|}{\beta} e^{\beta c} \right| e^{i(k\cos\theta a + k\sin\theta b - \omega_o t)} d\xi_1(\omega,\theta) \tag{4.72b}$$

$$z_1^{VF} = \int_0^{+\pi}\int_{-\infty}^{+\infty} -\frac{ik}{|k|} \left| e^{|k|c} - \frac{2k^2}{\beta^2} e^{\beta c} \right| e^{i(k\cos\theta a + k\sin\theta b - \omega_o t)} d\xi_1(\omega,\theta) \tag{4.72c}$$

$$p_1^{VF} = \int_0^{+\pi}\int_{-\infty}^{+\infty} -\rho \frac{ik}{|k|} \frac{2gk^2}{\beta^2} e^{\beta c} e^{i(k\cos\theta a + k\sin\theta b - \omega_o t)} d\xi_1(\omega,\theta) \tag{4.72d}$$

where the superscript *VF* has been used to denote solutions corresponding to viscous dynamics in which the waves are nondecaying (or viscous forced). Equations (4.72) reduces to first order inviscid solutions (3.35 - 3.38) if ν is set equal to zero. The effect of introducing the viscosity is to reduce the first order inviscid displacements by introducing additional terms with $e^{\beta c}$ depth dependence. These $e^{\beta c}$ terms are small compared to the inviscid $e^{|k|c}$ terms; the relative size being the ratio of the viscous length scale to the wave length. By equation (4.71) $e^{\beta c} = e^{\left(\frac{1-i}{l}\right)c}$. Thus $e^{\beta c}$ has both real and imaginary arguments. From the exponential of the imaginary argument, $e^{\beta c}$ fluctuates rapidly (in a sinusoidal manner) with depth (since $1/l \gg k$). The term also decays with depth due to the exponential of the real argument with an e-folding scale l, the thickness of the viscous boundary layer.

4.4.2. THE SECOND ORDER SOLUTIONS

Substitution of the first order solutions (4.72a) - (4.72c) into the second order differential equations (4.9) to (4.11) and continuity equation (4.12) and considering only the zero frequency interaction yields

$$x_{2tt}+gz_{2a}+\frac{p_{2a}}{\rho}-\nu\nabla^2 x_{2t}=\int_{-\pi}^{+\pi}\int_{-\pi}^{+\pi}\int_{-\infty}^{+\infty}\left|A_{11}^{VF}e^{2|k|c}+A_{22}^{VF}e^{|k|c+c/l}\right.$$
$$\left.+A_{33}^{VF}e^{2c/l}\right|e^{ik(\gamma_1 a+\gamma_2 b)}\,d\xi_1(\omega,\theta)\,d\xi_1(-\omega,\theta') \tag{4.73}$$

$$y_{2tt}+gz_{2b}+\frac{p_{2b}}{\rho}-\nu\nabla^2 y_{2t}=\int_{-\pi}^{+\pi}\int_{-\pi}^{+\pi}\int_{-\infty}^{+\infty}\left|B_{11}^{VF}e^{2|k|c}+B_{22}^{VF}e^{|k|c+c/l}+\right.$$
$$\left.B_{33}^{VF}e^{2c/l}\right|e^{ik(\gamma_1 a+\gamma_2 b)}\,d\xi_1(\omega,\theta)\,d\xi_1(-\omega,\theta') \tag{4.74}$$

$$z_{2tt}+gz_{2c}+\frac{p_{2c}}{\rho}-\nu\nabla^2 z_{2t}=\int_{-\pi}^{+\pi}\int_{-\pi}^{+\pi}\int_{-\infty}^{+\infty}\left|C_{11}^{VF}e^{2|k|c}+C_{22}^{VF}e^{|k|c+c/l}\right.$$
$$\left.+C_{33}^{VF}e^{2c/l}\right|e^{ik(\gamma_1 a+\gamma_2 b)}\,d\xi_1(\omega,\theta)\,d\xi_1(-\omega,\theta') \tag{4.75}$$

$$x_{2a}+y_{2b}+z_{2c}=\int_{-\pi}^{+\pi}\int_{-\pi}^{+\pi}\int_{-\infty}^{+\infty}\left|D_{11}^{VF}e^{2|k|c}+D_{22}^{VF}e^{|k|c+c/l}+D_{33}^{VF}e^{2c/l}\right|$$
$$e^{ik(\gamma_1 a+\gamma_2 b)}\,d\xi_1(\omega,\theta)\,d\xi_1(-\omega,\theta') \tag{4.76}$$

where

$$A_{11}^{VF}=(1+cos(\theta-\theta'))\frac{k\omega^2}{2}\left|i\gamma_1-k^2l^2\gamma_3\left(1+cos(\theta-\theta')\right)\right|$$

$$A_{22}^{VF}=k|k|l\omega^2\left|\gamma_3\left(cos\frac{c}{l}-sin\frac{c}{l}\right)(1+cos(\theta-\theta'))-i\gamma_1\left(cos\frac{c}{l}+sin\frac{c}{l}\right)\right|+$$

$$k^3l^2\omega^2\Bigg(\gamma_3\Big|cos\frac{c}{l}(1+3cos(\theta-\theta'))+\frac{|k|l}{2}(2cos^2(\theta-\theta')+3cos(\theta-\theta')-1)$$

$$\left(cos\frac{c}{l}+sin\frac{c}{l}\right)-\frac{k^2l^2}{2}sin\frac{c}{l}(1-cos(\theta-\theta'))\Big|-i\gamma_1\Big|sin\frac{c}{l}cos(\theta-\theta')$$

$$-\frac{|k|l}{2}(cos(\theta-\theta')-1)\left(cos\frac{c}{l}-sin\frac{c}{l}\right)-\frac{k^2l^2}{2}cos\frac{c}{l}(1-cos(\theta-\theta'))\Big|\Bigg)$$

$$A_{33}^{VF} = -k^3 l^2 \omega^2 \Big(\gamma_3 \big| 1 + 2\cos(\theta-\theta') + k^2 l^2 (\cos^2(\theta-\theta') - \cos(\theta-\theta')) \big| +$$

$$i\gamma_1 \big| 2 - \cos(\theta-\theta') - \frac{k^2 l^2}{2}(1 - 2\cos(\theta-\theta')) \big| \Big)$$

$$B_{11}^{VF} = (1+\cos(\theta-\theta'))\frac{k\omega^2}{2} \big| i\gamma_2 - k^2 l^2 \gamma_4 \Big(1 + \cos(\theta-\theta') biggrp \big|$$

$$B_{22}^{VF} = k|k| l\omega^2 \big| \gamma_4 (\cos\frac{c}{l} - \sin\frac{c}{l})(1+\cos(\theta-\theta')) - i\gamma_2 (\cos\frac{c}{l} + \sin\frac{c}{l}) \big| +$$

$$k^3 l^2 \omega^2 \Big(\gamma_4 \big| \cos\frac{c}{l}(1+3\cos(\theta-\theta')) + \frac{|k|l}{2}(2\cos^2(\theta-\theta') - \cos(\theta-\theta') + 1)$$

$$(\cos\frac{c}{l} + \sin\frac{c}{l}) - \frac{k^2 l^2}{2}\sin\frac{c}{l}(1-\cos(\theta-\theta')) \big| - i\gamma_2 \big| \sin\frac{c}{l}\cos(\theta-\theta') - \frac{|k|l}{2}(1-\cos(\theta-\theta'))$$

$$(\cos\frac{c}{l} - \sin\frac{c}{l}) - \frac{k^2 l^2}{2}\cos\frac{c}{l}(1-\cos(\theta-\theta')) \big| \Big)$$

$$B_{33}^{VF} = -k^3 l^2 \omega^2 \Big(\gamma_4 \big| 1 + 2\cos(\theta-\theta') + k^2 l^2 (\cos^2(\theta-\theta') - \cos(\theta-\theta')) \big| +$$

$$i\gamma_2 \big| 2 - \cos(\theta-\theta') - \frac{k^2 l^2}{2}(1 - 2\cos(\theta-\theta') \big| \Big)$$

$$C_{11}^{VF} = |k|\omega^2 (1+\cos(\theta-\theta'))$$

$$C_{22}^{VF} = -2|k|\omega^2 \cos\frac{c}{l}\cos(\theta-\theta') + k^2 l\omega^2 (\cos\frac{c}{l} + \sin\frac{c}{l})(\cos(\theta-\theta') - 1) +$$

$$k^2 |k| l^2 \omega^2 \Big(-\sin\frac{c}{l}(1-2\cos(\theta-\theta')) - |k| l (\cos\frac{c}{l} - \sin\frac{c}{l})(\cos^2(\theta-\theta') -$$

$$3\cos(\theta-\theta') + 1) + k^2 l^2 \cos\frac{c}{l}(\cos^2(\theta-\theta') - \cos(\theta-\theta') + 1) \Big)$$

$$C_{33}^{VF} = k^4 l^3 \omega^2 \Big(1 - 4\cos(\theta-\theta') \Big)$$

$$D_{11}^{VF}=k^2(1+cos(\theta-\theta'))^2/2$$

$$D_{22}^{VF}=-2k^2cos\frac{c}{l}cos(\theta-\theta')-k^2|k|l(cos\frac{c}{l}+sin\frac{c}{l})(cos^2(\theta-\theta')+1)-$$
$$k^4l^2sin\frac{c}{l}cos(\theta-\theta')$$

$$D_{33}^{VF}=k^4l^2\left(1+cos^2(\theta-\theta')\right)$$

$$\gamma_1=(cos\theta-cos\theta')$$

$$\gamma_2=(sin\theta-sin\theta')$$

$$\gamma_3=(cos\theta+cos\theta')$$

$$\gamma_4=(sin\theta+sin\theta'). \qquad (4.77)$$

Note that kl is a small parameter and the terms with bold parenthesis are higher order in kl. Therefore these terms are small but we will keep them for now in order to solve the following fourth order differential equations by balancing both sides of the equations. The right hand sides of equations (4.73) - (4.76) are independent of time. If we consider the possibility of unaccelerated motion (i.e., steady state), we can neglect the acceleration terms in (4.73) - (4.76). In order to solve these momentum equations we follow the same procedure as in section (4.4.1). An equation for u_2 (i.e., x_{2l}) alone can be derived by adding $\frac{\partial}{\partial b}[\frac{\partial}{\partial b}(4.73)-\frac{\partial}{\partial a}(4.74)]$ and $\frac{\partial}{\partial c}[\frac{\partial}{\partial c}(4.73)-\frac{\partial}{\partial a}(4.75)]$ and using $\frac{\partial^2}{\partial a\partial t}(4.76)$ to replace $v_{ab}+w_{ac}$. The result is

$$\nu\nabla^4u_2=\int_{-\pi}^{+\pi}\int_{-\pi}^{+\pi}\int_{-\infty}^{+\infty}|A_1^{VF}e^{2|k|c}+A_2^{VF}e^{|k|c+c/l}+A_3^{VF}e^{2c/l}|$$

$$e^{ik(\gamma_1a+\gamma_2b)}\,d\xi_1(\omega,\theta)\,d\xi_1(-\omega,\theta'). \qquad (4.78)$$

Similarly, for w_2 equation

$$\nu\nabla^4 w_2 = \int_{-\pi}^{+\pi}\int_{-\pi}^{+\pi}\int_{-\infty}^{+\infty} \left| C_2^{VF} e^{|k|c+c/l} + C_3^{VF} e^{2c/l} \right| e^{ik(\gamma_1 a+\gamma_2 b)} \, d\xi_1(\omega,\theta)\, d\xi_1(-\omega,\theta') \tag{4.79}$$

where

$$A_1^{VF} = k^5 l^2 \omega^2 (1+\cos(\theta-\theta'))^3 \gamma_3$$

$$A_2^{VF} = 2\omega^2 k \Big(\gamma_3 \left| |k|/l (\cos\tfrac{c}{l} + \sin\tfrac{c}{l})(1+\cos(\theta-\theta')) + k^2 \sin\tfrac{c}{l}(5\cos(\theta-\theta')+3) \right|$$
$$+ i\gamma_1 \left| |k|/l (\cos\tfrac{c}{l} - \sin\tfrac{c}{l})(1-\cos(\theta-\theta')) + k^2 \cos\tfrac{c}{l}(\cos(\theta-\theta')+1) \right| \Big)$$
$$-2k^3|k|l\omega^2 \Big(\gamma_3 (\cos\tfrac{c}{l} - \sin\tfrac{c}{l})(1+3\cos(\theta-\theta')+2\cos^2(\theta-\theta')) -$$
$$i\gamma_1 (\cos\tfrac{c}{l} + \sin\tfrac{c}{l})(3\cos(\theta-\theta')-1) \Big)$$

$$A_3^{VF} = 4k^3\omega^2 \left| \gamma_3 (1+2\cos(\theta-\theta')) - i\gamma_1 (2-\cos(\theta-\theta')) \right|$$

$$C_2^{VF} = 4k^2|k|\omega^2 \cos\tfrac{c}{l}(1-\cos(\theta-\theta'))^2 + 4k^4 l\omega^2 (\cos(\theta-\theta') - \cos^2(\theta-\theta'))$$
$$(\cos\tfrac{c}{l} + \sin\tfrac{c}{l}) - 4k^4|k|l^2\omega^2 (2\cos^2(\theta-\theta')3\cos(\theta-\theta')+1)\sin\tfrac{c}{l}$$

$$C_3^{VF} = -4k^4 l\omega^2 \left| \cos^2(\theta-\theta') - 3\cos(\theta-\theta')+2 \right|.$$

(4.80)

Equations (4.78) and (4.79) are valid in the whole fluid and determine the wave induced drift current. These inhomogeneous differential equations can be solved by applying the technique of undetermined coefficients. Particular solutions to these equations are

$$u_2^{VFp} = \int_{-\pi}^{+\pi}\int_{-\pi}^{+\pi}\int_{-\infty}^{+\infty} \frac{\omega k}{2} (A^{VF'}\gamma_3 + iB^{VF'}\gamma_1) e^{ik(\gamma_1 a+\gamma_2 b)} d\xi_1(\omega,\theta)\, d\xi_1(-\omega,\theta') \tag{4.81}$$

$$w_2^{VFp} = \int_{-\pi}^{+\pi}\int_{-\pi}^{+\pi}\int_{-\infty}^{+\infty} -2k^2 l^2 \omega C^{VF'} e^{ik(\gamma_1 a+\gamma_2 b)}\, d\xi_1(\omega,\theta)\, d\xi_1(-\omega,\theta') \tag{4.82}$$

Note that the particular solution for the vertical velocity w_2^{VFp} (4.82) is smaller than the horizontal velocity u_2^{VFp} (4.81) by an order of $(kl)^2$. Substituting (4.81) and (4.82) into the continuity equation differentiated with respect to t (i.e, $\frac{\partial}{\partial t}$(4.76)) gives

$$v_2^{VFp}=\int_{-\pi}^{+\pi}\int_{-\pi}^{+\pi}\int_{-\infty}^{+\infty}\frac{\omega k}{2}(A^{VF'}\gamma_4+iB^{VF'}\gamma_2)e^{ik(\gamma_1 a+\gamma_2 b)}\,d\xi_1(\omega,\theta)\,d\xi_1(-\omega,\theta') \tag{4.83}$$

where

$$\begin{aligned}
A^{VF'}&=(1+cos(\theta-\theta'))e^{2|k|c}-2|k|l(1+cos(\theta-\theta'))\,(cos\tfrac{c}{l}+sin\tfrac{c}{l})e^{|k|c+c/l}\\
&\quad+k^2l^2\left(2(1-cos(\theta-\theta'))sin\tfrac{c}{l}\,e^{|k|c+c/l}+(1+2cos(\theta-\theta'))e^{2c/l}\right)\\
B^{VF'}&=-2|k|l(1-cos(\theta-\theta'))\,(cos\tfrac{c}{l}-sin\tfrac{c}{l})e^{|k|c+c/l}\\
&\quad+k^2l^2\left(2(3-5cos(\theta-\theta'))cos\tfrac{c}{l}e^{|k|c+c/l}-(2-cos(\theta-\theta'))\,e^{2c/l}\right)\\
C^{VF'}&=\{|k|(1-cos(\theta-\theta'))^2cos\tfrac{c}{l}-k^2l(cos\tfrac{c}{l}+sin\tfrac{c}{l})(3cos^2(\theta-\theta')-4cos(\theta-\theta')+2)\\
&\quad-l^2k^2|k|sin\tfrac{c}{l}(2cos^3(\theta-\theta')-12cos^2(\theta-\theta')+13cos(\theta-\theta')-2)\}e^{|k|c+c/l}\\
&\quad+\frac{k^2l}{4}(cos^2(\theta-\theta')-3cos(\theta-\theta')+2)e^{2c/l}.
\end{aligned} \tag{4.84}$$

If we set $\nu=0$ then u_2^{VFp}, v_2^{VFp} in (4.81), (4.83) reduce to the inviscid fluid solutions given by (3.63), (3.61). Also the vertical velocity w_2^{VFp} given in (4.82) becomes zero when ν is set to zero. The viscosity causes solutions to differ greatly from inviscid solutions in the thin surface layer of thickness l. We will subsequently refer to this as the vorticity layer. Below the vorticity layer the viscous particular solutions are effectively identical to the inviscid solutions.

Weber (1983b) and Chang (1969) did not consider the terms with form $(.)e^{2c/l}$ (4.84) in their solutions. Although these terms are small compared to the $(.)e^{|k|c+c/l}$ terms, the vertical gradient of the $(.)e^{2c/l}$ terms near the surface is the same magnitude as the $(.)e^{|k|c+c/l}$ terms (i.e., $O(kl)$). Therefore, neglecting these terms from the solutions will introduce an error near the surface of the flow when the solutions are matched to the surface boundary conditions.

The above solutions satisfy the boundary condition at depth i.e., wave amplitude goes to zero as $c \to -\infty$. We must also ensure that the solutions (4.81) - (4.83) satisfy the second order surface boundary conditions (4.37) - (4.39). The zero-frequency second-order motion is driven by interactions between first-order viscous wave solutions. We therefore consider the case with no applied wind stress in the second order boundary conditions (4.37) - (4.39). The second order surface boundary conditions ($c=0$) are:

$$\rho\nu[x_{2tc}+z_{2ta}+x_{1tc}x_{1a}-x_{1ta}x_{1c}+x_{1tc}y_{1b}-x_{1tb}y_{1c}+z_{1ta}z_{1c}-z_{1tc}z_{1a}+ z_{1ta}y_{1b}-z_{1tb}y_{1a}-x_{1tb}z_{1b}-y_{1ta}z_{1b}-2x_{1ta}z_{1a}]+p_1z_{1a}\,|_{c=0}=0 \tag{4.85}$$

$$\rho\nu[y_{2tc}+z_{2tb}+y_{1tc}y_{1b}-y_{1tb}x_{1c}+y_{1tc}x_{1a}-y_{1ta}x_{1c}+z_{1tb}z_{1c}-z_{1tc}z_{1b}+ z_{1tb}x_{1a}-z_{1ta}x_{1b}-x_{1tb}z_{1a}-y_{1ta}z_{1a}-2y_{1tb}z_{1b}]+p_1z_{1b}\,|_{c=0}=0 \tag{4.86}$$

$$-p_2+\rho\nu[2z_{2tc}+2z_{1tc}x_{1a}+2z_{1tc}y_{1b}-2z_{1tb}y_{1c}-2z_{1ta}x_{1c}-x_{1tc}z_{1a}-z_{1ta}z_{1a}- y_{1tc}z_{1b}-z_{1tb}z_{1b}]\,|_{c=0}=0. \tag{4.87}$$

Equations (4.85) to (4.87) are identical to Weber's (1985) second-order boundary conditions without any wind forcing. Substituting the first-order solutions (4.72) into the second-order surface boundary conditions

(4.85) and (4.86) and considering only zero frequency interactions one finds

$$u_{2c}+w_{2a}|_{c=0} = \int_{-\pi}^{+\pi}\int_{-\pi}^{+\pi}\int_{-\infty}^{+\infty} |(-2k|k|+k^3 l)\,\omega\gamma_3 - ik^3 l\omega\gamma_1$$

$$-ik^3|k|l^2\omega\gamma_1(1+cos(\theta-\theta'))/2)|e^{ik(\gamma_1 a+\gamma_2 b)}d\xi_1(\omega,\theta)d\xi_1(-\omega,\theta') \quad (4.88)$$

$$v_{2c}+w_{2b}|_{c=0} = \int_{-\pi}^{+\pi}\int_{-\pi}^{+\pi}\int_{-\infty}^{+\infty} |(-2k|k|+k^3 l)\,\omega\gamma_4 - ik^3 l\omega\gamma_2$$

$$-ik^3|k|l^2\omega\gamma_2(1+cos(\theta-\theta'))/2)|e^{ik(\gamma_1 a+\gamma_2 b)}d\xi_1(\omega,\theta)d\xi_1(-\omega,\theta'). \quad (4.89)$$

The vertical boundary condition (4.87) does not provide any useful information because $p_2=0$ at the surface. We still need a surface boundary condition for the vertical velocity. We consider that the vertical drift velocity must be zero at the surface (see also Weber, 1985) i.e.,

$$w_2=0 \quad at \quad c=0 \quad (4.90)$$

Since $w_2=0$ at the surface, (4.88) reduces to

$$u_{2c}|_{c=0} = \int_{-\pi}^{+\pi}\int_{-\pi}^{+\pi}\int_{-\infty}^{+\infty} [(-2k|k|+k^3 l)\,\omega\gamma_3 - ik^3 l\omega\gamma_1$$

$$-ik^3|k|l^2\omega\gamma_1(1+cos(\theta-\theta'))/2)|e^{ik(\gamma_1 a+\gamma_2 b)}d\xi_1(\omega,\theta)d\xi_1(-\omega,\theta') \quad (4.91)$$

and (4.89) becomes,

$$v_{2c}|_{c=0} = \int_{-\pi}^{+\pi}\int_{-\pi}^{+\pi}\int_{-\infty}^{+\infty} |(-2k|k|+k^3 l)\,\omega\gamma_4 - ik^3 l\omega\gamma_2$$

$$-ik^3|k|l^2\omega\gamma_2(1+cos(\theta-\theta'))/2)|e^{ik(\gamma_1 a+\gamma_2 b)}d\xi_1(\omega,\theta)d\xi_1(-\omega,\theta'). \quad (4.92)$$

The particular solutions (4.81) - (4.83) do not satisfy the above boundary conditions at the free surface. Accordingly, the complete solution must also include solutions of the homogeneous versions of the equations (4.78) - (4.79). The homogeneous equations are

$$\nabla^4 u_2^{VFh}=0 \tag{4.93}$$

$$\nabla^4 w_2^{VFh}=0 \tag{4.94}$$

and the time derivative of the homogeneous version of the continuity equation (4.76) is

$$u_{2a}^{VFh}+v_{2b}^{VFh}+w_{2c}^{VFh}=0\,. \tag{4.95}$$

Solution for v_2^{VFh} is obtained by substituting the solutions of (4.93) and (4.94) into the equation (4.95). The homogeneous solutions must also satisfy the lower boundary condition

$$\begin{aligned} u_2^{VFh}&=0 \quad c\to-\infty \\ v_2^{VFh}&=0 \quad c\to-\infty \\ w_2^{VFh}&=0 \quad c\to-\infty\,. \end{aligned} \tag{4.96}$$

The solutions of the equations (4.93) and (4.94) involve finding the roots. It is clear that each equation has four roots of which two of them are

$$m_1=|2k\sin\frac{\theta-\theta'}{2}|$$

$$m_2=-|2k\sin\frac{\theta-\theta'}{2}|.$$

The other two roots are repeated roots. The negative roots are unacceptable because of the boundary conditions (4.96). Therefore, we can write the homogeneous solutions to the equations (4.93) and (4.94)

$$u_2^{VFh}=\int_{-\pi}^{+\pi}\int_{-\pi}^{+\pi}\int_{-\infty}^{+\infty}\left[(d\xi_{2x}+i\,d\xi_{2x}')\,e^{2k\phi c}+c\,(d\xi_{3x}+i\,d\xi_{3x}')\,e^{2k\phi c}\right]e^{ik(\gamma_1 a+\gamma_2 b)} \tag{4.97}$$

$$w_2^{VFh}=\int_{-\pi}^{+\pi}\int_{-\pi}^{+\pi}\int_{-\infty}^{+\infty}\left[d\xi_{2z}\,e^{2k\phi c}+c\,d\xi_{3z}\,e^{2k\phi c}\right]e^{ik(\gamma_1 a+\gamma_2 b)}. \tag{4.98}$$

Substituting (4.97) and (4.98) into (4.95) gives

$$v_2^{VFh}=\int_{-\pi}^{+\pi}\int_{-\pi}^{+\pi}\int_{-\infty}^{+\infty}-\frac{(\cos\theta-\cos\theta')}{(\sin\theta-\sin\theta')}\left[(d\xi_{2x}+i\,d\xi_{2x}')+c\,(d\xi_{3x}+i\,d\xi_{3x}')\right]e^{2k\phi c}$$

$$e^{ik(\gamma_1 a+\gamma_2 b)}+\int_{-\pi}^{+\pi}\int_{-\pi}^{+\pi}\int_{-\infty}^{+\infty}\frac{i}{(\sin\theta-\sin\theta')}\left[2\phi\,(d\xi_{2z}+c\,d\xi_{3z})+d\xi_{3z}/k\right]e^{2k\phi c}$$

$$e^{ik(\gamma_1 a+\gamma_2 b)} \tag{4.99}$$

where

$$\phi=\left|\sin\frac{\theta-\theta'}{2}\right|. \tag{4.100}$$

The unknown functions for the second order homogeneous solutions $d\xi_{2x}$, $d\xi_{2x}'$, $d\xi_{2z}$, $d\xi_{3x}$, $d\xi_{3x}'$, $d\xi_{2z}$, and $d\xi_{3z}$ are to be determined from the surface boundary conditions. We noticed that some of these constants are not independent. By taking $\frac{\partial}{\partial a}(4.75)-\frac{\partial}{\partial c}(4.73)]$ of the homogeneous versions of the second order momentum equations (4.73) and (4.75) and considering steady state one obtains

$$\nabla^2 u_{2c}^{VFh}-\nabla^2 w_{2a}^{VFh}=0$$

Substituting (4.97) and (4.98) for u_2^{VFh} and w_2^{VFh} into the above equation and equating the real and imaginary parts to zero gives

$$d\xi_{3x}=0$$

$$d\xi_{3x}'=-|\sin\frac{\theta+\theta'}{2}|d\xi_{3z}. \qquad (4.101a)$$

To determine the remaining constants we substitute the resulting expressions for $u_2^{VF}=u_2^{VFp}+u_2^{VFh}$, $v_2^{VF}=v_2^{VFp}+v_2^{VFh}$, and $w_2^{VF}=w_2^{VFp}+w_2^{VFh}$ into surface boundary conditions (4.91), (4.92), (4.90) and solve real and imaginary parts to give

$$d\xi_{2x}=\frac{-k\omega\gamma_3(1-\cos(\theta-\theta'))}{2\phi}d\xi_1(\omega,\theta)d\xi_1(-\omega,\theta')$$

$$d\xi_{2x}'=\omega k\gamma_1\left[\frac{F}{4\phi}-\frac{G}{8\phi}\right]d\xi_1(\omega,\theta)d\xi_1(-\omega,\theta')$$

$$d\xi_{3x}'=\omega k^2\gamma_1\frac{G}{4}d\xi_1(\omega,\theta)d\xi_1(-\omega,\theta')$$

$$d\xi_{2z}=2k^3l^2\omega(1-\cos(\theta-\theta'))^2\,d\xi_1(\omega,\theta)d\xi_1(-\omega,\theta')$$

$$d\xi_{3z}=\frac{\omega k^2}{2}\phi G\,d\xi_1(\omega,\theta)d\xi_1(-\omega,\theta')$$

where

$$F=kl(6\cos(\theta-\theta')-2)-k^2l^2(3-13\cos(\theta-\theta'))$$

and

$$G=kl(6\cos(\theta-\theta')-2)-k^2l^2(4\cos^2(\theta-\theta')-21\cos(\theta-\theta')+7) \qquad (4.101b)$$

Therefore, the total solutions satisfying the boundary conditions at the surface and at great depth are:

$$u_2^{VF} = u_2^{VFp} + u_2^{VFh}$$

$$u_2^{VF} = \int_{-\pi}^{+\pi}\int_{-\pi}^{+\pi}\int_{-\infty}^{+\infty} \frac{\omega k}{2}(A^{VF}\gamma_3 + iB^{VF}\gamma_1)\, e^{ik(\gamma_1 a+\gamma_2 b)}\, d\xi_1(\omega,\theta)\, d\xi_1(-\omega,\theta') \tag{4.102}$$

$$v_2^{VF} = v_2^{VFp} + v_2^{VFh}$$

$$v_2^{VF} = \int_{-\pi}^{+\pi}\int_{-\pi}^{+\pi}\int_{-\infty}^{+\infty} \frac{\omega k}{2}(A^{VF}\gamma_4 + iB^{VF}\gamma_2)\, e^{ik(\gamma_1 a+\gamma_2 b)}\, d\xi_1(\omega,\theta)\, d\xi_1(-\omega,\theta') \tag{4.103}$$

$$w_2^{VF} = w_2^{VFp} + w_2^{VFh}$$

$$w_2^{VF} = \int_{-\pi}^{+\pi}\int_{-\pi}^{+\pi}\int_{-\infty}^{+\infty} \omega k C^{VF}\, e^{ik(\gamma_1 a+\gamma_2 b)}\, d\xi_1(\omega,\theta)\, d\xi_1(-\omega,\theta') \tag{4.104}$$

where

$$A^{VF} = (1+cos(\theta-\theta'))\, e^{2|k|c} - 2|k|l\,(1+cos(\theta-\theta'))\,(cos\tfrac{c}{l}+sin\tfrac{c}{l})\, e^{|k|c+c/l} - (1-$$

$$cos(\theta-\theta'))\frac{e^{2k\phi c}}{\phi} + 2k^2l^2(1-cos(\theta-\theta'))\, sin\tfrac{c}{l}\, e^{|k|c+c/l} + k^2l^2\,(1+2cos(\theta-\theta'))\, e^{2c/l},$$

$$B^{VF} = -2|k|l\,(1-cos(\theta-\theta'))\,(cos\tfrac{c}{l}-sin\tfrac{c}{l})\, e^{|k|c+c/l} + [\,(F-G/2)/(2\phi) + ckG/2\,]$$

$$e^{2k\phi c} + 2k^2l^2(3-5cos(\theta-\theta'))\, cos\tfrac{c}{l}\, e^{|k|c+c/l} - k^2l^2\,(2-cos(\theta-\theta'))\, e^{2c/l},$$

$$C^{VF} = c\phi kG/2\, e^{2k\phi c}$$

$$+ 2k^2l^2[\,-(1-cos(\theta-\theta'))^2 cos\tfrac{c}{l}\, e^{|k|c+c/l} + (1-cos(\theta-\theta'))^2 e^{2k\phi c}\,], \tag{4.105}$$

and F, G are given by (4.101b). The above solutions (4.102 - 4.104) represent spatially varying horizontal and vertical shears in 3-D velocity field. Note that at first order in kl, the solution for vertical velocity does not equal zero.

Substituting $\theta=\theta'=0$ and neglecting k^2l^2 terms (4.102) reduces to

$$u_2^{VF}=\int_{-\infty}^{+\infty}\frac{\omega k}{2}|4e^{2|k|c}-8|k|l\,(\cos\frac{c}{l}+\sin\frac{c}{l})e^{|k|c+c/l}|\,d\xi_1(\omega,\theta)\,d\xi_1(-\omega,\theta').$$

(4.106)

Substituting for the wave amplitude from (3.66) and using the approximation $|k| \ll 1/l$ (as used by Weber (1983b)), equation (4.106) reduces to

$$u_2^{VF}=A_o^2\,\omega k|\,e^{2|k|c}-2|k|l\,(\cos\frac{c}{l}+\sin\frac{c}{l})e^{c/l}|.$$

(4.107)

Equation (4.107) is Weber's solution (1983b, eqn. (5.2)). Note also that (4.102) and the particular solution (4.81) are identical for $\theta=\theta'=0$. Thus for $\theta=\theta'=0$ the particular solution satisfies the boundary condition automatically, no homogeneous solution is therefore necessary to satisfy the boundary condition (see also Weber (1983b)). However, if we consider a random wave field of waves interacting at arbitrary angles then the particular solutions do not satisfy the surface boundary conditions. In this case we need homogeneous solutions to satisfy the surface boundary condition.

Thus inclusion of viscosity leads to solutions which constitute a random field of mass transport velocity both in the horizontal and vertical directions. Comparing the viscous solutions (4.102) and (4.103) with the corresponding inviscid solutions (3.63) and (3.61) one finds that the coefficients of $e^{2|k|c}$ in u_2^{VF} and v_2^{VF} (4.102, 4.103) (i.e., inviscid part of the viscous solutions) are identical to inviscid solutions (3.63, 3.61). The additional terms in (4.102) and (4.103) arise from the inclusion of the viscosity. These additional terms reduce the magnitude of the zero frequency second order velocity from that of the inviscid solutions. In

the limiting case of viscosity tending to zero, the viscous velocities (4.102, 4.103) do not reduce to inviscid solutions. Specifically, the homogeneous part of the horizontal solutions u_2^{VFh}, v_2^{VFh} (e.g., $d\xi_{2x}$, 4.101b) are nonzero for the zero viscosity (see also Weber (1985)). This must be due to applied external surface forcing which acts through the first order solutions to cause this nonzero velocity even when viscosity is zero. In the following section it will be shown that, in the absence of the applied external forcing (i.e., decaying wave case), the viscous solutions reduce to inviscid solutions as the viscosity goes to zero.

The vertical component of the mass transport velocity $(w_2^{VFp}+w_2^{VFh})$, goes to zero as $\nu \to 0$. It is also worth mentioning here that the dominant contribution in the total vertical solution is due to the homogeneous part w_2^{VFh} of the solution ($c\phi kG/2$, 4.105) which has a magnitude of order kl. The particular part w_2^{VFp} is of order $(kl)^2$ but is required to satisfy the surface boundary condition (4.90) for the vertical velocity. Neglecting w_2^{VFp} will cause $O(k^2l^2)$ vertical velocity at the surface ($z=0$). Later, in chapter 6, it will be shown by numerical integration that the vertical diffusion is almost totally due to the homogeneous part w_2^{VFh} of the solution.

The equations (4.102-4.105) represent solutions of the equations of motion up to second order in a perturbation expansion. As mentioned in the beginning of this chapter, these solutions have two small parameters in them: (1) perturbation expansion parameter ε and (2) $\varepsilon_1 (=kl)$. The perturbation expansion parameter ε $(=A_o/\lambda)$ is the wave slope (i.e., ratio of the wave amplitude to the wave length). For surface gravity waves, LeBlond and Mysak (1978) estimated the maximum value of $\varepsilon \approx 1/14 \approx 0.07$. An upper limit of 0.1 for ε is also reported by Kinsman (1984) from observations. It is conceivable that the lower limit of ε may be anything between 0.1 and zero. Now to estimate the second small parameter, $\varepsilon_1=kl$, we know that ε_1 is related to the eddy viscosity through

the viscous length scale $l=\sqrt{2\nu/\omega}$. Viscosity in the ocean has a large range having a lower limit of molecular viscosity $(1.0\times10^{-6})m^2/s$. For a typical large value of eddy-viscosity $\nu=(1.0\times10^{-2})m^2/s$ and the frequency range ω = (0.3-1.0) s^{-1}, k and l take the values from (0.009 - 0.1) m^{-1} and (0.26 -0.14) m respectively. These give a range of values for ε_1= (0.002 - 0.014). Having found the ranges of the two small parameters ε and $\varepsilon_1(=kl)$ it is important to realize that terms of $O(\varepsilon^2\varepsilon_1^2)$ may sometimes be of same order as $O(\varepsilon^3\varepsilon_1)$. The point we are trying to make is that if the third order perturbation solutions happen to contain terms of $O(\varepsilon_1^0)$ and $O(\varepsilon_1)$ then these terms may be of same order of magnitude as some terms of second order solution. In that case the third order perturbation solutions must be included. This is specially true for second order vertical solution (4.104) where the dominant terms in the solution are of $O(\varepsilon_1)$ and $O(\varepsilon_1^2)$. Nevertheless, we did not attempt to solve the third order perturbation equations of motion, therefore, the order of ε_1 in the order ε^3 vertical velocity field solution is unknown. This remains to be explored in the future.

Providing eddy-viscosity and wave amplitude are such that $\varepsilon^3\varepsilon_1 < \varepsilon^2\varepsilon_1^2$ i.e., $\varepsilon < \varepsilon_1$, then we can be assured that we don't need to consider $O(\varepsilon^3)$ solutions. Since $\varepsilon < \varepsilon_1$ is not generally true (except for very small amplitude waves and large eddy-viscosity) it follows that our solutions are not necessarily accurate up to $O(\varepsilon^2\varepsilon_1^2)$. Thus we retain only terms up to $O(\varepsilon^2\varepsilon_1)$ when calculating eddy-diffusivities. The $O(\varepsilon^2\varepsilon_1^2)$ terms in equations (4.105) have boxes drawn around them for ease of identification. However, we do not discard them totally since they would be useful should the $O(\varepsilon^3)$ solutions ever be explored in the future. Note that $O(\varepsilon^2\varepsilon_1)$ terms (i.e., $c\phi kG/2e^{2k\phi c}$ (4.105)) still have vertical zero frequency velocities.

To visualize the spatial behaviour of these solutions,

$u_2^{VF}, v_2^{VF}, w_2^{VF}$ (equations 4.102-4.104) are plotted as functions of a, b, c. Figure 4.2 shows the plot of the mass transport velocity due to two primary waves of frequency ω=1.43 rad/s each interacting at an angle $\pm 45^{0}$ with the a-axis. The arrow corresponding to u, v components of velocity is seen to be sheared in the horizontal plane as observed by the alternating direction of the arrows in the top plot. The direction of this random shearing changes as the angle of interaction changes. The motion in the vertical plane changes direction with the depth as shown in the lower plot.

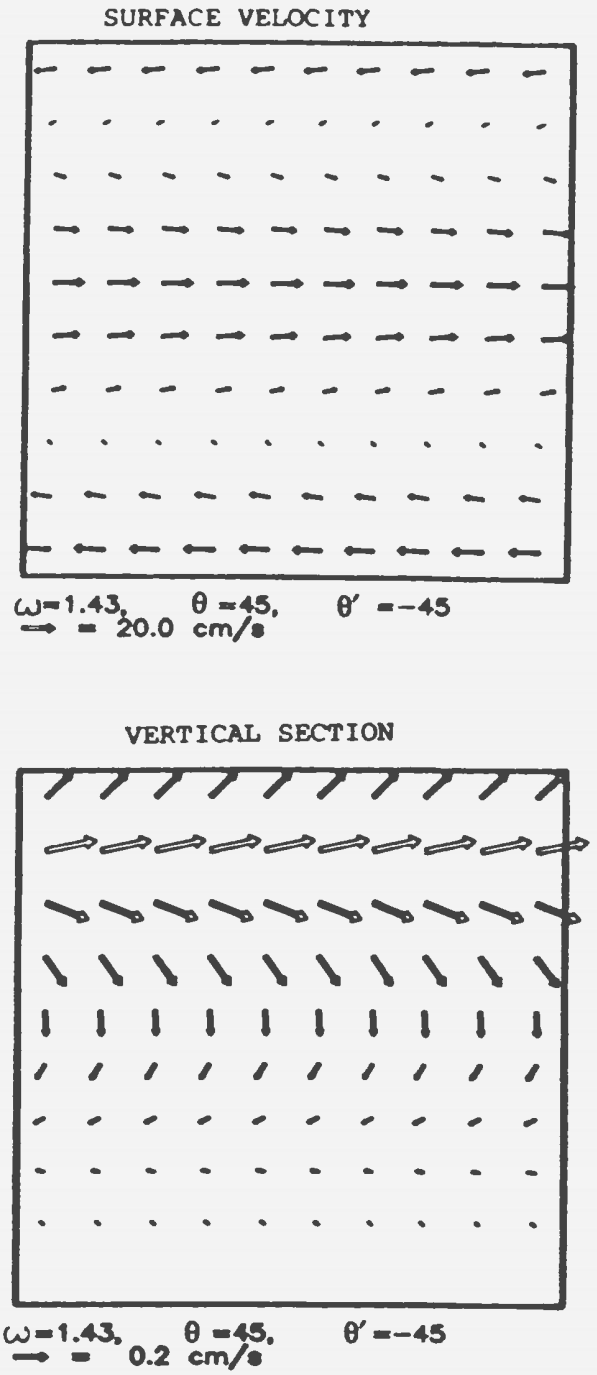

Figure 4-2: Interaction of two primary waves to give a horizontally and vertically sheared mean flow. The arrows show the magnitude and direction of current as a function of position (a,b,c). (a) A horizontal section through the surface c=0. Plot shows u_2^{VF} and v_2^{VF} velocities are sheared in the horizontal plane. (b) A vertical section in the (b,c) plane. Plot shows v_2^{VF} and w_2^{VF} are sheared with respect to b and c. The parameters used are $\omega = 1.43\ s^{-1}$, $\theta = 45^o$, $\theta' = -45^o$, a=b=20 m and $\nu = 0.01\ m^2/s$

4.5. SOLUTION FOR DECAYING VISCOUS GRAVITY WAVES

In this section we consider that the waves are established at time $t=0$ and that no further energy is supplied. Then, owing to viscous dissipation, the waves will attenuate in amplitude and eventually the whole motion will go to zero. The governing equations (4.1) to (4.3) and the continuity equation (3.6) remain unchanged from the nondecaying viscous wave problem.

4.5.1. FIRST ORDER SOLUTIONS

The first order momentum and continuity equations are given by (4.5) to (4.8). These equations are solved using a similar technique to that of nondecaying wave problem (section 4.4.1). Once again we will assume that spectral representations of first order solutions are given by equations (4.40)- (4.43). If there is no applied wind stress, then the general form of the first order boundary conditions (4.34) to (4.36) reduce to

$$z_{1ta}+x_{1tc}=0 \qquad (4.108)$$

$$z_{1tb}+y_{1tc}=0 \qquad (4.109)$$

$$-p_1+2\rho\nu z_{1tc}=0 \qquad (4.110)$$

$$at\ \ c=0,$$

and also

$$x_1, y_1, z_1 \ \rightarrow\ 0 \quad \text{as} \quad c \rightarrow -\infty$$

.

The surface boundary conditions for the horizontal component of the stress (4.108) and (4.109) are identical to nondecaying wave case (4.54, 4.55). The surface boundary conditions for the vertical component of

stress (4.56) was used to obtain the dispersion relation and magnitude of the applied stress τ_3'. Therefore, the relations (4.61) to (4.64) for the spectral density functions $d\xi_x$, $d\xi_y$, $d\xi_z$ and $d\xi_p$ are still satisfied. The vertical boundary condition (4.110) is different (zero applied stress) from that of the nondecaying wave case (4.56) in which a stress τ_3' was applied. Substituting for z_1 and p_1 from (4.42) and (4.43) into the boundary condition (4.110) and using (4.63) and (4.64) to express $d\xi_z$ and $d\xi_p$ in terms of $d\xi_1$ one obtains the following dispersion relation

$$\omega^2 = g|k| + k^2\omega^2\left(\frac{2\nu}{i\omega}\right) - \frac{2|k|\beta}{\beta^2+k^2}\left|\frac{gk^2}{\beta} + k^2\omega^2\left(\frac{2\nu}{i\omega}\right)\right|. \tag{4.111}$$

Neglecting terms that are small compared to 1 using (4.67b) and applying successive approximations gives

$$\omega^2 = \omega_0^2 - 4i\nu k^2\omega_0 + O\left(\frac{k^3}{\beta^3}\right)$$

$$= \omega_0^2(1-2ik^2l^2) + O(\ ). \tag{4.112}$$

where ω_0 is the real frequency given by (4.69a) and ν is being replaced by $l^2\omega_0/2$ using (4.71). By applying binomial expansion, ω may be written as

$$\omega = \omega_0(1-ik^2l^2) + O(kl)^4. \tag{4.113}$$

Thus the frequency consists of real and imaginary parts given by

$$\omega = \omega_R + i\,\omega_I \tag{4.114a}$$

where the real part is given by

$$\omega_R^2=\omega_o^2=g|k| \tag{4.114b}$$

and the imaginary part is given by

$$\omega_I=-k^2/2\omega_o=-2\nu k^2. \tag{4.114c}$$

Hence, for the decaying wave problem, the frequency of the waves is complex (contrary to nondecaying wave case where frequency was real in the present limit of our approximation, equation 4.69a).

Substituting (4.61) to (4.64) into (4.40) to (4.43) respectively and using equation (4.114) for ω one obtains the following first order solutions

$$x_1^{VD}=\int_{-\pi}^{+\pi}\int_{-\infty}^{+\infty}\cos\theta\,|\,e^{|k|c}-\frac{2|k|}{\beta}e^{\beta c}\,|\,e^{i(k\cos\theta a+k\sin\theta b-\omega_o t)-2\nu k^2 t}\,d\xi_1(\omega,\theta) \tag{4.115a}$$

$$y_1^{VD}=\int_{-\pi}^{+\pi}\int_{-\infty}^{+\infty}\sin\theta\,|\,e^{|k|c}-\frac{2|k|}{\beta}e^{\beta c}\,|\,e^{i(k\cos\theta a+k\sin\theta b-\omega_o t)-2\nu k^2 t}\,d\xi_1(\omega,\theta) \tag{4.115b}$$

$$z_1^{VD}=\int_{-\pi}^{+\pi}\int_{-\infty}^{+\infty}-\frac{ik}{|k|}\,|\,e^{|k|c}-\frac{2k^2}{\beta^2}e^{\beta c}\,|\,e^{i(k\cos\theta a+k\sin\theta b-\omega_o t)-2\nu k^2 t}\,d\xi_1(\omega,\theta) \tag{4.115c}$$

$$p_1^{VD}=\int_{-\pi}^{+\pi}\int_{-\infty}^{+\infty}\rho\frac{ik}{|k|}\,|\,4i|k|\nu\omega_o\,e^{|k|c}-\frac{2gk^2}{\beta^2}e^{\beta c}\,|$$

$$e^{i(k\cos\theta a+k\sin\theta b-\omega_o t)-2\nu k^2 t}\,d\xi_1(\omega,\theta). \tag{4.115d}$$

The superscript *VD* has been used to denote solutions corresponding to viscous dynamics in which the waves are decaying. The solutions decay in time due to the term $e^{-2\nu k^2 t}$. Apart from this decay term, the nondecaying wave solutions (4.72a) - (4.72c) are identical to decaying wave solutions (4.115a) - (4.115c). However, the pressure solution (4.72d) (for nondecaying wave) is different from (4.115d). Equation (4.115d) contains an additional term $-4k\rho\nu\omega_o e^{|k|c}$ (compared to 4.72d) which plays a dominant role in balancing the first order surface boundary condition for the vertical component of stress. It will be shown latter that this term and the exponentially decaying term in the first order solutions cause a significant change in the second order surface boundary conditions on the horizontal component of the stress (compared to the nondecaying wave surface boundary conditions). In the limiting case of zero viscosity, the first order solutions reduce to inviscid solutions (3.35) - (3.38).

Using (4.53) to replace $d\xi_1$ in (4.115) by $d\xi_{,x}$ one obtains

$$x_1^C = \int_{-\pi}^{+\pi}\int_{-\infty}^{+\infty} \left[e^{|k|c} - \frac{2|k|}{\beta} e^{\beta c} \right] e^{i(k\cos\theta a + k\sin\theta b - \omega_o t) - 2\nu k^2 t} d\xi_{,x}(\omega,\theta) \tag{4.116a}$$

$$y_1^C = \int_{-\pi}^{+\pi}\int_{-\infty}^{+\infty} \tan\theta \left[e^{|k|c} - \frac{2|k|}{\beta} e^{\beta c} \right] e^{i(k\cos\theta a + k\sin\theta b - \omega_o t) - 2\nu k^2 t} d\xi_{,x}(\omega,\theta) \tag{4.116b}$$

$$z_1^C = \int_{-\pi}^{+\pi}\int_{-\infty}^{+\infty} \frac{-ik}{|k|}\cos\theta \left[e^{|k|c} - \frac{2k^2}{\beta^2} e^{\beta c} \right] e^{i(k\cos\theta a + k\sin\theta b - \omega_o t) - 2\nu k^2 t} d\xi_{,x}(\omega,\theta) \tag{4.116c}$$

$$p_1^C = \int_{-\pi}^{+\pi}\int_{-\infty}^{+\infty}\int_{-\infty}^{+\infty} \frac{-i\rho}{k}\cos\theta \left[(\omega^2 - |k|g) e^{|k|c} + \frac{2gk^2|k|}{\beta^2} e^{\beta c} \right] e^{i(k\cos\theta a + k\sin\theta b - \omega_o t) - 2\nu k^2 t} d\xi_{,x}(\omega,\theta) \tag{4.116d}$$

These are the 3-D extensions of the Chang's (1969) first order solutions (superscript *C* stands for Chang). For $\theta=0$ the above solutions should reduce to Chang's (1969) first order solutions. For $\theta=0$, equation

(4.116a) and Chang's first order x_1-solution are identical. However, solutions for ${z_1}^C$ and ${p_1}^C$ (4.116c and 4.116d) do not agree with those of Chang's. In Chang's paper, first order z_1 and p_1 solutions, have a sign discrepency in front of the viscous term. Further examination shows that due to this sign discrepency, Chang's first order solutions do not satisfy the first order continuity equation.

4.5.2. THE SECOND ORDER SOLUTIONS

Substitution of the first order solutions into the second order differential equations (4.9) - (4.12) and considering only zero frequency interactions yields

$$x_{2tt}+gz_{2a}+\frac{p_{2a}}{\rho}-\nu\nabla^2 x_{2t}=\int_{-\pi}^{+\pi}\int_{-\pi}^{+\pi}\int_{-\infty}^{+\infty}[A_{11}{}^{VD}e^{2|k|c}+A_{22}{}^{VD}e^{|k|c+c/l}+ A_{33}{}^{VD}e^{2c/l}]e^{ik(\gamma_1 a+\gamma_2 b)-\delta t}d\xi_1(\omega,\theta)\,d\xi_1(-\omega,\theta') \tag{4.117}$$

$$y_{2tt}+gz_{2b}+\frac{p_{2b}}{\rho}-\nu\nabla^2 y_{2t}=\int_{-\pi}^{+\pi}\int_{-\pi}^{+\pi}\int_{-\infty}^{+\infty}[B_{11}{}^{VD}e^{2|k|c}+B_{22}{}^{VD}e^{|k|c+c/l}+ B_{33}{}^{VD}e^{2c/l}]e^{ik(\gamma_1 a+\gamma_2 b)-\delta t}d\xi_1(\omega,\theta)\,d\xi_1(-\omega,\theta') \tag{4.118}$$

$$z_{2tt}+gz_{2c}+\frac{p_{2c}}{\rho}-\nu\nabla^2 z_{2t}=\int_{-\pi}^{+\pi}\int_{-\pi}^{+\pi}\int_{-\infty}^{+\infty}[C_{11}{}^{VD}e^{2|k|c}+C_{22}{}^{VD}e^{|k|c+c/l}+ C_{33}{}^{VD}e^{2c/l}]e^{ik(\gamma_1 a+\gamma_2 b)-\delta t}d\xi_1(\omega,\theta)\,d\xi_1(-\omega,\theta') \tag{4.119}$$

$$x_{2a}+y_{2b}+z_{2c}=\int_{-\pi}^{+\pi}\int_{-\pi}^{+\pi}\int_{-\infty}^{+\infty}\left| D_{11}^{VD}e^{2|k|c}+D_{22}^{VD}e^{|k|c+c/l}+D_{33}^{VD}e^{2c/l}\right|$$

$$e^{ik(\gamma_1 a+\gamma_2 b)-\delta t}\,d\xi_1(\omega,\theta)\,d\xi_1(-\omega,\theta') \tag{4.120}$$

where

$$A_{11}^{VD}=(1+cos(\theta-\theta'))\frac{k\omega^2}{2}\left| i\gamma_1\,(1+k^4l^4cos(\theta-\theta'))-k^2l^2\gamma_3(cos(\theta-\theta')+3)\right|$$

$$A_{22}^{VD}=k|k|l\omega^2\left|\gamma_3\,(cos\frac{c}{l}-sin\frac{c}{l})(1+cos(\theta-\theta'))-i\gamma_1\,|k|k|l\omega^2(cos\frac{c}{l}+sin\frac{c}{l})\right|+$$

$$k^3l^2\omega^2\Bigg(\gamma_3\left|\,cos\frac{c}{l}(1+3cos(\theta-\theta'))+\frac{|k|l}{2}(2cos^2(\theta-\theta')+3cos(\theta-\theta')-1)\right.$$

$$\left.(cos\frac{c}{l}+sin\frac{c}{l})+\frac{k^2l^2}{2}sin\frac{c}{l}(3-cos(\theta-\theta'))\right|-i\gamma_1\left|sin\frac{c}{l}cos(\theta-\theta')\right.$$

$$\left.-\frac{|k|l}{2}(cos(\theta-\theta')-3)\,(cos\frac{c}{l}-sin\frac{c}{l})-\frac{k^2l^2}{2}cos\frac{c}{l}(1-7\,cos(\theta-\theta'))\right|\Bigg)$$

$$A_{33}^{VD}=-k^3l^2\omega^2\Bigg(\gamma_3\left|\,1+2cos(\theta-\theta')+k^2l^2(cos^2(\theta-\theta')+cos(\theta-\theta')-2)\right|+$$

$$i\gamma_1\left|\,2-cos(\theta-\theta')+\frac{k^2l^2}{2}(1+6\,cos(\theta-\theta'))\right|$$

$$B_{11}^{VD}=(1+cos(\theta-\theta'))\frac{k\omega^2}{2}\left[\,i\gamma_2\,(1+k^4l^4cos(\theta-\theta'))-k^2l^2\gamma_4(cos(\theta-\theta')+3)\right|$$

$$B_{22}^{VD}=k|k|l\omega^2\left[\,\gamma_4\,(cos\frac{c}{l}-sin\frac{c}{l})\,(1+cos(\theta-\theta'))-i\,\gamma_2\left|\,(cos\frac{c}{l}+sin\frac{c}{l})\right.\right.$$

$$+k^3l^2\omega^2\Bigg(\gamma_4\left|\,cos\frac{c}{l}(1+3cos(\theta-\theta'))+\frac{|k|l}{2}(2cos^2(\theta-\theta')+3cos(\theta-\theta')-1)\right.$$

$$\left.(cos\frac{c}{l}+sin\frac{c}{l})+\frac{k^2l^2}{2}sin\frac{c}{l}(3-cos(\theta-\theta'))\right|-i\,\gamma_2\left|sin\frac{c}{l}cos(\theta-\theta')\right.$$

$$\left.-\frac{|k|l}{2}(cos(\theta-\theta')-3)\,(cos\frac{c}{l}-sin\frac{c}{l})-\frac{k^2l^2}{2}cos\frac{c}{l}(1-7\,cos(\theta-\theta'))\right|\Bigg)$$

$$B_{33}^{VD}=-k^3l^2\omega^2\Bigg(\gamma_4\left|\,1+2cos(\theta-\theta')+k^2l^2\,(cos^2(\theta-\theta')+cos(\theta-\theta')-2)\right|+$$

$$i\gamma_2\left|\,2-cos(\theta-\theta')+\frac{k^2l^2}{2}(1+6\,cos(\theta-\theta')\right|\Bigg)$$

$$C_{11}^{VD}=|k|\omega^2(1+cos(\theta-\theta'))(1+k^4l^4cos(\theta-\theta'))$$

$$C_{22}^{VD}=-2|k|\omega^2cos\tfrac{c}{l}\,cos(\theta-\theta')+k^2l\omega^2(cos\tfrac{c}{l}+sin\tfrac{c}{l})(cos(\theta-\theta')-1)+$$

$$k^2|k|l^2\omega^2\Big(-sin\tfrac{c}{l}(1+2cos(\theta-\theta'))+|k|l(sin\tfrac{c}{l}-cos\tfrac{c}{l})(cos^2(\theta-\theta')-$$

$$cos(\theta-\theta')-1)+k^2l^2cos\tfrac{c}{l}(cos^2(\theta-\theta')-cos(\theta-\theta')-3)\Big)$$

$$C_{33}^{VD}=k^4l^3\omega^2(1-2cos(\theta-\theta'))$$

$$D_{11}^{VD}=k^2(1+cos(\theta-\theta'))^2/2$$

$$D_{22}^{VD}=-2k^2cos\tfrac{c}{l}cos(\theta-\theta')-k^2|k|l(cos\tfrac{c}{l}+sin\tfrac{c}{l})(cos^2(\theta-\theta')+1)$$

$$-k^4l^2sin\tfrac{c}{l}cos(\theta-\theta')$$

$$D_{33}^{VD}=k^4l^2(1+cos^2(\theta-\theta'))$$

$$\delta=4\nu k^2. \qquad (4.121)$$

Note that right hand sides of equations (4.117) - (4.120) are time dependent. In the nondecaying wave case, right hand sides of the second order momentum equations (4.73) - (4.76) are independent of time. In equations (4.117) to (4.121), terms up to $O(kl)^2$ are identical to nondecaying case (4.73) to (4.77). Only the terms of order $(kl)^3$ and $(kl)^4$ are changed by the introduction of the time-decay term $e^{-2\nu k^2 t}$. Major differences appear, however, in the second order boundary conditions (derived latter) which will in turn effect the homogeneous solutions.

The x_2-momentum equation (4.117) reduces to Weber's (1983b) eqn. (4.1) if we drop $(kl)^2$ order terms, horizontal derivative terms (e.g., z_{2a}, p_{2a}, x_{2aa} and x_{2bb} which are small compared to vertical derivative term x_{2cc}) and substitute $\theta=\theta'=0$. Weber solved this u_2-momentum equation (accurate to first order in kl) to get the u_2-component of the mass transport velocity. He did not solve for the vertical component of

the mass transport velocity. The fact that the vertical gradient of the pressure is not negligible compared to the vertical gradient of the velocity in w_2- equation of motion (4.119), implies that (4.119) cannot be solved using the Weber's technique. Therefore, Weber's technique is of little help in solving the three dimensional problem. Since we are considering decaying wave problem we will not consider the steady state case (as in section 4.4.2). A more general approach is adopted to solve (4.117)-(4.120).

Following the same procedure as in section (4.4.2), the momentum equations (4.117) - (4.119) can be expressed as the following single variable equations in x_2, y_2 and z_2:

$$\nabla^2 x_{2tt} - \nu\nabla^4 x_{2t} = \int_{-\pi}^{+\pi}\int_{-\pi}^{+\pi}\int_{-\infty}^{+\infty} |A_1{}^{VD} e^{2|k|c} + A_2{}^{VD} e^{|k|c+c/l} + A_3{}^{VD} e^{2c/l}|$$
$$e^{ik(\gamma_1 a+\gamma_2 b)-\delta t}\, d\xi_1(\omega,\theta) d\xi_1(-\omega,\theta') \tag{4.122}$$

$$\nabla^2 y_{2tt} - \nu\nabla^4 y_{2t} = \int_{-\pi}^{+\pi}\int_{-\pi}^{+\pi}\int_{-\infty}^{+\infty} |B_1{}^{VD} e^{2|k|c} + B_2{}^{VD} e^{|k|c+c/l} + B_3{}^{VD} e^{2c/l}|$$
$$e^{ik(\gamma_1 a+\gamma_2 b)-\delta t}\, d\xi_1(\omega,\theta) d\xi_1(-\omega,\theta') \tag{4.123}$$

$$\nabla^2 z_{2tt} - \nu\nabla^4 z_{2t} = \int_{-\pi}^{+\pi}\int_{-\pi}^{+\pi}\int_{-\infty}^{+\infty} |C_1{}^{VD} e^{2|k|c} + C_2{}^{VD} e^{|k|c+c/l} + C_3{}^{VD} e^{2c/l}|$$
$$e^{ik(\gamma_1 a+\gamma_2 b)-\delta t}\, d\xi_1(\omega,\theta) d\xi_1(-\omega,\theta') \tag{4.124}$$

where

$$A_1^{VD} = -k^5 l^2 \omega^2 (1+cos(\theta-\theta'))^2 (3+cos(\theta-\theta')) [\gamma_3 - i k^2 l^2 \gamma_1]$$

$$A_2^{VD} = -2\omega^2 k \Big(\gamma_3 [\,|k|/l (cos\tfrac{c}{l} + sin\tfrac{c}{l})(1+cos(\theta-\theta')) + k^2 sin\tfrac{c}{l}(5cos(\theta-\theta')+3)\,]$$

$$-i\gamma_1 [\,|k|/l (cos\tfrac{c}{l} - sin\tfrac{c}{l})(cos(\theta-\theta')-1) + k^2 cos\tfrac{c}{l}(cos(\theta-\theta')+1)\,] \Big)$$

$$+ 2k^3 |k| l \omega^2 \Big(\gamma_3 (cos\tfrac{c}{l} - sin\tfrac{c}{l}) cos(\theta-\theta')(2cos(\theta-\theta')+5)$$

$$-i\gamma_1 (cos\tfrac{c}{l} + sin\tfrac{c}{l})(cos(\theta-\theta')-2) \Big)$$

$$A_3^{VD} = -\gamma_3 4k^3\omega^2(1+2cos(\theta-\theta')) + i\gamma_1 4k^3\omega^2(2-cos(\theta-\theta'))$$

$$B_1^{VD} = -k^5 l^2 \omega^2 (1+cos(\theta-\theta'))^2 (3+cos(\theta-\theta')) [\gamma_4 - i k^2 l^2 \gamma_2]$$

$$B_2^{VD} = -2\omega^2 k \Big(\gamma_4 [\,|k|/l (cos\tfrac{c}{l} + sin\tfrac{c}{l})(1+cos(\theta-\theta')) + k^2 sin\tfrac{c}{l}(5cos(\theta-\theta')+3)\,]$$

$$-i\gamma_2 [\,|k|/l (cos\tfrac{c}{l} - sin\tfrac{c}{l})(cos(\theta-\theta')-1) + k^2 cos\tfrac{c}{l}(cos(\theta-\theta')+1)\,] \Big)$$

$$+ 2k^3 |k| l \omega^2 \Big(\gamma_4 (cos\tfrac{c}{l} - sin\tfrac{c}{l}) cos(\theta-\theta')(2cos(\theta-\theta')+5)]$$

$$-i\gamma_2 (cos\tfrac{c}{l} + sin\tfrac{c}{l})(cos(\theta-\theta')-2) \Big)$$

$$B_3^{VD} = -4k^3\omega^2\gamma_4(1+2cos(\theta-\theta')) + i\gamma_2 4k^3\omega^2(2-cos(\theta-\theta'))$$

$$C_1^{VD} = 2k^6 |k| l^4 \omega^2 (1+cos(\theta-\theta'))^2 (3+cos(\theta-\theta'))$$

$$C_2^{VD} = -4k^2 |k| \omega^2 cos\tfrac{c}{l}(1-cos(\theta-\theta'))^2 + 4k^4 l \omega^2 cos^2(\theta-\theta')(cos\tfrac{c}{l} + sin\tfrac{c}{l})$$

$$+ 4k^4 |k| l^2 \omega^2 (cos^2(\theta-\theta') + cos(\theta-\theta') + 3) sin\tfrac{c}{l}$$

$$C_3^{VD} = 4k^4 l \omega^2 |\, cos^2(\theta-\theta') - 3cos(\theta-\theta') + 2\,].$$

(4.125)

Now if we carefully examine the equations (4.122) - (4.124) we will see that, for time variation of the form $e^{-2\nu k^2 t}$, the acceleration term $\nabla^2 \mathbf{x}_{2tt}$ and friction term $\nu\nabla^4 \mathbf{x}_{2t}$ are of equal magnitude. The acceleration term cannot, therefore, be neglected. This is in contrast to inviscid and

nondecaying wave cases where we have dropped the acceleration term by assuming that the mass transport velocity does not have acceleration. Furthermore, an attempt to solve the above equations considering unaccelerated motion gave particular solutions which do not reduce to inviscid solutions (3.63) to (3.61) as $\nu \to 0$. Therefore these equations are solved in a different manner from that used to solve the inviscid and nondecaying wave problems.

Retaining both the acceleration and friction terms in equations (4.122) to (4.124) and applying the technique of undetermined coefficients, the particular solutions to these equations are given by

$$x_2^{VDp} = \int_{-\pi}^{+\pi}\int_{-\pi}^{+\pi}\int_{-\infty}^{+\infty} -\frac{\omega k}{2\delta}(A'^{VD}\gamma_3 + iB'^{VD}\gamma_1)\, e^{ik(\gamma_1 a+\gamma_2 b)-\delta t} \, d\xi_1(\omega,\theta)\, d\xi_1(-\omega,\theta') \quad (4.126a)$$

$$y_2^{VDp} = \int_{-\pi}^{+\pi}\int_{-\pi}^{+\pi}\int_{-\infty}^{+\infty} -\frac{\omega k}{2\delta}(A'^{VD}\gamma_4 + iB'^{VD}\gamma_2)\, e^{ik(\gamma_1 a+\gamma_2 b)-\delta t} \, d\xi_1(\omega,\theta)\, d\xi_1(-\omega,\theta') \quad (4.126b)$$

$$z_2^{VDp} = \int_{-\pi}^{+\pi}\int_{-\pi}^{+\pi}\int_{-\infty}^{+\infty} C'^{VD}\, e^{ik(\gamma_1 a+\gamma_2 b)-\delta t}\, d\xi_1(\omega,\theta)\, d\xi_1(-\omega,\theta') \quad (4.126c).$$

The particular solution for pressure is obtained by substituting (4.126c) into second order z_2-momentum equation (4.119)

$$p_2^{VDp} = -\int_{-\pi}^{+\pi}\int_{-\pi}^{+\pi}\int_{-\infty}^{+\infty} \omega^2 \rho\, D'^{VD}\, e^{ik(\gamma_1 a+\gamma_2 b)-\delta t}\, d\xi_1(\omega,\theta)\, d\xi_1(-\omega,\theta') \quad (4.126d)$$

where

$$A'^{VD} = (1+\cos(\theta-\theta'))\,e^{2|k|c} - 2|k|l\,(1+\cos(\theta-\theta'))\,(\cos\tfrac{c}{l}+\sin\tfrac{c}{l})\,e^{|k|c+c/l}$$

$$+k^2l^2\left(2(1-\cos(\theta-\theta'))\sin\tfrac{c}{l}\,e^{|k|c+c/l} + (1+2\cos(\theta-\theta'))\,e^{2c/l}\right)$$

$$B'^{VD} = -2|k|l\,(1-\cos(\theta-\theta'))\,(\cos\tfrac{c}{l}-\sin\tfrac{c}{l})\,e^{|k|c+c/l} - k^2l^2\Big((1+\cos(\theta-\theta'))$$

$$e^{2|k|c} - 2(3-5\cos(\theta-\theta'))\cos\tfrac{c}{l}\,e^{|k|c+c/l} + (2-\cos(\theta-\theta'))\,e^{2c/l}\Big)$$

$$C'^{VD} = \frac{k}{2}(1+\cos(\theta-\theta'))\,e^{2|k|c} + \{\,|k|(1-\cos(\theta-\theta'))^2\cos\tfrac{c}{l} - k^2l\,(\cos\tfrac{c}{l}+\sin\tfrac{c}{l})$$

$$(3\cos^2(\theta-\theta') - 4\cos(\theta-\theta') + 2) - l^2k^2|k|\sin\tfrac{c}{l}(2\cos^3(\theta-\theta') - 12\cos^2(\theta-\theta') +$$

$$13\cos(\theta-\theta') - 2)\,\}\,e^{|k|c+c/l} + \frac{k^2l}{4}(\cos^2(\theta-\theta') - 3\cos(\theta-\theta') + 2)\,e^{2c/l}$$

$$D'^{VD} = |\cos\tfrac{c}{l}(1-\cos(\theta-\theta'))^2 - kl\,(\cos\tfrac{c}{l}+\sin\tfrac{c}{l})\,(3\cos^2(\theta-\theta') - 5\cos(\theta-\theta') + 2)$$

$$-l^2k^2\sin\tfrac{c}{l}(2\cos^3(\theta-\theta') - 12\cos^2(\theta-\theta') + 15\cos(\theta-\theta') - 3)\,|\,e^{|k|c+c/l}$$

(4.126*e*)

The solutions (4.126) represent second order displacements and pressure due to a group of decaying deep water surface gravity waves. Once again the vertical displacement z_2^{VDp} (4.126c) is smaller than the horizontal displacements by a factor $\delta = 2k^2l^2\omega$. By differentiating (4.126a) - (4.126c) with respect to t one obtains particular solutions for the velocities $(u_2^{VDp}, v_2^{VDp}, w_2^{VDp})$ for decaying waves

$$u_2^{VDp} = \int_{-\pi}^{+\pi}\int_{-\pi}^{+\pi}\int_{-\infty}^{+\infty}\frac{\omega k}{2}(A'^{VD}\gamma_3 + iB'^{VD}\gamma_1)\,e^{ik(\gamma_1 a+\gamma_2 b)-\delta t}\,d\xi_1(\omega,\theta)\,d\xi_1(-\omega,\theta')$$

(4.127*a*)

$$v_2^{VDp} = \int_{-\pi}^{+\pi}\int_{-\pi}^{+\pi}\int_{-\infty}^{+\infty}\frac{\omega k}{2}(A'^{VD}\gamma_4 + iB'^{VD}\gamma_2)\,e^{ik(\gamma_1 a+\gamma_2 b)-\delta t}\,d\xi_1(\omega,\theta)\,d\xi_1(-\omega,\theta')$$

(4.127*b*)

$$w_2^{VDp} = \int_{-\pi}^{+\pi}\int_{-\pi}^{+\pi}\int_{-\infty}^{+\infty} -2k^2l^2\omega C'^{VD}\,e^{ik(\gamma_1 a+\gamma_2 b)-\delta t}\,d\xi_1(\omega,\theta)\,d\xi_1(-\omega,\theta')$$

(4.127*c*)

where $A'^{VD}, B'^{VD}, C'^{VD}$ are given by equations (4.126e). The above solutions satisfy the lower boundary condition for the deep water surface gravity waves i.e., $u_2^{VDp}, v_2^{VDp}, w_2^{VDp} \to 0$, $c \to -\infty$. Far below the vorticity layer l, u_2^{VDp}, v_2^{VDp} tend to the inviscid solutions (3.63) and (3.61). The particular solutions u_2^{VDp} and v_2^{VDp} are very similar to u_2^{VFp} and v_2^{VFp} for nondecaying waves (4.81, 4.83) except that u_2^{VDp} and v_2^{VDp} each have one additional term of order k^2/l^2 (see B'^{VF} and B'^{VD} terms, equations 4.84, 4.126e). Similarly, nondecaying vertical velocity w_2^{VFp} (4.82) and decaying vertical velocity w_2^{VDp} (4.127c) solutions are similar except that C'^{VD} (4.126e) has one additional term than that of C'^{VF} (4.84). In the limiting case of $\theta=\theta'=0$, u_2^{VDp} (4.127a) reduces to Weber's(1983a) and Chang's(1969) particular solutions.

The solutions (4.127) represent damped wave motion. Such motion will decay with time. In order to estimate the magnitude of damping produced by the surface gravity waves usually encountered in the ocean (typical frequency range 0.3 to 1.0 rad/s) the wave number k ranges between .009 to 0.1 m^{-1}. For $\nu=0.01\ m^2/s$, $\delta=2k^2/l^2\omega$ lies between 3×10^{-6} to $4\times10^{-4}\ s^{-1}$. So the damping is slow and can be neglected if the time interval under analysis is of the order of minutes.

Now the solutions must match the boundary conditions at the surface. The second order surface boundary conditions are obtained by substituting first order solutions (4.115) into the boundary equations (4.85) to (4.87) and considering zero frequency interaction. Using the same argument as in section (4.4.2) the vertical velocity at the surface must be zero i.e.

$$w_2^{VD}=0 \text{ at } c=0 \qquad (4.128)$$

The boundary conditions are therefore

$$u_{2c}^{VD}|_{t=0} = \int_{-\pi}^{+\pi}\int_{-\pi}^{+\pi}\int_{-\infty}^{+\infty} | k^3 l\omega\gamma_3 - i k^3 l\omega\gamma_1 (1 + |k|l(1+cos(\theta-\theta'))/2)| \; e^{ik(\gamma_1 a + \gamma_2 b) - \delta t} d\xi_1(\omega,\theta) d\xi_1(-\omega,\theta') \quad (4.129)$$

$$v_{2c}^{VD}|_{t=0} = \int_{-\pi}^{+\pi}\int_{-\pi}^{+\pi}\int_{-\infty}^{+\infty} | k^3 l\omega\gamma_4 - i k^3 l\omega\gamma_2 (1 + |k|l(1+cos(\theta-\theta'))/2)| \; e^{ik(\gamma_1 a + \gamma_2 b) - \delta t} d\xi_1(\omega,\theta) d\xi_1(-\omega,\theta') \quad (4.130)$$

The boundary conditions (4.129), (4.130) for a, b-components of surface stress involve terms of smaller order in kl than the surface boundary conditions (4.91), (4.92) for surface stress in the case of nondecaying wave. The large magnitude of the surface values for the nondecaying waves may be attributed to the applied surface stress and also dropping of the decaying part ($e^{-\delta t}$) of the solution. Unluta and Mei (1970) and Weber (1983a) reported that the second order boundary conditions are of order ($k^2/2$) and they set the right hand side of (4.129) and (4.130) equal to zero. If we drop k^2/β^2 term in first order z_1 and p_1 solutions (4.115c) (4.115d) (as done by Chang, 1969), then the boundary conditions become of the same order as those of Unluta and Mei (1970) and Weber (1983a) i.e., $O(k^2/2)$. The k^2/β^2 term is small ($O(k^2/2)$) but its gradient at the surface is of the order kl.

The particular solutions (4.126) do not satisfy the above boundary conditions (4.128)-(4.130). Accordingly, the complete solution must also include the homogeneous solutions of the homogeneous versions of the equations (4.122) - (4.124). That is, the homogeneous equations are

$$\nabla^2 u_{2t}^{VDh} - \nu \nabla^4 u_2^{VDh} = 0 \tag{4.131}$$

$$\nabla^2 v_{2t}^{VDh} - \nu \nabla^4 v_2^{VDh} = 0 \tag{4.132}$$

$$\nabla^2 w_{2t}^{VDh} - \nu \nabla^4 w_2^{VDh} = 0 \tag{4.133}$$

where u_2^{VDh}, v_2^{VDh} and w_2^{VDh} represent velocities from the homogeneous solutions. The homogeneous solutions must satisfy the condition at $c=-\infty$ which are

$$\begin{aligned} u_2^{VDh} &= 0 \quad c \to -\infty \\ v_2^{VDh} &= 0 \quad c \to -\infty \\ w_2^{VDh} &= 0 \quad c \to -\infty. \end{aligned} \tag{4.134}$$

Attempts to solve equations (4.131) to (4.133) subject to condition (4.134) using a separation of variables technique (similar to nondecaying-wave case) were unsuccessful. The differential equations (4.131) - (4.133) have four roots namely,

$$m_{1,2} = \pm 2 \left| k \sin \frac{\theta - \theta'}{2} \right|$$

$$m_{3,4} = \pm 2i \left| k \cos \frac{\theta - \theta'}{2} \right|$$

of which only one root m_1 (with + sign) gives solution which decays with depth. The other 3 roots are unphysical because they are either oscillatory with depth or increase exponentially with depth. Moreover, the root m_1 leads to a singularity when boundary conditions are applied as θ approaches θ'. The reason is that when the horizontal length scale of the forcing function (which is from the nonlinear interaction of the first order solutions) tends to infinity (i.e., when $\theta=\theta'$) and when the forcing

terms have been acting for an infinitely long time in one direction (i.e., when $\omega=\omega'$), then momentum will diffuse to infinite depth. This explains why zero frequency, zero angle interaction cannot satisfy the condition $u,v,w \to 0$ as $c \to -\infty$.

Weber (1983a) used a different approach to solve the homogeneous part of his x_2-momentum equation (eqn. 4.117 with $\theta=-\theta'=0$). He applied a Laplace transform by introducing an initial condition for the homogeneous velocity. Following Weber (1983a) we also assume that the second order homogeneous solutions are zero at time $t=0$ i.e.,

$$\begin{aligned} u_2^{VDh}&=0 \quad at \quad t=0 \\ v_2^{VDh}&=0 \quad at \quad t=0 \\ w_2^{VDh}&=0 \quad at \quad t=0. \end{aligned} \tag{4.135}$$

Physically the above initial conditions mean that initially we will start with a wave field given by the particular solutions (4.127). The wave field described by the particular solutions (4.127) decay in time because of the action of viscosity. But since the original momentum cannot be destroyed, the homogeneous solutions (which are zero initially) satisfying the surface boundary conditions distribute the momentum from the surface to the layer below. The depth of this layer is initially infinitesimally small and grows to order k^{-1} in the time taken for the wave field to decay (Longuet-Higgins, 1969).

Equations (4.131) to (4.133) are solved subject to the boundary conditions (4.128) to (4.130) and initial conditions (4.135) by applying the Laplace transform in the time variable. The Laplace transform of a function $f(t)$ is given by

$$F(s)=\int_0^\infty f(t)e^{-st}dt$$

where s is the Laplace transform of t. Therefore, the Laplace transform of the equations (4.131) to (4.133) are

$$\nabla^2 U_2^{VDh}-\nu/s\,\nabla^4 U_2^{VDh}=0 \tag{4.136}$$

$$\nabla^2 V_2^{VDh}-\nu/s\,\nabla^4 V_2^{VDh}=0 \tag{4.137}$$

$$\nabla^2 W_2^{VDh}-\nu/s\,\nabla^4 W_2^{VDh}=0 \tag{4.138}$$

where $U_2^{VDh}, V_2^{VDh}, W_2^{VDh}$ are the Laplace transforms of the second order homogeneous velocities $u_2^{VDh}, v_2^{VDh}, w_2^{VDh}$ respectively and s being the Laplace transform of t. Equations (4.136) to (4.138) are fourth order differential equations in (a,b,c) spatial variables only (t dependence appears as a coefficient of the spatial derivatives). Assuming same (a,b) dependence as in particular solutions (4.127) i.e., $e^{ik(\gamma_1 a+\gamma_2 b)}$, the equations (4.136)-(4.138) are now solved for unknown dependence in c. Out of four roots (two positive and two negative) of the above equations, only two (positive roots) are acceptable. The negative roots result in solutions that do not decay as $c\to-\infty$. The homogeneous solutions are, therefore, given by

$$U_2^{VDh}=\int_{-\pi}^{+\pi}\int_{-\pi}^{+\pi}\int_{-\infty}^{+\infty}[(d\xi_{2x}{}^{VD}+i\,d\xi_{2x}{}^{'VD})e^{\lambda_1 c}+(d\xi_{3x}{}^{VD}+i\,d\xi_{3x}{}^{'VD})e^{\lambda_2 c}]$$
$$e^{ik(\gamma_1 a+\gamma_2 b)} \quad (4.139a)$$

$$V_2^{VDh}=\int_{-\pi}^{+\pi}\int_{-\pi}^{+\pi}\int_{-\infty}^{+\infty}[(d\xi_{2y}{}^{VD}+i\,d\xi_{2y}{}^{'VD})e^{\lambda_1 c}+(d\xi_{3y}{}^{VD}+i\,d\xi_{3y}{}^{'VD})e^{\lambda_2 c}]$$
$$e^{ik(\gamma_1 a+\gamma_2 b)} \quad (4.139b)$$

$$W_2^{VDh}=\int_{-\pi}^{+\pi}\int_{-\pi}^{+\pi}\int_{-\infty}^{+\infty}[d\xi_{2z}{}^{VD}e^{\lambda_1 c}+d\xi_{3z}{}^{VD}e^{\lambda_2 c}]e^{ik(\gamma_1 a+\gamma_2 b)} \quad (4.139c)$$

where

$$\lambda_1=\sqrt{\frac{s}{\nu}+2k^2(1-cos(\theta-\theta'))}$$

$$\lambda_2=\sqrt{2k^2(1-cos(\theta-\theta'))} \quad (4.139d)$$

The unknown constants $d\xi_{2x}{}^{VD}$, $d\xi_{2x}{}^{'VD}$, $d\xi_{3x}{}^{VD}$, $d\xi_{3x}{}^{'VD}$, $d\xi_{2y}{}^{VD}$, $d\xi_{2y}{}^{'VD}$, $d\xi_{3y}{}^{VD}$, $d\xi_{3y}{}^{'VD}$, $d\xi_{2z}{}^{VD}$, and $d\xi_{3z}{}^{VD}$ are determined by satisfying the Laplace transform of the boundary conditions (4.128) - (4.130), homogeneous versions of the continuity equation (4.120) and one vorticity equation. The continuity and vorticity equations are used to relate some of the constants which are not independent. Solving the real and imaginary parts of the resulting equations as in section 4.4.2, the constants are given by

$$d\xi_{2x}{}^{VD}=\frac{k|k|\omega\gamma_3(1+cos(\theta-\theta'))}{(s+\delta)\lambda_1}d\xi_1(\omega,\theta)d\xi_1(-\omega,\theta')$$

$$d\xi_{2x}{}^{'VD}=\{-\frac{\gamma_1}{(s+\delta)\lambda_1}\frac{Q}{2k(1-cos(\theta-\theta'))}+\frac{\nu}{s(s+\delta)}[\frac{\lambda_2}{\lambda_1}(Q+\lambda_1{}^2R)sin(\frac{\theta+\theta'}{2})]\}$$
$$d\xi_1(\omega,\theta)d\xi_1(-\omega,\theta')$$

$$d\xi_{3x}{}^{VD}=0$$

$$d\xi_{3x}{}^{VD} = -d\xi_{3z}{}^{VD} \sin(\frac{\theta+\theta'}{2})$$

$$d\xi_{2y}{}^{VD} = \frac{k|k|\omega\gamma_4(1+\cos(\theta-\theta'))}{(s+\delta)\lambda_1} d\xi_1(\omega,\theta) d\xi_1(-\omega,\theta')$$

$$d\xi_{2y}{}^{VD} = \{ -\frac{\gamma_2}{(s+\delta)\lambda_1} \frac{Q}{2k(1-\cos(\theta-\theta'))} \frac{\nu}{s(s+\delta)} - [\frac{\lambda_2}{\lambda_1}(Q+\lambda_1{}^2 R)\cos(\frac{\theta+\theta'}{2})] \}$$
$$d\xi_1(\omega,\theta) d\xi_1(-\omega,\theta')$$

$$d\xi_{3y}{}^{VD} = -d\xi_{3z}{}^{VD} \cos(\frac{\theta+\theta'}{2})$$

$$d\xi_{2z}{}^{VD} = -\nu \frac{Q+\lambda_2{}^2 R}{s(s+\delta)} d\xi_1(\omega,\theta) d\xi_1(-\omega,\theta')$$

$$d\xi_{3z}{}^{VD} = \nu \frac{Q+\lambda_1{}^2 R}{s(s+\delta)} d\xi_1(\omega,\theta) d\xi_1(-\omega,\theta')$$

where

$$Q = 2k^4 l\omega(1-\cos(\theta-\theta'))[(1-3\cos(\theta-\theta')) + \frac{kl}{2}(5-11\cos(\theta-\theta'))]$$

and

$$R = \frac{\delta k}{2}[(2\cos^2(\theta-\theta') - 3\cos(\theta-\theta') + 3) - \frac{kl}{2}(11\cos^2(\theta-\theta') - 13\cos(\theta-\theta') + 6)].$$

(4.139e)

The solutions (4.139) are accurate up to the order of $(kl)^2$. Performing the inverse Laplace transform on (4.139) gives homogeneous solutions (not presented here for brevity) which contain many terms including terms of order $(kl)^2$. These solutions fail to satisfy the initial condition (4.135) by a small term of the order $O(kl)^2$. Hildebrand (1962, page 73) showed through an example that (in the case of simultaneous equations resulting from two differential equations), the method of Laplace transform may supply erroneous solutions which fail to satisfy certain prescribed initial conditions i.e. the same initial conditions used to do

the transformation initially. Clearly, the solutions with the coefficients given by (4.139e) fall in this catagory. But the order of the error is $O(kl)^2$ and the solutions satisfy the boundary conditions and initial conditions up to the $O(kl)$. Also note that $O(kl)$ terms are the dominant terms in the solutions and latter on we will drop the $O(kl)^2$ terms anyway.

The next logical step is, therefore, to see if the initial condition is still violated if we drop the small terms of order $(kl)^2$ from the particular solutions (4.127) and repeat the procedure of Laplace transform to solve the same homogeneous equations (4.136) - (4.138) as before. The second order boundary conditions (4.129) and (4.130) are now similar to Unluta and Mei (1970) and Weber (1983a) (as we drop k^2/β^2 term from (4.115c, d)) as discussed before (i.e., $O(k^2l^2)$). Therefore, the surface boundary conditions for the horizontal component of the stress are now

$$u_{2c}^{VD}|_{c=0}=0$$
$$v_{2c}^{VD}|_{c=0}=0 \qquad (4.140)$$

The homogeneous solutions thus obtained (in Laplace transformed variables) are similar to equations (4.139). But the coefficients $d\xi_{2x}^{VD}, d\xi_{2x}'^{VD}, d\xi_{2y}^{VD}$ etc. (equation 4.139e) are now given by

$$d\xi_{2x}^{VD}=\frac{k|k|\omega\gamma_3(1+cos(\theta-\theta'))(1+kl)}{(s+\delta)\lambda_1}d\xi_1(\omega,\theta)d\xi_1(-\omega,\theta')$$

$$d\xi_{2x}'^{VD}=\{\frac{\gamma_1}{(s+\delta)\lambda_1}k^3l\omega(1-cos(\theta-\theta'))-\frac{\nu}{s(s+\delta)}[\frac{Q\lambda_2}{\lambda_1}sin(\frac{\theta+\theta'}{2})]\}$$
$$d\xi_1(\omega,\theta)d\xi_1(-\omega,\theta')$$

$$d\xi_{3x}^{VD}=0$$

$$d\xi_{3x}'^{VD}=-d\xi_{3z}^{VD}sin(\frac{\theta+\theta'}{2})$$

$$d\xi_{2y}{}^{VD}=\frac{k|k|\omega\gamma_4(1+cos(\theta-\theta'))(1+kl)}{(s+\delta)\lambda_1}d\xi_1(\omega,\theta)\,d\xi_1(-\omega,\theta')$$

$$d\xi_{2y}{}'^{VD}=\{\frac{\gamma_2}{(s+\delta)\lambda_1}k^3l\omega(1-cos(\theta-\theta'))+\frac{\nu}{s(s+\delta)}|\frac{Q\lambda_2}{\lambda_1}cos(\frac{\theta+\theta'}{2})|\}$$
$$d\xi_1(\omega,\theta)\,d\xi_1(-\omega,\theta')$$

$$d\xi_{3y}{}^{VD}=0$$

$$d\xi_{3y}{}'^{VD}=-d\xi_{3z}{}^{VD}\,cos(\frac{\theta+\theta'}{2})$$

$$d\xi_{2z}{}^{VD}=\nu\frac{Q}{s(s+\delta)}d\xi_1(\omega,\theta)\,d\xi_1(-\omega,\theta')$$

$$d\xi_{3z}{}^{VD}=-\nu\frac{Q}{s(s+\delta)}d\xi_1(\omega,\theta)\,d\xi_1(-\omega,\theta')$$

$$Q=2k^4l\omega(1-cos(\theta-\theta'))^2$$

(4.141)

The inverse Laplace transform of (4.139a-4.139c) with $d\xi_{2x}{}^{VD}$, $d\xi_{2x}{}'^{VD}$, $d\xi_{3x}{}^{VD}$ etc. given by (4.141) give the homogeneous solutions for the decaying wave problem

$$u_2^{VDh}=\int_{-\pi}^{+\pi}\int_{-\pi}^{+\pi}\int_{-\infty}^{+\infty}\Big[\gamma_3\omega k|k|(1+kl)(1+cos(\theta-\theta'))\sqrt{\frac{\nu}{\pi}}e^{-\delta t}\int_0^t\frac{e^{\delta\zeta-\lambda_2^2\nu\zeta-\frac{c^2}{4\nu\zeta}}}{\sqrt{\zeta}}d\zeta$$

$$+i\gamma_1\omega k^3 l(1-cos(\theta-\theta'))\sqrt{\frac{\nu}{\pi}}e^{-\delta t}\int_0^t\frac{e^{\delta\zeta-\lambda_2^2\nu\zeta-\frac{c^2}{4\nu\zeta}}}{\sqrt{\zeta}}d\zeta-\frac{i\gamma_1\omega k^3 l}{2}$$

$$(1-cos(\theta-\theta'))^2\sqrt{\frac{\nu}{\pi}}\left(\int_0^t\frac{e^{-\lambda_2^2\nu\zeta-\frac{c^2}{4\nu\zeta}}}{\sqrt{\zeta}}d\zeta-e^{-\delta t}\int_0^t\frac{e^{\delta\zeta-\lambda_2^2\nu\zeta-\frac{c^2}{4\nu\zeta}}}{\sqrt{\zeta}}d\zeta\right)$$

$$-\frac{i\gamma_2 k^2 l\omega}{2}sin(\frac{\theta-\theta'}{2})(1-cos(\theta-\theta'))(1-e^{-\delta t})e^{\lambda_2 c}\Big]e^{ik(\gamma_1 a+\gamma_2 b)}$$

$$d\xi_1(\omega,\theta)\,d\xi_1(-\omega,\theta') \qquad (4.142a)$$

$$v_2^{VDh}=\int_{-\pi}^{+\pi}\int_{-\pi}^{+\pi}\int_{-\infty}^{+\infty}\Big[\gamma_4\omega k|k|(1+kl)(1+cos(\theta-\theta'))\sqrt{\frac{\nu}{\pi}}e^{-\delta t}\int_0^t\frac{e^{\delta\zeta-\lambda_2^2\nu\zeta-\frac{c^2}{4\nu\zeta}}}{\sqrt{\zeta}}d\zeta$$

$$+i\gamma_2\omega k^3 l(1-cos(\theta-\theta'))\sqrt{\frac{\nu}{\pi}}e^{-\delta t}\int_0^t\frac{e^{\delta\zeta-\lambda_2^2\nu\zeta-\frac{c^2}{4\nu\zeta}}}{\sqrt{\zeta}}d\zeta-\frac{i\gamma_2\omega k^3 l}{2}$$

$$(1-cos(\theta-\theta'))^2\sqrt{\frac{\nu}{\pi}}\left(\int_0^t\frac{e^{-\lambda_2^2\nu\zeta-\frac{c^2}{4\nu\zeta}}}{\sqrt{\zeta}}d\zeta-e^{-\delta t}\int_0^t\frac{e^{\delta\zeta-\lambda_2^2\nu\zeta-\frac{c^2}{4\nu\zeta}}}{\sqrt{\zeta}}d\zeta\right)$$

$$-\frac{i\gamma_2 k^2 l\omega}{2}sin(\frac{\theta-\theta'}{2})(1-cos(\theta-\theta'))(1-e^{-\delta t})e^{\lambda_2 c}\Big]e^{ik(\gamma_1 a+\gamma_2 b)}$$

$$d\xi_1(\omega,\theta)\,d\xi_1(-\omega,\theta') \qquad (4.142b)$$

$$w_2^{VDh}=\int_{-\pi}^{+\pi}\int_{-\pi}^{+\pi}\int_{-\infty}^{+\infty}\Big[k^4 l\nu\omega(1-cos(\theta-\theta'))^2\Big((1-cos(\theta-\theta'))$$

$$\int_0^t e^{-\lambda_2^2\nu\zeta}\,Erfc(\frac{|c|}{\sqrt{4\nu\zeta}})d\zeta+(1+cos(\theta-\theta'))\,e^{-\delta t}\int_0^t e^{\delta\zeta-\lambda_2^2\nu\zeta}\,Erfc(\frac{|c|}{\sqrt{4\nu\zeta}})d\zeta\Big)$$

$$-\frac{k^2 l\omega}{2}(1-cos(\theta-\theta'))^2(1-e^{-\delta t})e^{\lambda_2 c}\Big]e^{ik(\gamma_1 a+\gamma_2 b)}\,d\xi_1(\omega,\theta)\,d\xi_1(-\omega,\theta')$$

(4.142c)

Notice now that the above homogeneous solutions satisfy the initial condition (4.135). For $\theta=\theta'=0$ and using the approximation $kl \ll 1$, equation (4.142a) reduces to

$$u_2^{VDh}=\int_{-\infty}^{+\infty} 4\omega k|k|\sqrt{\frac{\bar{\nu}}{\pi}}e^{-\delta t}\int_0^t \left|\frac{e^{\delta\zeta-\frac{\epsilon^2}{4\nu\zeta}}}{\sqrt{\zeta}}d\zeta\right| d\xi_1(\omega)\,d\xi_1(-\omega) \tag{4.143}$$

Using the relation for the monochromatic wave amplitude as in (3.66), u_2^{VDh} can be written as

$$u_2^{VDh}=2A_0^2\omega k^2\sqrt{\frac{\bar{\nu}}{\pi}}e^{-\delta t}\int_0^t \frac{e^{\delta\zeta-\frac{\epsilon^2}{4\nu\zeta}}}{\sqrt{\zeta}}d\zeta \tag{4.144}$$

which is the Weber's solution (1983a, eqn. 6.7) with $\zeta=t-t_1$.

By dropping the $O(k^2l^2)$ terms from the particular solutions (4.127) the horizontal velocities are not significantly changed. We also lose w_2^{VDp}, the particular solution for the vertical velocity (4.127c) (which is $O(k^2l^2)$). This is the limitation of our solution. However, this will effect the total vertical velocity solution w_2^{VD} in an insignificant way because the homogeneous solution for the vertical velocity w_2^{VDh} is of order (kl) whereas the particular solution w_2^{VDp} is of order k^2l^2. The error introduced by dropping $O(k^2l^2)$ terms from w_2^{VDp} solution is estimated to be of order 0.1 to 0.2 % of the total solution which is quite negligible. In the nondecaying wave case (section 4.4.2) the homogeneous solution for the vertical velocity w_2^{VFh} (4.98) (see G in 4.101b) is of order $O(kl)$ whereas the corresponding particular solution w_2^{VFp} (4.82) is of order $O(k^2l^2)$.

The above homogeneous solutions (4.142a-4.142c) are different from those of the viscous nondecaying-wave solutions (4.81) - (4.83) and they decay with depth and time. The solutions of Chang (1969) do not decay with depth (because Chang (1969) chose an

oscillatory root for the solution to her homogeneous equation that satisfies the boundary condition at the surface only). A most interesting point is that the homogeneous decaying wave solutions (4.142) go to zero as viscosity goes to zero implying that the total viscous decaying wave solutions reduce to the inviscid solution as viscosity tends to zero. This is contrary to nondecaying wave case where homogeneous solutions (4.97 and 4.99) do not go to zero as viscosity is set equal to zero (probably because of the applied forcing).

The total solutions for the viscous decaying waves are therefore:

$$u_2^{VD} = u_2^{VDp} + u_2^{VDh}$$

$$u_2^{VD} = \int_{-\pi}^{+\pi}\int_{-\pi}^{+\pi}\int_{-\infty}^{+\infty} \frac{\omega k}{2}(A^{VD}\gamma_3 + iB^{VD}\gamma_1)\, e^{ik(\gamma_1 a+\gamma_2 b)}\, d\xi_1(\omega,\theta)\, d\xi_1(-\omega,\theta') \tag{4.145a}$$

$$v_2^{VD} = v_2^{VDp} + v_2^{VDh}$$

$$v_2^{VD} = \int_{-\pi}^{+\pi}\int_{-\pi}^{+\pi}\int_{-\infty}^{+\infty} \frac{\omega k}{2}(A^{VD}\gamma_4 + iB^{VD}\gamma_2)\, e^{ik(\gamma_1 a+\gamma_2 b)}\, d\xi_1(\omega,\theta)\, d\xi_1(-\omega,\theta') \tag{4.145b}$$

$$w_2^{VD} = w_2^{VDp} + w_2^{VDh}$$

$$w_2^{VD} = \int_{-\pi}^{+\pi}\int_{-\pi}^{+\pi}\int_{-\infty}^{+\infty} \omega k C^{VD}\, e^{ik(\gamma_1 a+\gamma_2 b)}\, d\xi_1(\omega,\theta)\, d\xi_1(-\omega,\theta') \tag{4.145c}$$

where

$$A^{VD} = |\,(1+\cos(\theta-\theta'))\, e^{2|k|c} - 2|k|l(1+\cos(\theta-\theta'))\,\left(\cos\frac{c}{l}+\sin\frac{c}{l}\right) e^{|k|c+c/l}\,]\, e^{-\delta t}$$

$$+2|k|(1+kl)(1+\cos(\theta-\theta'))\sqrt{\frac{\nu}{\pi}}\, e^{-\delta t}\int_0^t \frac{e^{\delta\zeta-\lambda_2^2\nu\zeta-\frac{c^2}{4\nu\zeta}}}{\sqrt{\zeta}}\, d\zeta$$

$$B^{VD} = -2|k|l(1-cos(\theta-\theta'))\,(cos\frac{c}{l}-sin\frac{c}{l})e^{|k|c+c/l}e^{-\delta t}$$

$$+2k^2l(1-cos(\theta-\theta'))\sqrt{\frac{\bar{\nu}}{\pi}}e^{-\delta t}\int_0^t \frac{e^{\delta\zeta-\lambda_2^2\nu\zeta-\frac{c^2}{4\nu\zeta}}}{\sqrt{\zeta}}d\zeta - k^2l$$

$$(1-cos(\theta-\theta'))^2\sqrt{\frac{\bar{\nu}}{\pi}}\left(\int_0^t \frac{e^{-\lambda_2^2\nu\zeta-\frac{c^2}{4\nu\zeta}}}{\sqrt{\zeta}}d\zeta - e^{-\delta t}\int_0^t \frac{e^{\delta\zeta-\lambda_2^2\nu\zeta-\frac{c^2}{4\nu\zeta}}}{\sqrt{\zeta}}d\zeta\right)$$

$$-kl\,sin(\frac{\theta-\theta'}{2})(1-cos(\theta-\theta'))(1-e^{-\delta t})e^{\lambda_2 c}$$

$$C^{VD} = k^3l\nu(1-cos(\theta-\theta'))^2\left((1-cos(\theta-\theta'))\int_0^t e^{-\lambda_2^2\nu\zeta}\,Erfc(\frac{|c|}{\sqrt{4\nu\zeta}})d\zeta\right.$$

$$\left.+(1+cos(\theta-\theta'))\,e^{-\delta t}\int_0^t e^{\delta\zeta-\lambda_2^2\nu\zeta}\,Erfc(\frac{|c|}{\sqrt{4\nu\zeta}})d\zeta\right)$$

$$-\frac{kl}{2}(1-cos(\theta-\theta'))^2(1-e^{-\delta t})e^{\lambda_2 c}\int e^{ik(\gamma_1 a+\gamma_2 b)}\,d\xi_1(\omega,\theta)d\xi_1(-\omega,\theta') \qquad (4.145d)$$

In order to understand the three solutions (e.g., inviscid (3.61, 3.63), viscous with forcing (4.102-4.104) and viscous decaying (4.145a-c)), the second order zero frequency velocities at $a=10m$, $b=10m$ are now plotted as a function of depth. The real part of the velocities are computed for single frequency interaction for amplitude equal to 1 m. (A bigger wave amplitude is possible which will give a larger magnitude for these velocities). Figure (4.3a) shows the plot of a-component of motion against depth of the inviscid u_2^{IN}, viscous decaying u_2^{VD} and viscous nondecaying (forcing) u_2^{VF} solutions. The top plot in Figure 4-3 shows that when $\theta=\theta'=0$ the velocity due to decaying wave solution u_2^{VD} is the largest near the surface. The next largest velocity at the surface is that due to inviscid solution u_2^{IN} which overlaps u_2^{VF}. The viscous nondecaying solution u_2^{VF} generates the smallest of the three velocities near the surface for $\theta=\theta'=0$ interactions. The three solutions tend to

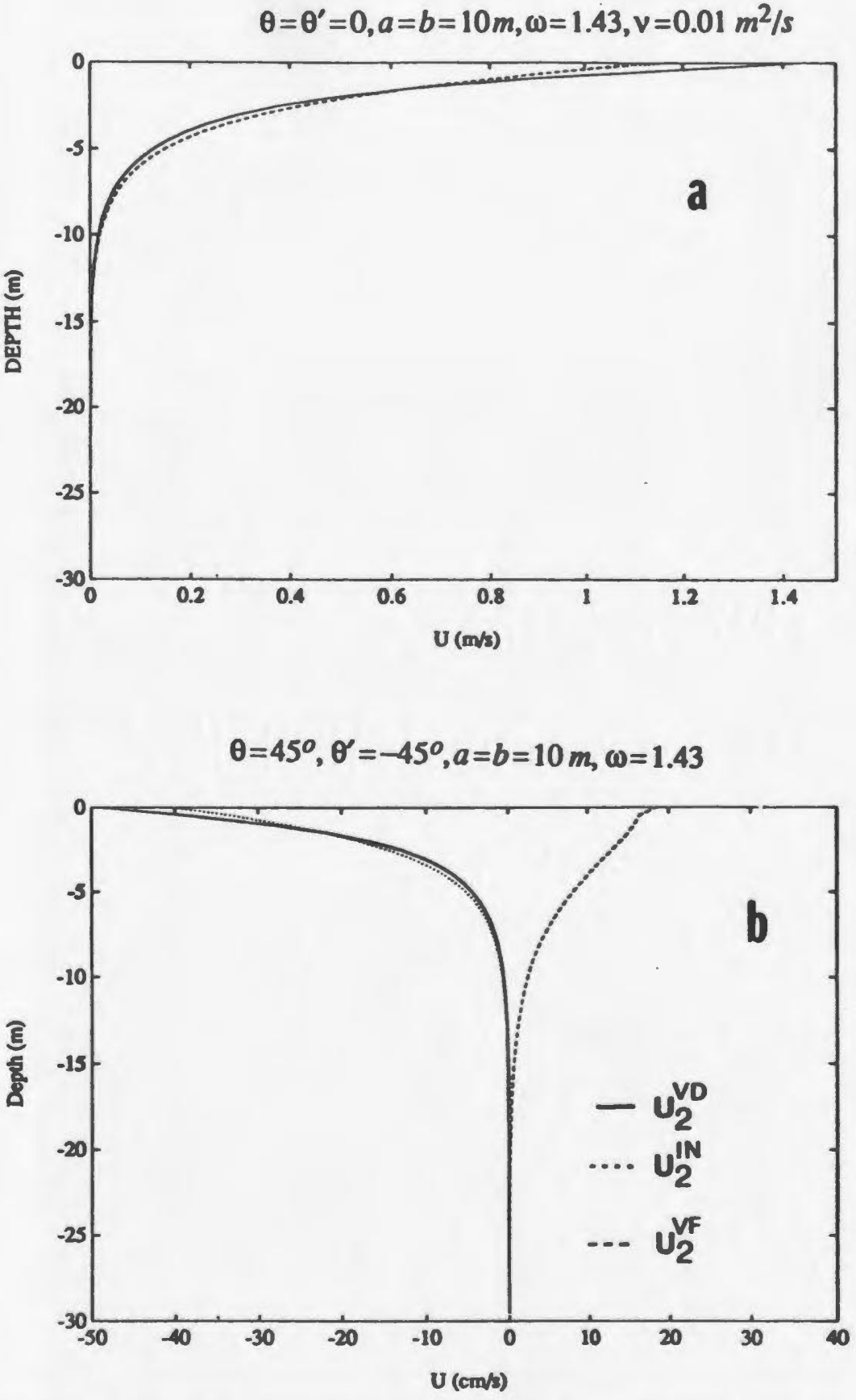

Figure 4-3: Plots of inviscid (3.63, 3.61), viscous nondecaying (4.102-4.104) and viscous decaying (4.145a-c) solutions versus depth. Note that magnitude and direction of the velocities vary as θ and θ′ change. Parameters used in the calculations are shown on the plots.

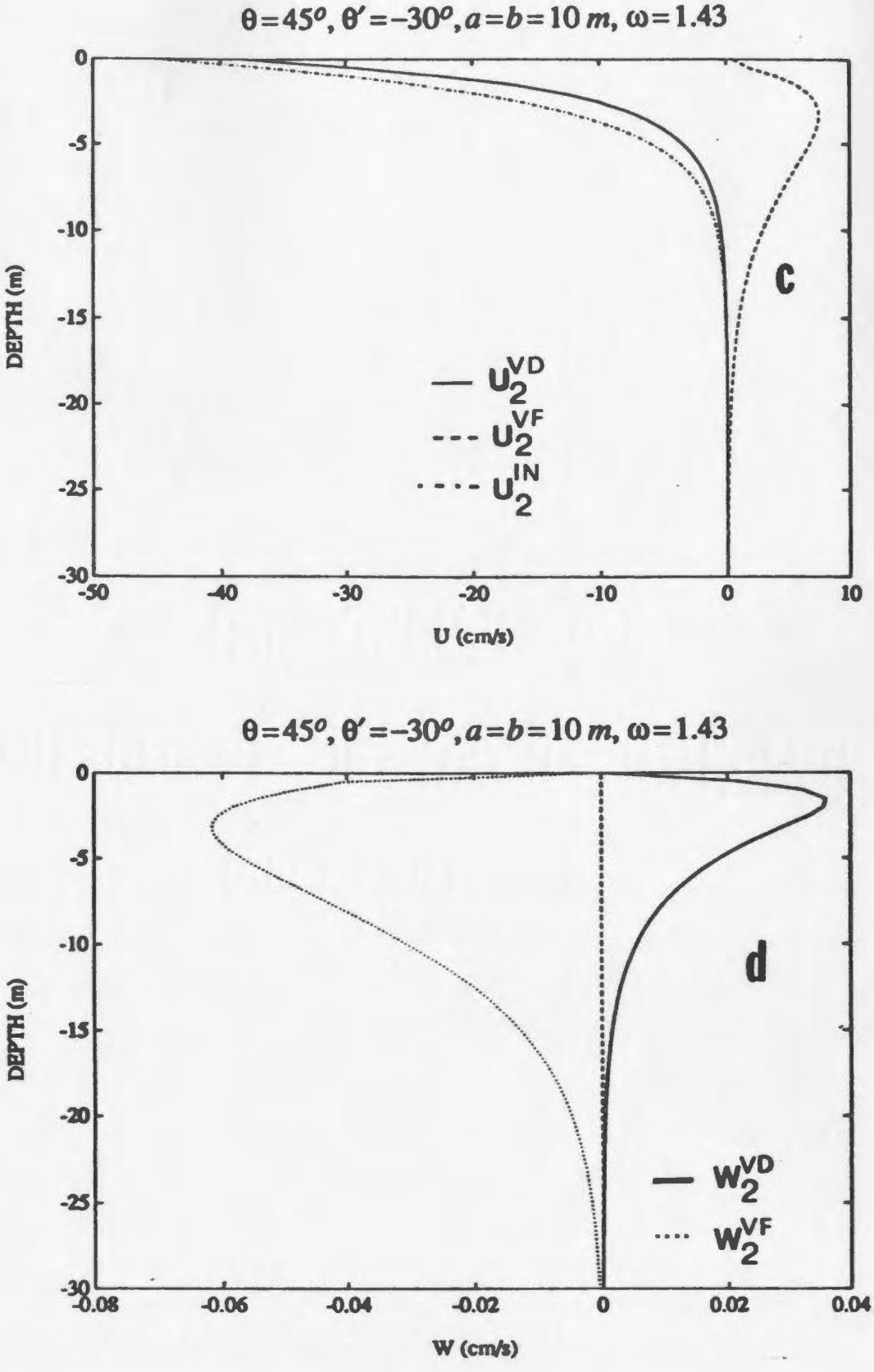

FIGURE 4-3 (CONCLUDED)

converge below the surface. Figures (4.3b) and (4.3c) display the same velocities for the nonzero angles of interaction. In these cases the inviscid u_2^{IN} and viscous decaying u_2^{VD} solutions are almost in phase and of similar magnitude. The viscous nondecaying solution $u_2{}^{VF}$ not only decays more slowly with depth but also has a different direction and amplitude from that of the inviscid and viscous decaying motions. The vertical motions generated by the viscous decaying w_2^{VD} and viscous nondecaying $w_2{}^{VF}$ solutions are at different directions (Fig. 4.3d). The inviscid solution does not give any vertical motion. The vertical motion due to the viscous forcing solution, $w_2{}^{VF}$, is larger than w_2^{VD} and decays more slowly with depth compared to the viscous decaying motion w_2^{VD}.

4.5.3. SUMMARY

The 3-D Lagrangian equations of motion are solved analytically for a homogeneous, nonrotating and viscous ocean. The ocean is considered to be deep so that the waves do not feel the effect of the bottom. The solutions are obtained following two approaches: decaying and nondecaying wave solutions.

The nondecaying wave solutions are based on application of a small external stress (along the vertical direction) that are just enough to maintain the wave against decay. The solutions so obtained decay with depth (but do not decay in time). The solutions show random motion in both horizontal and vertical plane. The horizontal component of the velocity (4.102) reduces to Weber's (1983b) solution as $\theta=\theta'=0$. The total solutions do not reduce to inviscid solutions as the viscosity is set equal to zero.

The decaying wave solutions, on the other hand, decay with both depth and time. The particular solutions of the horizontal motions (4.127a, 4.127b) are similar to nondecaying wave case (4.81, 4.83) for

time t=0. Unlike nondecaying wave case, the time and space dependence of the homogeneous solutions are inseparable. Homogeneous equations are solved by applying Laplace transform following the technique of Weber (1983a). The total horizontal solutions reduce to Weber's (1983a) solutions for the monochromatic wave situation with $\theta=\theta'=0$. The total solutions (4.145a, b) also reduce to inviscid solutions (3.63) and (3.61) when viscosity is set to zero.

The magnitude of the x- component of the viscous decaying wave solution u_2^{VD} is large near the surface for $\theta=\theta'=0$ compared to inviscid u_2^{IN} and viscous decaying solutions u_2^{VD} (Fig. 4.3a). However, for interactions with non-zero angle between the primary waves, u_2^{IN} can cause larger horizontal motion at the surface (e.g., Fig. 4.3c) than that for the viscous solutions. On the other hand, the viscous decaying solution u_2^{VD} and inviscid solution u_2^{IN} decays more quickly with depth compared to viscous nondecaying solution (Fig. 4.3b,4.3c). The zero-frequency vertical velocity for viscous decaying w_2^{VD} and viscous nondecaying u_2^{VF} waves have different directions (Fig. 4.3d,e). Once again, the viscous nondecaying solution w_2^{VF} decays more slowly with depth and penetrates deeper.

Chapter 5

CALCULATION OF EDDY DIFFUSIVITIES

5.1. INTRODUCTION

In the last two chapters it was shown that, surface waves can cause zero-frequency motions in both the horizontal directions and the vertical direction. The zero-frequency velocity of a fluid particle may be viewed as the average velocity of a particle at a given depth for the averaging time large compared with the wave period. It is also averaged over the wave group. Since the wave field consists of a superposition of statistically independent waves, the zero-frequency velocity associated with individual particles will experience fluctuations relative to the mean value for small time. From random walk theory, such random velocity fluctuations can result in a particle dispersion which, for large dispersion times (compared to integral time scale) can be represented as a Fickian diffusion process. Experiments by Schott et al. (1978) show that the horizontal components of diffusion coefficients tend to increase with the increase of the surface wave height. We are now in a position to investigate how the viscous surface waves might contribute to the eddy-diffusion. Herterich and Hasselmann (1982) calculated horizontal components of single-particle, two-particle and patch diffusivities from their solutions for the zero-frequency drift velocities. They did not find solutions resulting in vertical diffusion. In this chapter, we derive expressions for the eddy-diffusivity tensor for single particle, two-particle and cluster of particles following the technique of Herterich and

Hasselmann (1982) and Sanderson and Okubo (1988). The equations for both vertical and horizontal eddy-diffusivities are then integrated numerically by using the Pierson-Moskowitz spectrum (Pierson and Moskowitz, 1964) for a fully developed sea. Eddy-diffusivities from the viscous solutions will then be compared with the eddy-diffusivities from the inviscid solutions.

5.2. MATHEMATICAL DERIVATION

SINGLE-PARTICLE DIFFUSION

The single particle eddy-diffusivity tensor, D_{ij}, for long-time (relative to integral time scale) is defined as

$$D_{ij}=\frac{1}{2}\int_{-\infty}^{+\infty} R_{ij}(\tau)\,d\tau \tag{5.1}$$

$$D_{ij}=\pi G_{ij}(0) \tag{5.2}$$

where

$$R_{ij}(\tau)=\langle u_i'(t+\tau)\,u_j'(t)\rangle \tag{5.3}$$

is the covariance function and

$$G_{ij}(\omega)=\frac{1}{2\pi}\int_{-\infty}^{+\infty} R_{ij}(\tau)\,e^{-i\omega\tau}\,d\tau \tag{5.4}$$

is the cross-spectrum of the particle velocity fluctuations $u'_i=u_i-\langle u_i\rangle$. The angle brackets represent averages over an ensemble of particles. Here u_i ($i=1,2,3$) denotes velocities in the a, b and c directions. As the wave groups propagate by, the velocities of individual water particles fluctuate randomly as functions of space and time.

The integral time scale is a measure of the time interval for which a particle's motion remains correlated to its initial value. Herterich and Hasselmann (1982) argued that for narrow bandwidth

deep water surface gravity waves, the integral time scale is of the order of the inverse of the spectrums' bandwidth. We will use the frequency band appropriate to the Pierson-Moskowitz spectrum [ω = (1.0 - 0.3) 1/s]. Following the argument of Herterich and Hasselmann (1982), this gives an estimation of the range of integral time scale of (1 - 3) s. By definition, the integral covariance time scales are

$$\tau_{ij}=\frac{\int_{-\infty}^{+\infty} R_{ij}(\tau)\,d\tau}{R_{ij}(0)}=\frac{2\pi G_{ij}(0)}{\int_{-\infty}^{+\infty} G_{ij}(\omega)\,d\omega}. \tag{5.5}$$

For t much greater than τ_{ij} the covariance of the positions of an infinite ensemble of particles is

$$<(x_i-<x_i>)(x_j-<x_j>)>=2D_{ij}t \tag{5.6}$$

which increases linearly with time (Taylor, 1921). If t is less than the integral covariance time scale, then the diffusion is non-Fickian and spreading increases proportional to time raised to a power greater than 1. In that case, (5.6) is given by

$$<(x_i-<x_i>)(x_j-<x_j>)>=\int_0^t K_{ij}(t')\,dt' \tag{5.7}$$

where

$$K_{ij}(t')=\int_{-t'}^{t'} R_{ij}(\tau)\,d\tau.$$

In calculating the diffusivity tensor D_{ij}, we shall use the spectral representation (5.2) rather than the correlation integral (5.1). Setting the first-order spectrum to zero at zero frequency, only the

second-order perturbation velocities contribute to the zero-frequency energy density.

Before we proceed to derive the expression for the diffusivity tensor, we will first rewrite the mass transport velocities ($u_{2i}^{IN}, u_{2i}^{VF}, u_{2i}^{VD}$) in a more convenient notation. The second order inviscid solutions (3.63 and 3.61) may be written as

$$u_{2i}^{IN} = \int_{-\pi}^{+\pi}\int_{-\pi}^{+\pi}\int_{-\infty}^{+\infty} \alpha_i^{IN}\, e^{ik(\gamma_1 a + \gamma_2 b)}\, d\xi_1(\omega,\theta)\, d\xi_1(-\omega,\theta') \tag{5.8}$$

where

$$i = 1,2$$

and

$$\alpha_1^{IN} = \frac{\omega k}{2} A^{IN} \gamma_3$$

$$\alpha_2^{IN} = \frac{\omega k}{2} A^{IN} \gamma_4 \tag{5.9}$$

and A^{IN} is given by (3.62) $\gamma_1, \gamma_2, \gamma_3, \gamma_4$ are given by (4.77). Similarly, the second order viscous forced (nondecaying) solutions, u_{2i}^{VF} (4.102-4.104), are expressed as

$$u_{2i}^{VF} = \int_{-\pi}^{+\pi}\int_{-\pi}^{+\pi}\int_{-\infty}^{+\infty} \alpha_i^{VF}\, e^{ik(\gamma_1 a+\gamma_2 b)}\, d\xi_1(\omega,\theta)\, d\xi_1(-\omega,\theta') \tag{5.10}$$

where

$$i=1,2,3 \quad \text{and}$$

$$\alpha_1^{VF} = \frac{\omega k}{2}(A^{VF}\gamma_3 + iB^{VF}\gamma_1)$$

$$\alpha_2^{VF} = \frac{\omega k}{2}(A^{VF}\gamma_4 + iB^{VF}\gamma_2)$$

$$\alpha_3^{VF} = \omega k C^{VF}. \tag{5.11}$$

A^{VF}, B^{VF}, C^{VF} are given by (4.105). Following the same procedure, the second order viscous decaying wave solutions, u_{2i}^{VD} (4.145a-4.145c), can be expressed as

$$u_{2i}^{VD} = \int_{-\pi}^{+\pi}\int_{-\pi}^{+\pi}\int_{-\infty}^{+\infty} \alpha_i^{VD}\, e^{ik(\gamma_1 a+\gamma_2 b)}\, d\xi_1(\omega,\theta)\, d\xi_1(-\omega,\theta') \tag{5.12}$$

where

$$i=1,2,3$$

and

$$\alpha_1^{VD} = \frac{\omega k}{2}(A^{VD}\gamma_3 + iB^{VD}\gamma_1)$$

$$\alpha_2^{VD} = \frac{\omega k}{2}(A^{VD}\gamma_4 + iB^{VD}\gamma_2)$$

$$\alpha_3^{VD} = \omega k C^{VD} \tag{5.13}$$

and A^{VD}, B^{VD}, C^{VD} are given by (4.145d).

The single particle diffusivity tensor for times greater than the integral time scale is given by

$$D_{ij}=\pi G_{ij}(0)=\pi\int_{-\pi}^{+\pi}\int_{-\pi}^{+\pi}\int_{-\infty}^{+\infty}\alpha_{ij}S_1(\omega,\theta)S_1(\omega,\theta')d\omega\,d\theta\,d\theta' \tag{5.14}$$

where

$$\alpha_{ij}=\alpha_i\alpha_j \tag{5.15}$$

$$<d\xi_1(\omega,\theta)d\xi_1{}^*(\omega'',\theta'')>=S_1(\omega,\theta)\,d\omega d\theta\,d\theta' \qquad \omega=\omega'',\theta=\theta'' \tag{5.16}$$

$$<d\xi_1(\omega,\theta)d\xi_1{}^*(\omega'',\theta'')>=0 \quad \textit{otherwise.}$$

The angle brackets represent the ensemble average and the superscript asterisk denotes the complex conjugate. The symbol S_1 represents the wave spectrum. For inviscid motion, the single particle diffusivities, D_{ij}^{IN}, are similar to (5.14) except that α_{ij} is replaced by α_{ij}^{IN} where

$$\alpha_{ij}^{IN}=\alpha_i^{IN}\alpha_j^{IN}. \tag{5.17}$$

Similarly, the single particle diffusivities for viscous forced motion, D_{ij}^{VF}, are similar to (5.14) except that α_{ij} is replaced by α_{ij}^{VF} where

$$\alpha_{ij}^{VF}=\alpha_i^{VF}\alpha_j^{VF}. \tag{5.18}$$

A similar expression holds for viscous decaying diffusivity (D_{ij}^{VD}) where α_{ij} in (5.14) is replaced by α_{ij}^{VD} where

$$\alpha_{ij}^{VD}=\alpha_i^{VD}\alpha_j^{VD}. \tag{5.19}$$

PAIR DIFFUSION

The particle pair diffusion equation is useful for interpreting experiments with clusters of drifters. In such experiments the reference point for single particle diffusion, i.e., ensemble mean velocity, is not always well defined by the finite buoy cluster. A dispersion formulation in terms of pair separations avoids this difficulty. For a pair of particles that are initially separated by a distance r_i, the zero-frequency component of the relative velocity is calculated following Herterich and Hasselmann (1982). Let (a_1, b_1, c_1) and (a_2, b_2, c_2) be the positions of two particles. Then the relative motion between them is given by

$$U_{2i}^{(2)}(r_1, r_2, r_3) = U_{2i}(a_1, b_1, c_1) - U_{2i}(a_2, b_2, c_2) \quad i = 1, 2, 3 \tag{5.20}$$

where

$$(r_1, r_2, r_3) = (a_2 - a_1, b_2 - b_1, c_2 - c_1)$$

To get a picture of the two-particle eddy-diffusivity by varying all the three variables (i.e., a, b, c) is difficult because of the anisotropy of the velocity. Herterich and Hasselmann (1982), Sanderson and Okubo (1988) calculated two-particle eddy-diffusivities only as a function of horizontal separation between a pair of particles. They did not consider separation in the vertical plane in their calculations of two-particle diffusivities. Here we will consider two cases: 1) the two particles are initially at the same depth level but located at two horizontal positions (i.e., horizontal separation) and 2) the two particles are initially in the same vertical plane but separated by a vertical distance (i.e., vertical separation).

CASE 1

Let the two particles be at same depth but at two different horizontal positions given by (a_1, b_1, c_1) and (a_1+r_1, b_1+r_2, c_1). Then the two-particle inviscid velocity, $U_{2i}^{IN(2)}$, is similar to the single particle inviscid velocity U_{2i}^{IN} (5.8) except that $\alpha_i^{IN}; i=1,2$ is replaced by

$$\alpha_i^{IN(2)} = \alpha_i^{IN}\{1 - e^{ik(cos\theta - cos\theta')r_1 + ik(sin\theta - sin\theta')r_2}\}. \qquad (5.21)$$

The inviscid two-particle diffusivity tensor $D_{ij}^{IN(2)}$, is therefore given by (5.14) with α_{ij} replaced by $\alpha_{ij}^{IN(2)}$, where

$$\alpha_{ij}^{IN(2)} = 2\alpha_{ij}^{IN}\{1 - cos|k(cos\theta - cos\theta')r_1 + k(sin\theta - sin\theta')r_2|\}. \qquad (5.22)$$

Following the same technique, the viscous forced two-particle velocities are given by (5.10) with α_i^{VF} replaced by

$$\alpha_i^{VF(2)} = \alpha_i^{VF}\{1 - e^{ik(cos\theta - cos\theta')r_1 + ik(sin\theta - sin\theta')r_2}\} \qquad (5.23)$$

and the forced viscous two-particle diffusivity tensor, $D_{ij}^{VF(2)}$, is given by (5.14) with α_{ij} replaced by $\alpha_{ij}^{VF(2)}$, where

$$\alpha_{ij}^{VF(2)} = 2\alpha_{ij}^{VF}\{1 - cos|k(cos\theta - cos\theta')r_1 + k(sin\theta - sin\theta')r_2|\}. \qquad (5.24)$$

Similarly, for viscous decaying wave motion, the two-particle eddy-diffusivity tensor, $D_{ij}^{VD(2)}$, is given by 5.14 with α_{ij} replaced by $\alpha_{ij}^{VD(2)}$, where

$$\alpha_{ij}^{VD(2)} = 2\alpha_{ij}^{VD}\{1 - cos|k(cos\theta - cos\theta')r_1 + k(sin\theta - sin\theta')r_2|\}. \qquad (5.25)$$

CASE 2

Now consider the situation that the two particles are at same horizontal position but separated by a vertical distance r_3. Let the coordinates of the two particles be (a,b,c_1) and (a,b,c_2). The components of the velocities will then depend on the distance of vertical separation between the two particles. In this case, the inviscid two-particle velocities for a pair of particles separated by a vertical distance $(r_3=c_2-c_1)$ are given by

$$U'^{IN(2)}_{2i}(a,b,r_3)=U^{IN}_{2i}(a,b,c_1)-U^{IN}_{2i}(a,b,c_2) \quad i=1,2,3 \qquad (5.26)$$

and the two-particle viscous diffusion tensor $D'^{IN(2)}_{i,j}$ is given by (5.14) with $\alpha_{i,j}$ replaced by $\alpha'^{IN(2)}_{i,j}$, where

$$\alpha'^{IN(2)}_{i,j}=\alpha'^{IN(2)}_{i}\alpha'^{IN(2)}_{j}$$

and

$$\alpha'^{IN(2)}_{i}=\alpha^{IN}_{i}(c_1)-\alpha^{IN}_{i}(c_1+r_3). \qquad (5.27)$$

Similarly, the viscous forced two-particle diffusion tensor $D'^{VF(2)}_{ij}$ is given by (5.14) with α_{ij} replaced by $\alpha'^{VF(2)}_{ij}$ where

$$\alpha'^{VF(2)}_{i,j}=\alpha'^{VF(2)}_{i}\alpha'^{VF(2)}_{j}$$

and

$$\alpha'^{VF(2)}_{i}=\alpha^{VF}_{i}(c_1)-\alpha^{VF}_{i}(c_1+r_3). \qquad (5.28)$$

Note that pair-diffusivity goes to zero as the separation scale $\mathbf{r} \to 0$.

Following the same procedure, one could also write an expression for the two-particle diffusivity tensor for the viscous decaying waves (5.12). However, the viscous decaying (5.10) and inviscid (5.8) solutions behave somewhat similarly to one another (see Figure 4.3). Besides, the viscous decaying solutions take large computational time since it involves four dimensional integration. Therefore, two-particle, patch- and patch-averaged diffusivities for the viscous decaying wave solutions will not be pursued.

PATCH DIFFUSION

Often in real cases of practical importance one is not interested in the motion of pairs of particles, rather one is interested in the diffusion of the whole patch. In that case one has no recourse other than to consider dispersion relative to the motion of the centroid of the tracer patch. The centroid position and velocity of the patch at a given depth is defined by

$$x_{2i} = \int\int x_{2i} C(a',b')\,da'\,db'$$

$$U_{2i} = \int\int U_{2i} C(a',b')\,da'\,db'$$

where $C(a',b')$ is the normalized tracer concentration (Herterich and Hasselmann, 1982). The motion of a particle relative to the centroid of a patch of material is the same as the single particle case except that α_i is replaced by

$$\alpha_i^{(p)} = \alpha_i \{ 1 - \int\int C(a',b')\, e^{ik(cos\theta - cos\theta')(a'-a) + ik(sin\theta - sin\theta')(b'-b)}\, da'\,db' \}. \tag{5.29}$$

The inviscid eddy-diffusion relative to the patch centroid, $D_{ij}^{IN(p)}$, is given by (5.14) except that α_{ij} is replaced by

$$\alpha_{ij}^{IN(p)} = \alpha_{ij}^{IN}\{1 + cm^2 + sm^2 - 2\,cm\cos[k(\cos\theta - \cos\theta')a + k(\sin\theta - \sin\theta')b] - 2\,sm\sin[k(\cos\theta - \cos\theta')a + k(\sin\theta - \sin\theta')b]\} \quad (5.30)$$

where

$$cm = \int\int C(a',b')\cos[k(\cos\theta - \cos\theta')a' + k(\sin\theta - \sin\theta')b']\,da'\,db' \quad (5.31)$$

$$sm = \int\int C(a',b')\sin[k(\cos\theta - \cos\theta')a' + k(\sin\theta - \sin\theta')b']\,da'\,db'. \quad (5.32)$$

The viscous nondecaying (forced) patch-eddy-diffusivity tensor $D_{ij}^{VF(p)}$, is given by (5.14) with α_{ij} replaced by $\alpha_{ij}^{VF(p)}$ where

$$\alpha_{ij}^{VF(p)} = \alpha_{ij}^{VF}\{1 + cm^2 + sm^2 - 2\,cm\cos[k(\cos\theta - \cos\theta')a + k(\sin\theta - \sin\theta')b] - 2\,sm\sin[k(\cos\theta - \cos\theta')a + k(\sin\theta - \sin\theta')b]\}. \quad (5.33)$$

For very large patch, $cm \to 0$, $sm \to 0$, and $\alpha_{ij}^{IN(p)}$, and $\alpha_{ij}^{VF(p)}$ reduces to α_{ij}^{IN}, and α_{ij}^{VF} respectively. Thus the patch diffusivity tends to single particle diffusivity. As the patch size becomes much smaller than the scale of the surface waves, $cm \to 1$, $sm \to 0$, and the patch diffusivity tends to zero.

Note that the patch diffusivity (5.30 - 5.33) is a function of position within the patch. In experiments, one usually has insufficient data to determine the diffusivity as a function of position within the patch. Rather, it is usual to determine the diffusivity averaged throughout the area of the patch. This patch averaged diffusivity for the inviscid motion, $D_{ij}^{IN(pa)}$, can therefore be calculated from (5.14) by replacing α_{ij} with

$$\alpha_{ij}^{IN(pa)} = \int\int \alpha_{ij}^{IN(p)}(a,b)\, C(a,b)\, da\, db \qquad (5.34)$$

where $\alpha_{ij}^{IN(p)}$ is given by (5.30 - 5.32). Similarly, to obtain the patch-averaged diffusivity for the viscous forced motion, $D_{ij}^{VF(pa)}$, replace α_{ij} in (5.14) with

$$\alpha_{ij}^{VP(pa)} = \int\int \alpha_{ij}^{VF(p)}(a,b)\, C(a,b)\, da\, db \qquad (5.35)$$

where $\alpha_{ij}^{VF(p)}$ given by (5.33).

5.3. NUMERICAL CALCULATION

In order to obtain an estimate of the magnitude of the eddy-diffusivities derived in the previous section, the equations (5.14) are numerically integrated for the cases of single-particle, two-particle and patch diffusion. The wave spectrum is assumed to be separable into a frequency dependent part $f(\omega)$ and an angular spreading part $\Theta(\theta)$ i.e.,

$$S_1(\omega,\theta) = f(\omega)\,\Theta(\theta). \qquad (5.36)$$

The spectrum used in this calculation is the empirical spectrum of Pierson-Moskowitz (1964) for the fully developed sea given by

$$f(\omega) = \alpha_p g^2 \omega^{-5} exp\left[-5/4\left(\frac{\omega_m}{\omega}\right)^4\right] \qquad (5.37)$$

where α_p=0.0081 is the Phillip's constant and ω_m is the peak frequency.

The parameters in (5.37) are chosen from Hasselmann et al. (1973). The peak frequency ω_m is determined by the wind speed U at 19.5 m height above the sea level through the relation

$$\omega_m = 0.140 2\pi g/U. \tag{5.38}$$

The peak frequency of the fully developed Pierson-Moskowitz spectrum for the wind speed $U = 10\ m/s$ is 0.88 rad/s. The angular spreading term $\Theta(\theta)$ is normalized such that

$$\int_{-\pi}^{\pi} \Theta(\theta) d\theta = 1.$$

First, we calculate the single particle eddy-diffusivities as a function of the narrowness of the spreading function $\Theta(\theta)$. Single particle eddy-diffusivities are calculated by numerically integrating equation (5.14) with $S_1(\omega,\theta)$ specified by (5.36) and using Pierson-Moskowitz spectrum (5.37). The narrowness of the spreading function is represented by

$$\begin{aligned} \Theta(\theta) &= A_n \cos^n(\theta) \quad |\theta| < \pi/2 \\ \Theta(\theta) &= 0 \quad \pi/2 < |\theta| > \pi \end{aligned} \tag{5.39}$$

where the exponent n characterizes the narrowness and the coefficient A_n is given by

$$A_n=\frac{2\times4\times6\ldots\times n}{1\times3\times5\ldots\times(n-1)\pi} \quad n \text{ even,}$$

and (5.40)

$$A_n=\frac{1}{2}\frac{1\times3\times5\ldots\times n}{2\times4\times6\ldots\times(n-1)} \quad n \text{ odd.}$$

The infinite range of integration for frequency, ω, is replaced by a finite range from 0.3 to 5.0 *rad/s*. Single-particle eddy-diffusivities for inviscid, viscous forcing and viscous decaying solutions are calculated for two viscosities: 1.0×10^{-6} (i.e., molecular viscosity) and 1.0×10^{-2} m^2/s. The latter viscosity is used by Weber (1985) to calculate the mass transport velocity from the zero frequency interaction of two deep water surface gravity waves. In order to use any large viscosity in our calculation, we must ensure that the viscous length scale l and wave number k satisfy the condition $kl \ll 1$. Using the peak frequency ω_m and $\nu=1.0\times10^{-2} m^2/s$ one finds that $kl=0.01$. It is, therefore, safe to use the latter viscosity in our calculation.

Figure 5.1 plots the single particle diffusivities D_{ii}^{IN}, D_{ii}^{VF} and D_{ii}^{VD} against the directionality parameter n. The inviscid solutions reproduce Herterich and Hasselmann's result (Herterich and Hasselmann, 1982 Fig.1). The inviscid and viscous (forced and decaying) eddy-diffusivities are strongly anisotropic. With the increase of the narrowness parameter n, the eddy-diffusivity in the a- direction increases and in the b-direction decreases. The change in the eddy-diffusivity along b-direction is very small compared to that along the a-direction for the same change in the directionality n. The plot demonstrates that for eddy-viscosity $\nu=0.01\ m^2/s$ the viscous decaying diffusivity D_{11}^{VD} is larger than the inviscid diffusivity D_{11}^{IN} and the viscous forced diffusivity D_{ii}^{VF} by factors of 1.2 and 1.7 respectively at the surface. This can also be seen

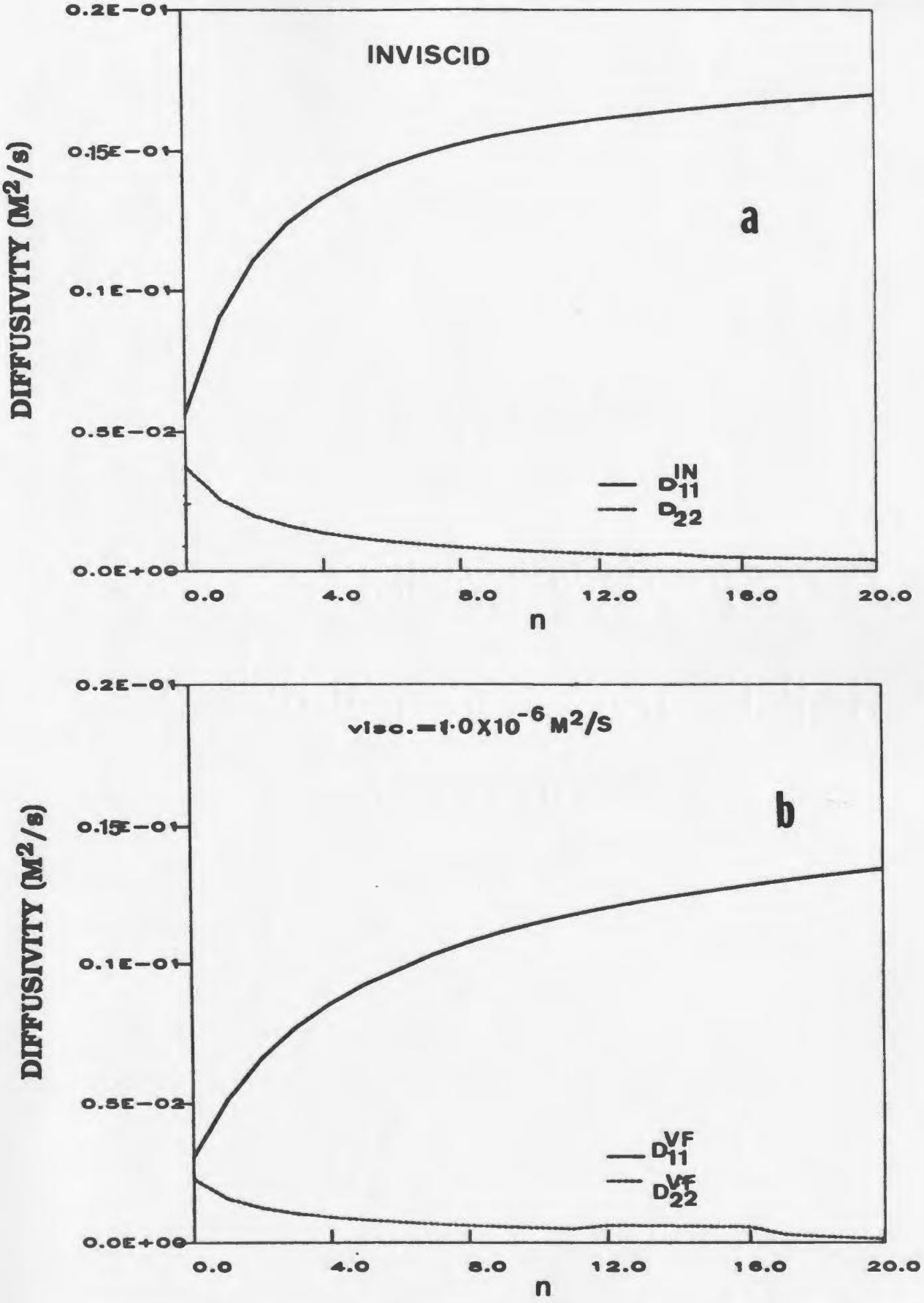

Figure 5-1: Plots of single particle diffusivities as a function of exponent n of the directionality function (eqn. 5.39). (a) inviscid case, (b) D_{ii}^{VF} with viscosity $\nu = 1.0\times10^{-6}\ m^2/s$, (c) D_{ii}^{VF} with viscosity $\nu = 1.0\times10^{-2}\ m^2/s$ and (d) D_{ii}^{VD} with $\nu = 1.0\times10^{-2}\ m^2/s$.

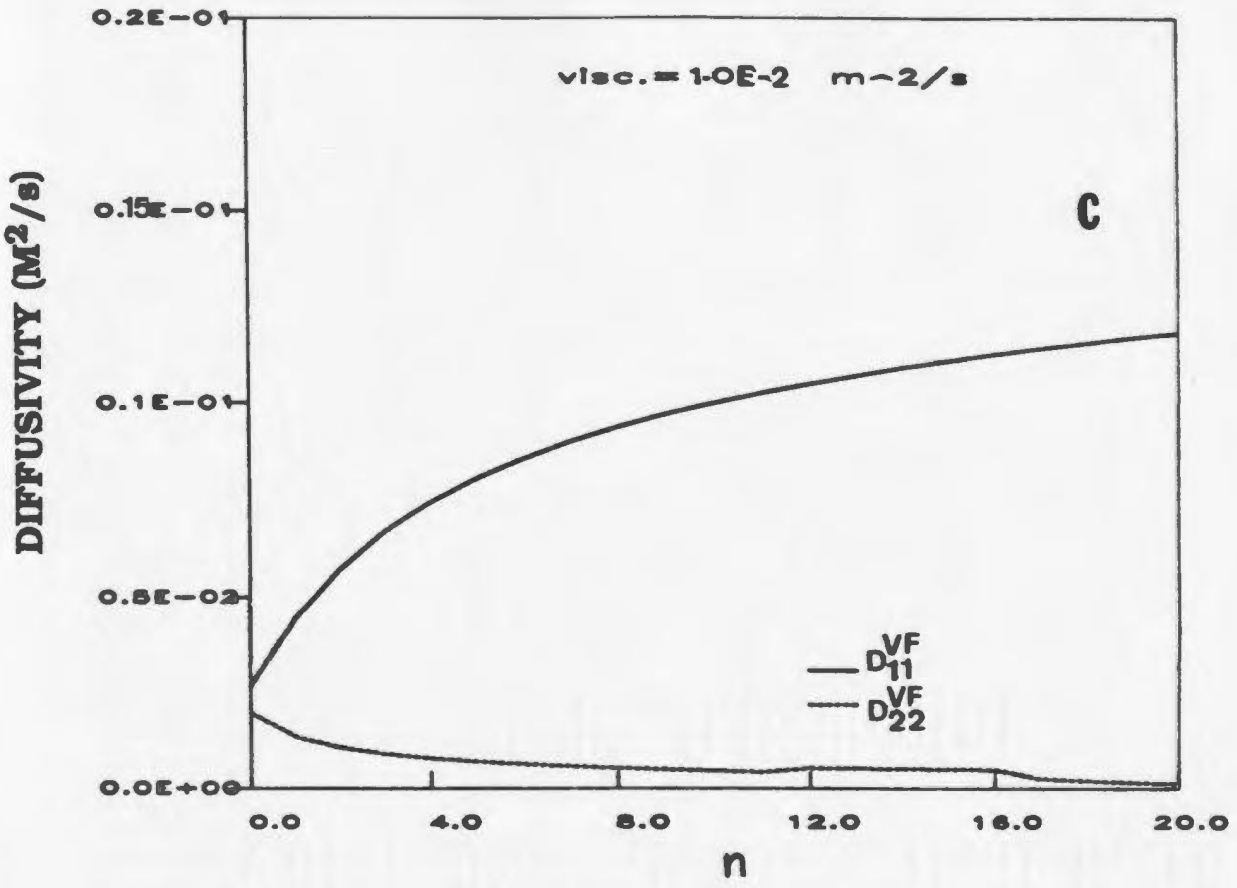

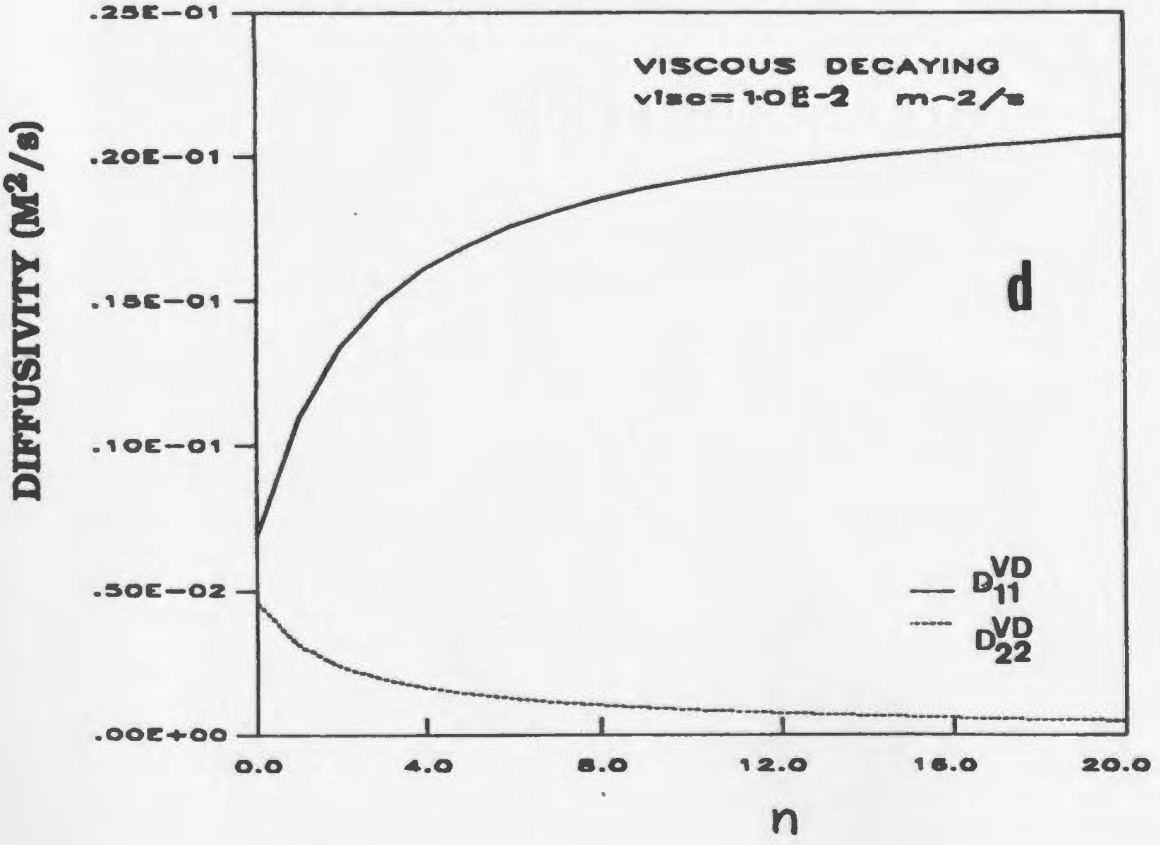

FIGURE 5-1 (CONCLUDED)

in Figure 4.3 which shows that the velocity due to the viscous forcing solution u_2^{VF} is smaller than the inviscid u_2^{IN} and viscous decaying u_2^{VD} velocities. Thus the viscous forced solutions give smaller horizontal diffusivities than the inviscid solutions, whereas the viscous decaying solutions give larger horizontal diffusivities than the inviscid solutions. In the case of viscous forced solutions an increase of viscosity ν by four orders of magnitude resulted in horizontal diffusivities being decreased by less than a factor of 2.

For a symmetrical spreading about the wind direction which we define as the a-axis, $\Theta(\theta)=1/2\pi$. The non-diagonal components of the diffusivity tensor vanish for the isotropic case. Unless explicitly specified we will take $\Theta(\theta)=\frac{1}{2\pi}$ throughout the following work.

One might think that effect of viscosity is felt up to the depth of the viscous length scale l below which viscous and nonviscous solutions merge together. The viscous length scales $l=(2\nu/\omega_m)^{1/2}$ for the two viscosities 1.0×10^{-6} and 1.0×10^{-2} m^2/s are respectively 1.5 cm and 15.0 cm. In order to investigate the depth dependence of the single-particle diffusivities, figure 5.2 plots the horizontal component of eddy-diffusivities against depth for the inviscid and the two viscous cases. The viscous decaying and inviscid diffusivities converge to the same solution slightly below the depth of the viscous length scale. The viscous forcing diffusivity D_{ii}^{VF} decays more slowly with depth until it converges with the inviscid and viscous decaying diffusivities at a depth of about 10 m. The e-folding depth for the inviscid diffusivity (which is half the Stokes' depth $=1/(2\times k_m)$) is about 3.3 m. Also recall that the total viscous forcing solutions (4.102-4.104) do not reduce to inviscid solutions (3.63, 3.61) as viscosity tends to zero. But the viscous decaying solutions (4.145) go to inviscid solution when viscosity is set equal to zero. The primary effect of viscosity in the viscous decaying solution is to create additional shear

and diffusion near the surface, but otherwise to leave things unchanged from the inviscid case.

The Pierson-Moskowitz spectrum (5.37) is dependent upon wind speed through the relation (5.37). It is, therefore, a matter of interest to investigate how the eddy-diffusivities depend on the wind speed U. For the given Pierson-Moskowitz spectrum (5.37) together with (5.38), the horizontal eddy-diffusivity (5.14) may be expressed as

$$D_{ij}=0.37\,\alpha_p{}^2\frac{U^3}{g}\overline{D}_{ij} \qquad (5.40)$$

$$i,j=1,2$$

where $\overline{D}_{ij}$ is a nondimensional diffusivity. Substituting equation (5.17) into (5.14) and applying transformation of variables, the inviscid non-dimensional diffusivity $\overline{D}_{ii}^{IN}$ is given by

$$\overline{D_{ii}{}^{IN}}=\int_{-\pi}^{+\pi}\int_{-\pi}^{+\pi}\int_{0}^{+\infty} y^2\gamma_k{}^2(1+cos(\theta-\theta'))^2 e^{-\frac{5}{2}y^4+\frac{4\omega_m{}^2 c}{gy^2}}\,dy\,d\theta\,d\theta' \qquad (5.41a)$$

where

$$i=1,2\quad k=3,4\quad \text{and}$$

$$y=\frac{\omega_m}{\omega}. \qquad (5.41b)$$

Thus the horizontal eddy-diffusivity increases with wind speed raised to the power of 3. Herterich and Hasselmann (1982) also obtained a similar power law between the wind speed and the inviscid eddy-diffusivity from dimensional arguments. However, their relation has a printing mistake (Herterich and Hasselmann, 1982, eqn. 3.5; g appears as multiplicative constant instead of division) that makes it dimensionally incorrect. Nevertheless Herterich and Hasselmann (1982) do give the correct

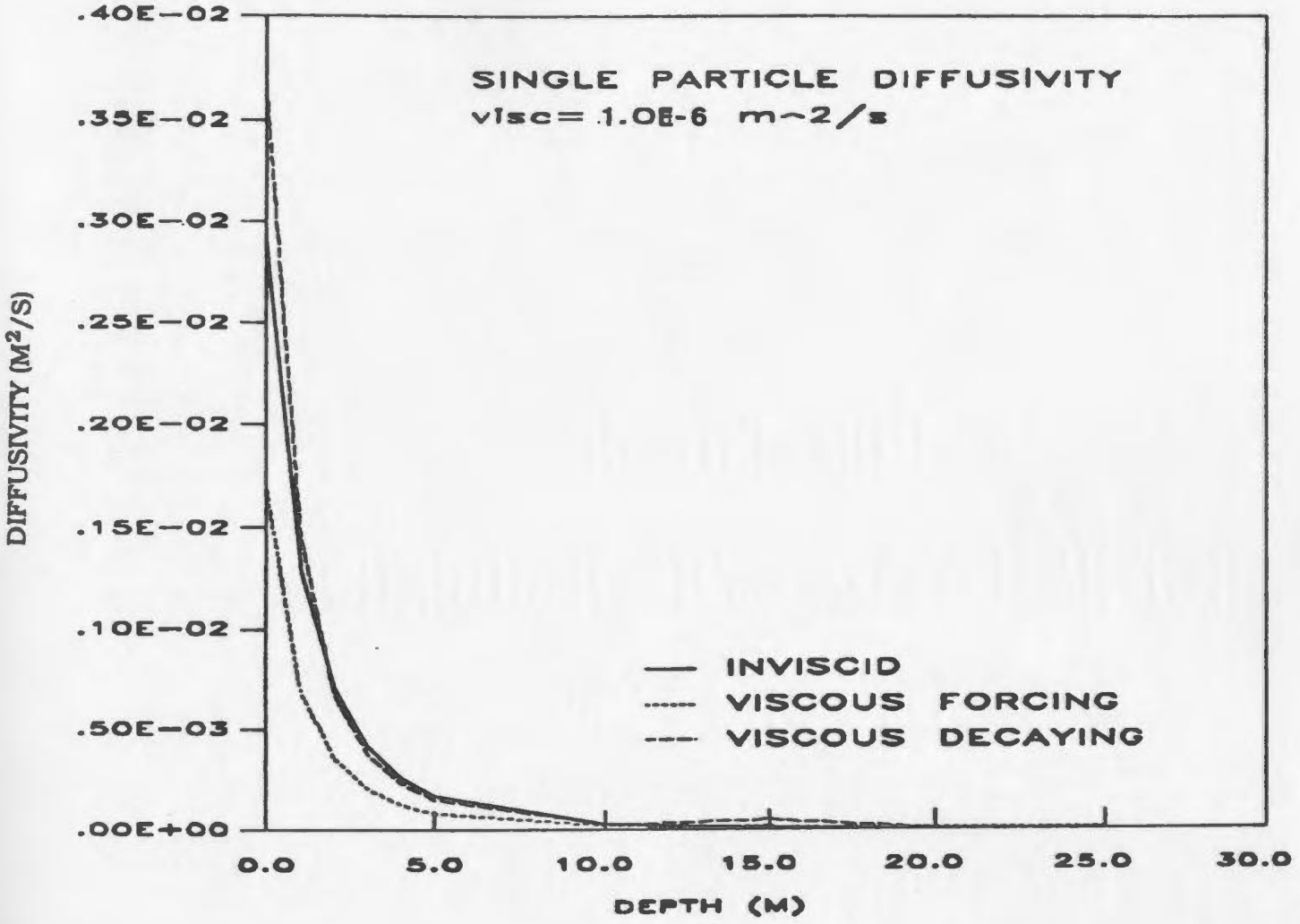

Figure 5-2: Single-particle diffusivity D_{ii}^{IN}, D_{ii}^{VF}, D_{ii}^{VD} plotted as a function of depth for $\nu = 1.0\times10^{-6}\ m^2/s$ and t=100s.

exponent for U. A similar power law holds between the viscous forced eddy-diffusivity D_{ii}^{VF} and the wind speed U. Figure 5.3 shows the plot of the a-component of the inviscid and viscous forced eddy-diffusivities (D_{11}^{IN}, D_{11}^{VF}) as a function of wind speed. A full expression for the non-dimensional diffusivity, $\overline{D_{ii}^{VF}}$ (which involves a large number of terms), is avoided for the sake of brevity. Keeping only the dominant terms, the nondimensional form of the viscous forcing horizontal diffusivity $\overline{D_{ii}^{VF}}$ is given by

$$\overline{D_{ii}^{VF}} \approx \int_{-\pi}^{+\pi}\int_{-\pi}^{+\pi}\int_{0}^{+\infty} y^2 \left[\gamma_k{}^2(1+\cos(\theta-\theta'))^2 e^{\frac{4\omega_m{}^2 c}{gy^2}} + 2\gamma_k{}^2(1-\cos(\theta-\theta')) e^{\frac{4\omega_m{}^2\phi c}{gy^2}} - \frac{2\sin^2(\theta-\theta')\gamma_k{}^2}{\phi} e^{\frac{2\omega_m{}^2 c(1+\phi)}{gy^2}} \right] e^{-\frac{5}{2}y^4}\, dy\, d\theta\, d\theta' \tag{5.42}$$

From Figure 5.3, the slope of the lines is observed to be 3.

The vertical component of the eddy-diffusivities $D_{33}{}^{VF}$ and $D_{33}{}^{VD}$ are calculated by using (5.14) with α_{ij} replaced by (5.18) and (5.19) respectively. Once again the Pierson-Moskowitz spectrum (5.37) is used. The vertical component of the viscous forced eddy-diffusivity $D_{33}{}^{VF}$ depends on depth c, viscosity ν (through l), and on wind speed U. The vertical component of the viscous decaying eddy-diffusivity depends on all of the above mentioned parameters and time t. First, we will investigate how the vertical component of the eddy-diffusivities $D_{33}{}^{VF}$ and $D_{33}{}^{VD}$ (viscous forcing and viscous decaying) compare to one another. Figure 5.4 plots $D_{33}{}^{VF}$ and $D_{33}{}^{VD}$ as a function of depth. The vertical component of the viscous decaying eddy-diffusivity $D_{33}{}^{VD}$ is zero at the surface and increases up to a depth of 1 m. Below this depth, $D_{33}{}^{VD}$ decreases with the increase of depth. The viscous forcing eddy-

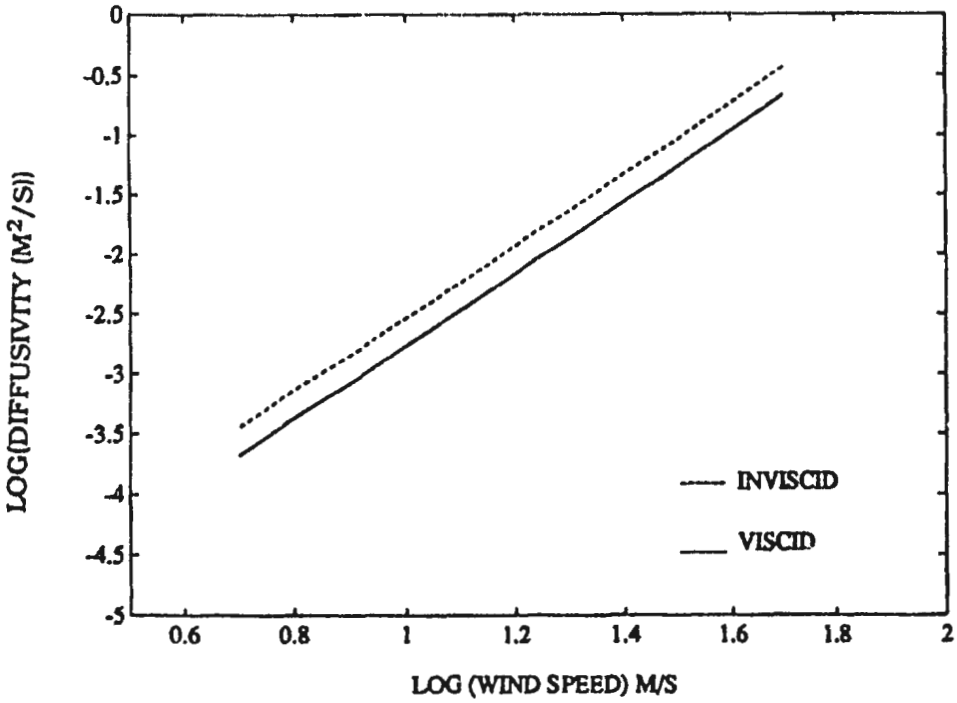

Figure 5-3: Single-particle diffusivities D_{11}^{IN} and D_{11}^{VF} plotted as a function of wind speed U. The following parameters are used : c=0, $\nu = 1.0\times10^{-6}\, m^2/s$.

diffusivity, D_{33}^{VF}, is also zero at the surface and reaches a maximum value at a depth of about 4 m below the surface. It decays more slowly with depth than the viscous decaying eddy-diffusivity D_{33}^{VD}. Note that D_{33}^{VF} and D_{33}^{VD} are smaller than the eddy-viscosity ν by magnitudes of approximately 4 decades and 6 decades respectively.

Since the viscous nondecaying diffusivity D_{33}^{VF} has larger magnitude and also penetrates deeper in the water column than that of the D_{33}^{VD}, the behaviour of the former diffusivity is further investigated.

The vertical component of the viscous forcing eddy-diffusivity D_{33}^{VF} consists of terms that are contributed from both particular and homogeneous solutions. In order to find the dominant terms in D_{33}^{VF}, D_{33}^{VF} may be written explicitly by using (5.14) and (5.18)

$$D_{33}^{VF} = \pi \int_{-\pi}^{\pi} \int_{-\pi}^{\pi} \int_{0}^{\infty} \omega^2 k^2 C^{VF^2} S_1(\omega,\theta) S_1(\omega,\theta') \, d\omega \, d\theta \, d\theta'$$

$$= term1 + term2 + term3 \qquad (5.43)$$

where C^{VF} is given by (4.105). Taking the square of C^{VF} and rearranging

$$term1 = \pi \int_{-\pi}^{\pi} \int_{-\pi}^{\pi} \int_{0}^{\infty} \omega^2 c^2 k^4 \phi^2 G^2/4 \; e^{4k\phi c} S_1(\omega,\theta) S_1(\omega,\theta') \, d\omega \, d\theta \, d\theta'$$

$$term2 = \pi \int_{-\pi}^{\pi} \int_{-\pi}^{\pi} \int_{0}^{\infty} 2k^5 f^2 \omega^2 c \, \phi G \, e^{2k\phi c} S_1(\omega,\theta) S_1(\omega,\theta')$$

$$\left(-(1-cos(\theta-\theta'))^2 \cos\frac{c}{l} e^{|k|c+c/l} + (1-cos(\theta-\theta'))^2 \, e^{2k\phi c} \right) d\omega \, d\theta \, d\theta',$$

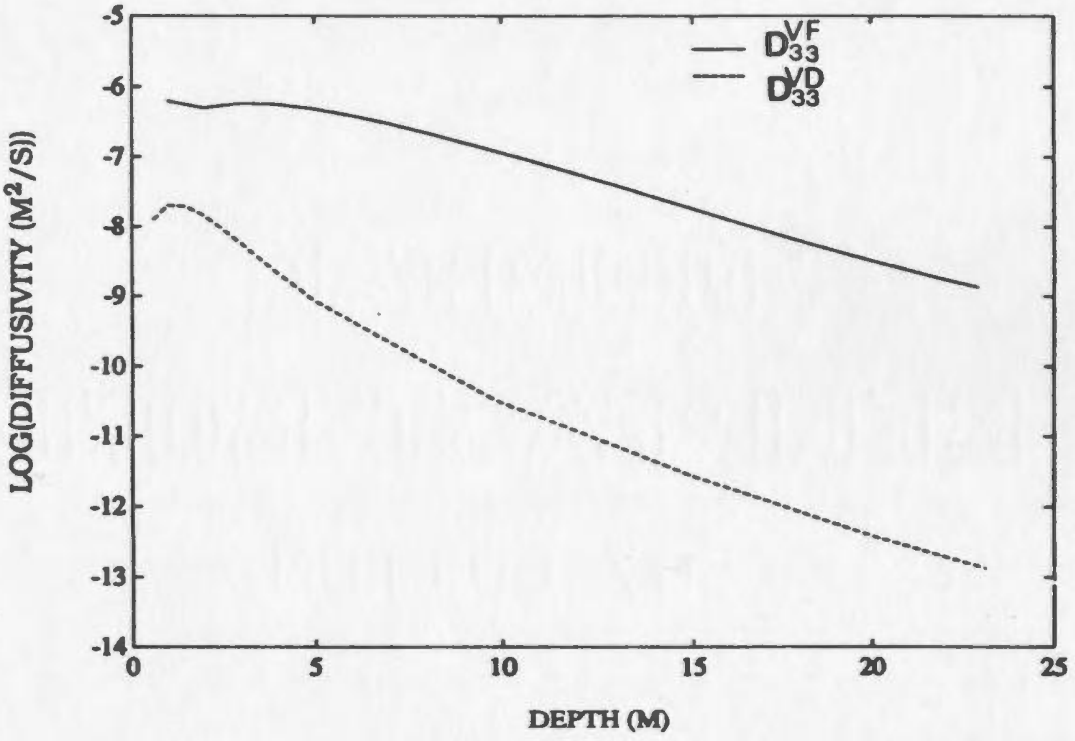

Figure 5-4: Single-particle vertical diffusivities D_{33}^{VF} and D_{33}^{VD} plotted as a function of depth. The following parameters were used : $U = 10\ m/s$, $\nu = 1.0\times10^{-2}\ m^2/s$, t= 100 s

$$term3=\pi\int_{-\pi}^{\pi}\int_{-\pi}^{\pi}\int_{0}^{\infty} 4\,\omega^2 k^6 l^4 S_1(\omega,\theta)S_1(\omega,\theta')$$

$$\left(-(1-cos(\theta-\theta'))^2 cos\frac{c}{l}\,e^{|k|c+c/l}+(1-cos(\theta-\theta'))^2\,e^{2k\phi c}\right)^2 d\omega d\theta d\theta'. \tag{5.44}$$

The constant G is given by (4.101b) and *term*1, *term*2, *term*3 represent contributions from different terms in (5.43) grouped in ascending powers of (kl).

Figure (5.5) shows the plot's of different terms in D_{33}^{VF} as a function of c for viscosity $\nu=1.0\times10^{-6}m^2/s$. Total contribution from all three terms are also shown on the same plot (Fig. 5.5). First note that the vertical eddy-diffusivity is much smaller than the viscosity. The top curve is due to *term*1 and to within the plots resolution it over lies the diffusivity obtained from all three terms. The other two lines are due to *term*2 and *term*3. It is clear on the plot that the main contribution to the vertical diffusivity comes from the *term*1 which constitutes the homogeneous part of the solution. Recall that the homogeneous solution (4.98) has a term which is of $O(kl)$ (G, 101b) and the rest of the terms are of $O(kl)^2$ or higher, therefore, much smaller. Equation (5.43) may, therefore, be simplified by keeping only *term*1 and dropping remaining terms in (5.44). This analysis also supports our previous assumption in section 4.5.2 that the particular solution (4.127c) of second order viscous decaying waves is negligible compared to the homogeneous solution that forms the dominant part in the total solution (4.145c) of the viscous decaying problem.

From equations (5.43) and (5.44) it is clear that the vertical eddy-diffusivity D_{33}^{VF} is a function of viscosity, wind speed and depth. The depth dependence is shown in Figure 5.5, in which D_{33}^{VF} (top line) is

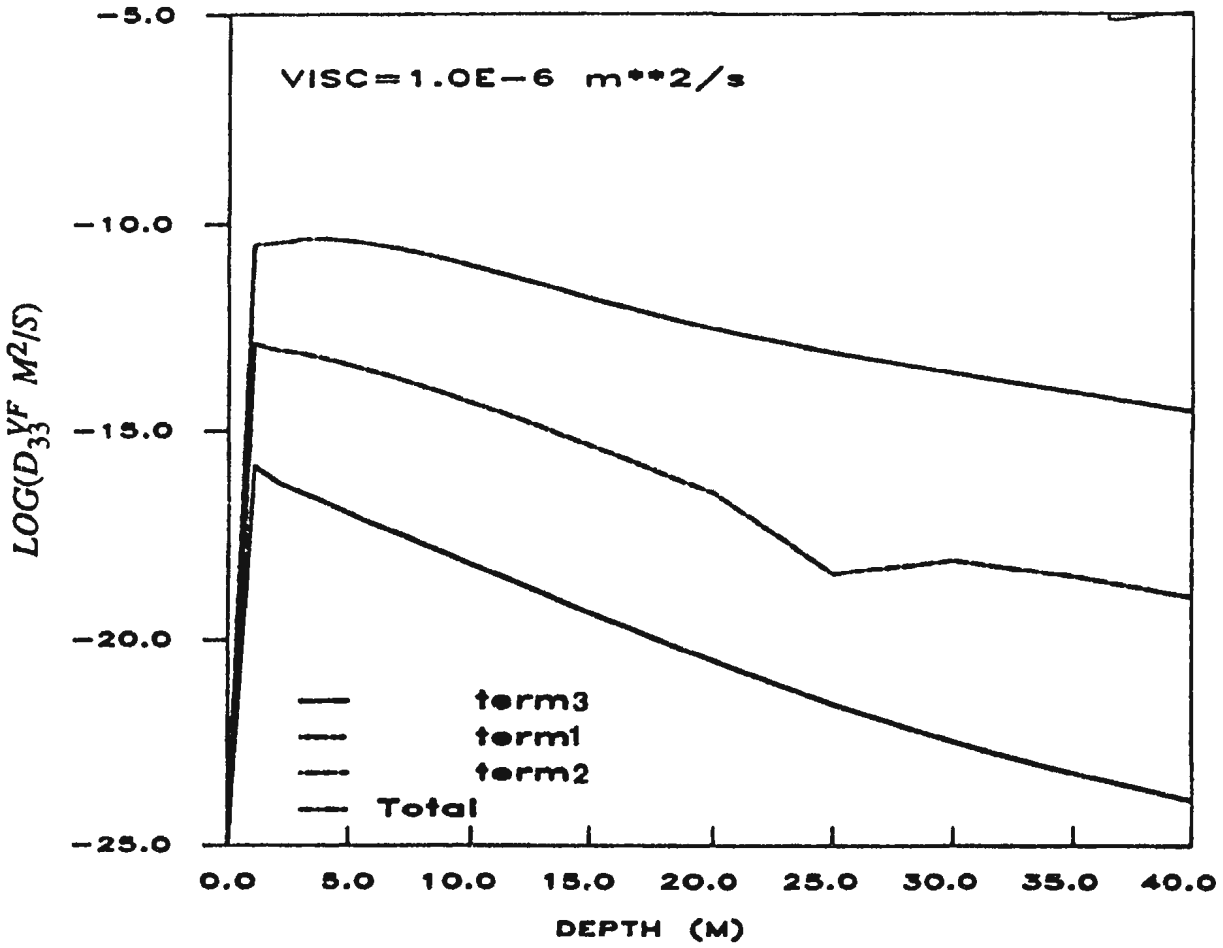

Figure 5-5: Single-particle diffusivities D_{33}^{VF} as function of depth for $\nu = 1.0 \times 10^{-6}$ m^2/s. Contributions from different terms in (5.44) are shown. The top line corresponds to *term*1 and total D_{33}^{VF}. The middle line (dashed) and the bottom line (solid) are due to *term*2 and *term*3 respectively.

plotted as a function of c. As expected, the vertical diffusivity D_{33}^{VF} is zero at the surface and increases to a maximum value at about 4 m depth. Beyond this depth D_{33}^{VF} decreases monotonically with depth c (Figure 5.5, top line). The effect of varying the viscosity ν appears in Figure 5.6 where D_{33}^{VF} is plotted as a function of viscosity ν. The plot also demonstrates how the different terms in equation (5.43) contribute to the vertical diffusion. Figure 5.6 again demonstrates that total diffusivity D_{33}^{VF} (the top line) is mainly due to *term*1. The slope of the total D_{33}^{VF} line (top line) is unity. The apparent deviation from the straight line (towards the end of the top line, Figure 5.6) indicates that *term*2 and *term*3 become important as ν increases. Nevertheless, the condition that $kl \ll 1$ imposes a limitation on the maximum value of ν that can be used in our calculation of eddy-diffusivities. Thus it reassures our previous conclusion that dropping the $O(kl)^2$ terms does not affect the accuracy of our solution.

As the wind speed increases, the peak of the Pierson-Moskowitz spectrum shifts towards the low frequency end of the spectrum. The dependence of vertical eddy-diffusivity D_{33}^{VF} on the wind speed U is shown in Figure 5.7. The vertical eddy-diffusivity D_{33}^{VF} increases rapidly with the wind speed up to $U=10\ m/s$. Beyond that speed, D_{33}^{VF} increases slowly with U with a tendency to saturate after $U=20\ m/s$. Experiments by Kullenberg (1971) also show that vertical diffusivity increases with wind speed.

An order of magnitude estimate of the vertical eddy-diffusivity may be done using a scaling argument. For a random wave field characterized by a narrow spectrum of bandwidth $\Delta\omega=1.0-0.3\ s^{-1}$, the integral time scale $\tau\sim(\Delta\omega)^{-1}$. The vertical velocity w roughly scales as $\langle w\rangle\approx(kl)\langle u\rangle$. Taking $\langle u\rangle=0.1-0.2\ m/s$, $\nu=0.01\ m^2/s$ and using $D_{33}\approx\langle w^2\rangle\tau$ for the vertical eddy-diffusivity we have $D_{33}=2\times10^{-6}-7\times10^{-5}\ m^2/s$. This is

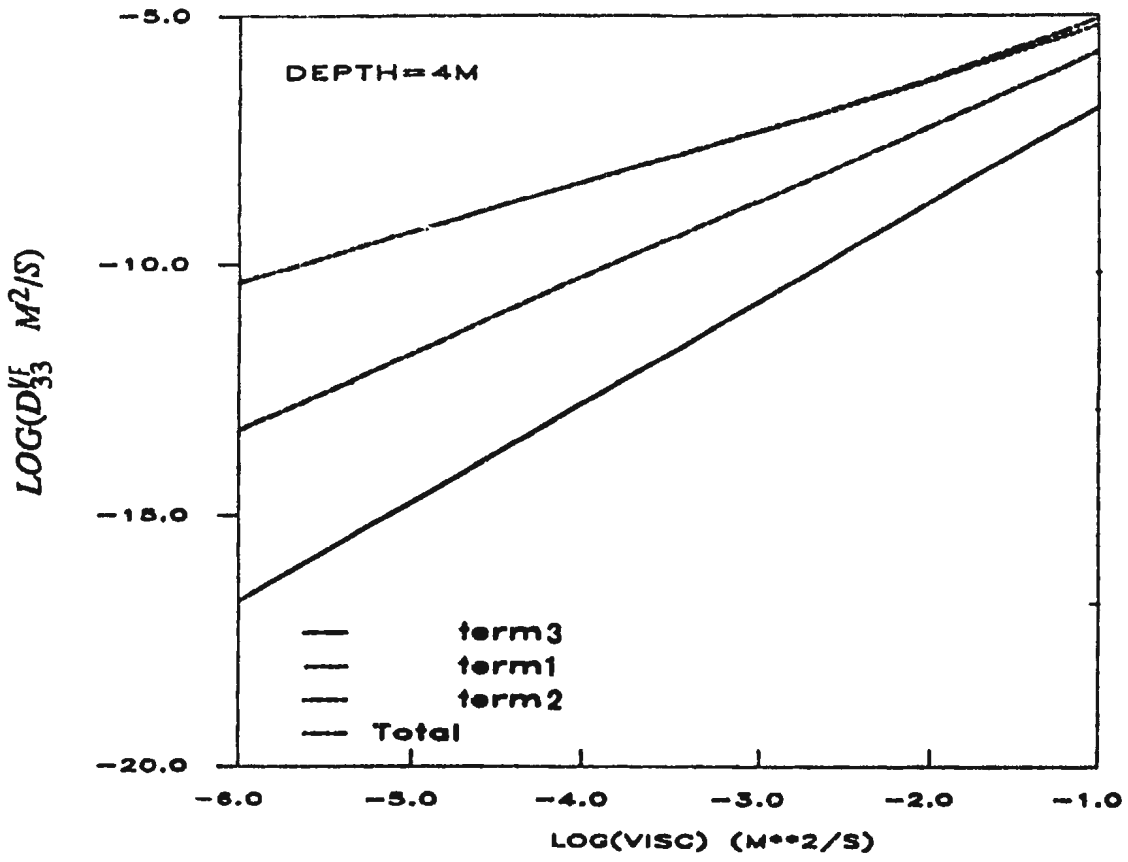

Figure 5-6: Plots of D_{33}^{VF} versus viscosity for depth c=-4.0 m. The top line corresponds to *term*1 and total D_{33}^{VF}. The middle line (dashed) and the lowest line (solid) are due to *term*2 and *term*3.

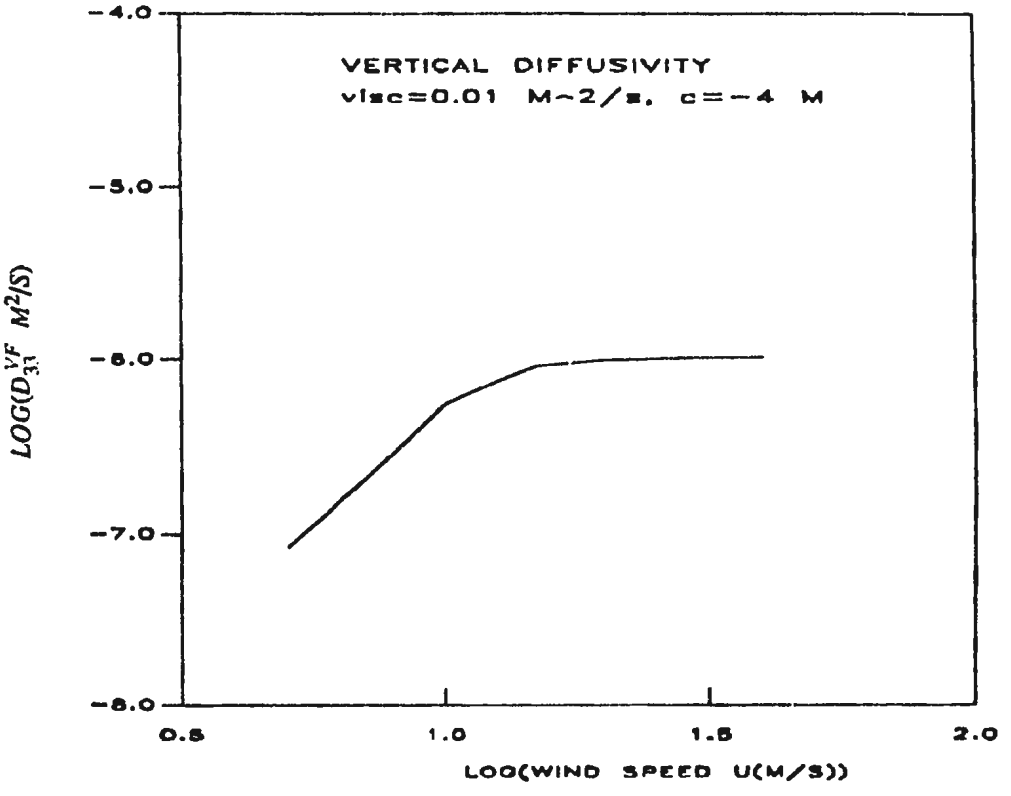

Figure 5-7: Plot of single-particle vertical diffusivity D_{33}^{VF} as a function of wind speed U.

comparable with the orders of magnitudes of the vertical eddy-diffusivity obtained by the numerical integration of equation (5.43) (see Fig. 5.4).

The two-particle diffusivities are calculated both as a function of horizontal separation r and vertical separation r_3 for the inviscid and viscous forcing solutions. For the horizontal diffusivities, we will consider depth c=0.0. Single-particle diffusivity is plotted (Fig. 5.8) as a straight line since separation scale has no meaning for single particle diffusivity. For two-particle and patch diffusivity, the separation in the b direction is set to zero. Figure 5.8 displays the plots of inviscid D_{11}^{IN} and viscous forcing D_{11}^{VF} diffusivities as a function of horizontal separation r. Patch-diffusivities are calculated only for horizontal separation r. For patch-diffusion, r is the distance of a particle from the centroid of the patch. The patch diffusion is computed for an isotropic, normalized Gaussian tracer concentration

$$C(a,b)=\frac{1}{2\pi\lambda^2}exp\left[-(a^2+b^2)/(2\lambda^2)\right] \tag{5.46}$$

with a horizontal scale given by λ centered at the origin of the coordinate system. The patch scale λ is chosen as 200 m. This will ensure that the patch is neither sufficiently small for the patch to move as a single particle (single particle diffusion limit), nor sufficiently large for the two particle diffusion limit. Choosing b=0, (5.30) becomes

$$\alpha_{ij}^{IN(p)}=\alpha_{ij}^{IN}\left\{1+cm^2-2cm\cos\left[k(\cos\theta-\cos\theta')a\right]\right\} \tag{5.47}$$

where

$$cm=exp\left[-k^2\lambda^2(1-\cos(\theta-\theta'))\right]$$

A similar expression holds for $\alpha_{ij}^{VF(p)}$. From Figure 5.8, the two-particle diffusivity is twice the single particle diffusivity and the patch-diffusivity is in between the two- and single- particle diffusivities.

However, when the two particles designated by (a_1,b_1,c_1) and (a_1,b_1,c_2) are separated by a vertical distance, we get a different result.

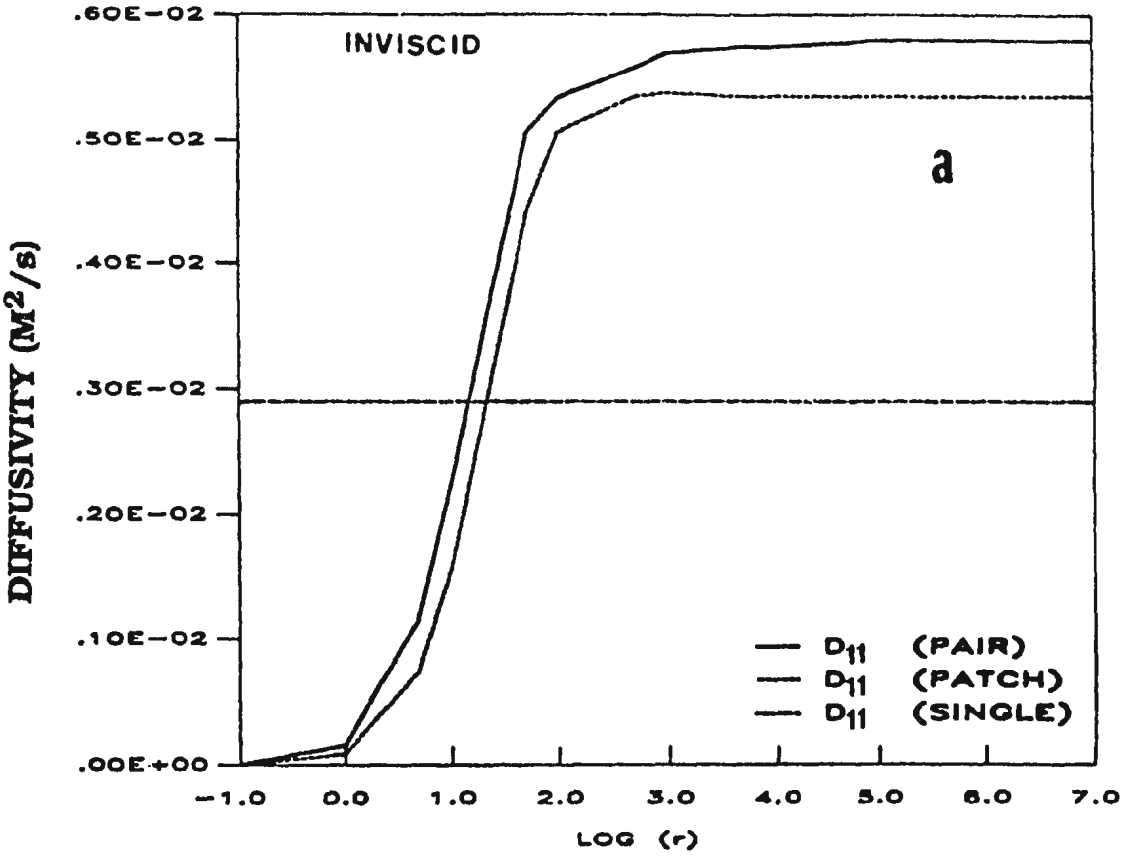

Figure 5-8: Single-particle, two-particle and patch-diffusivity plotted as a function of horizontal separation scale r. (a) inviscid case, (b) viscous forcing with $\nu=1.0\times10^{-2}$ m^2/s and (c) viscous forcing with $\nu=1.0\times10^{-2}$ m^2/s. Parameters used were $c=0.0$, $\lambda=200$ m.

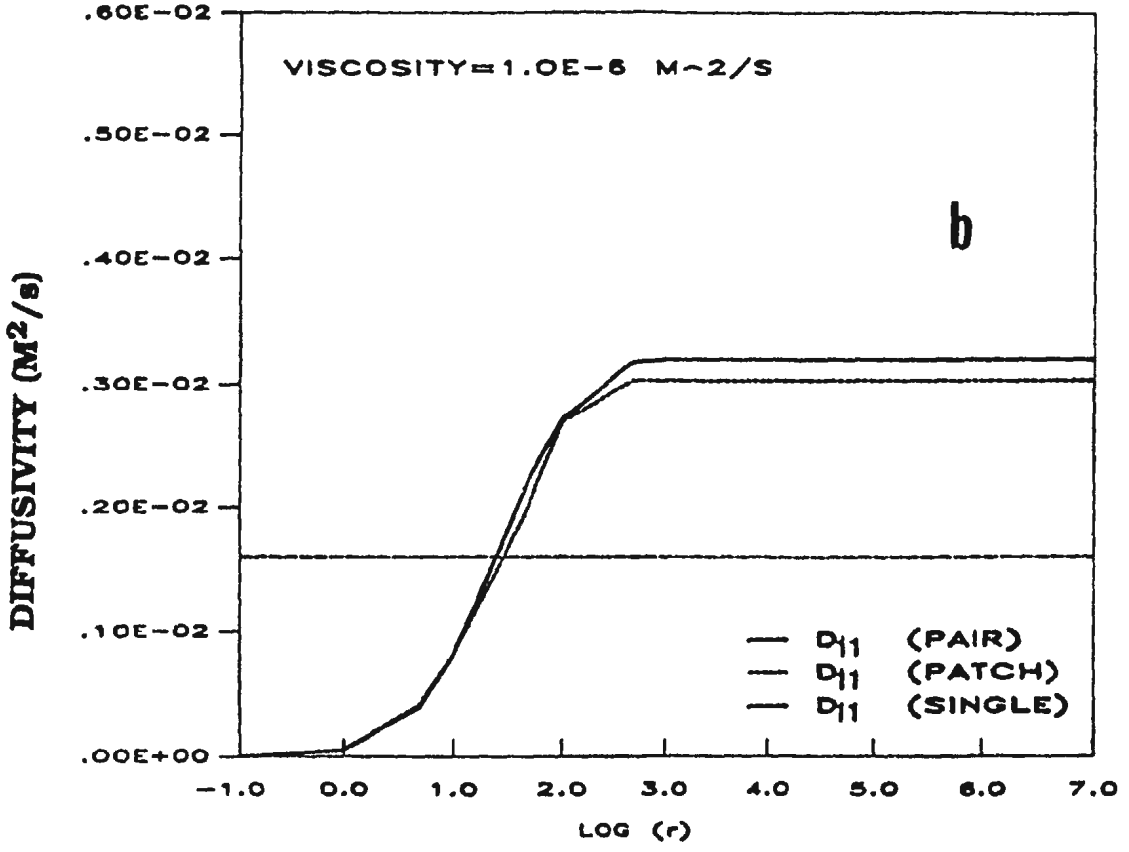

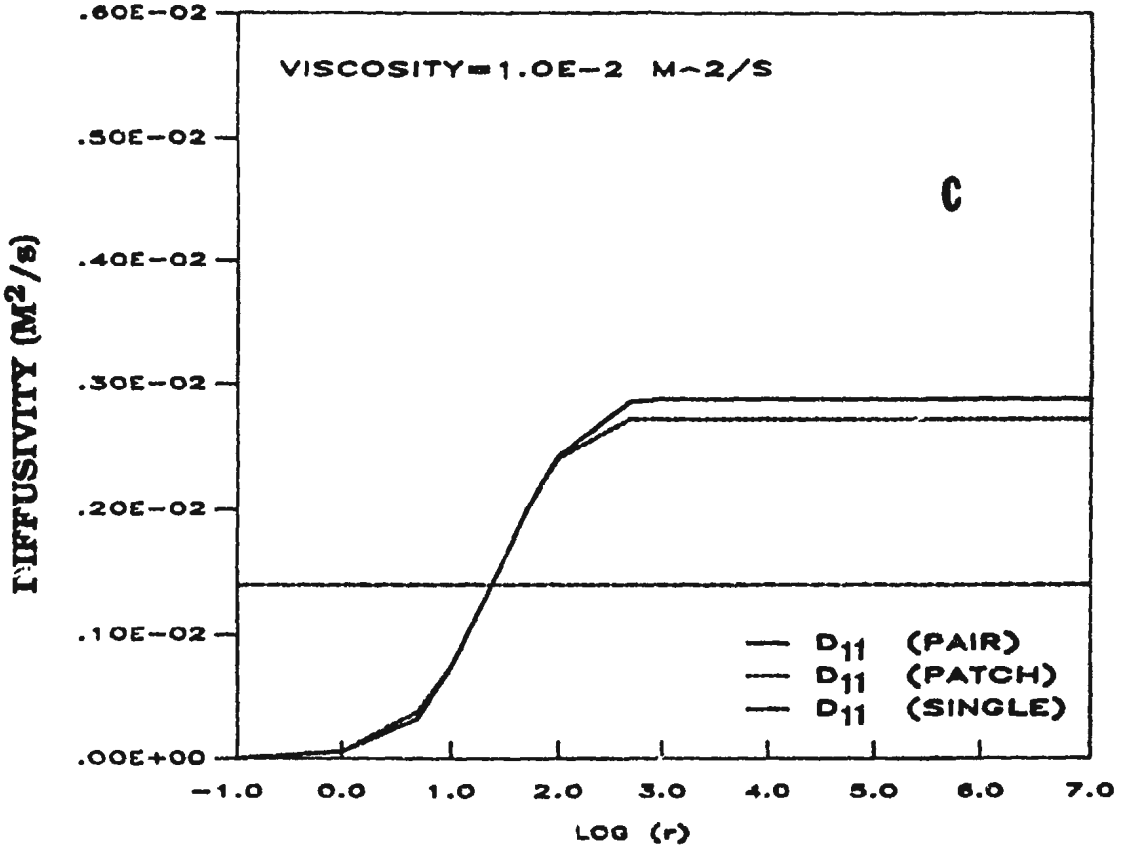

FIGURE 5-8 (CONCLUDED)

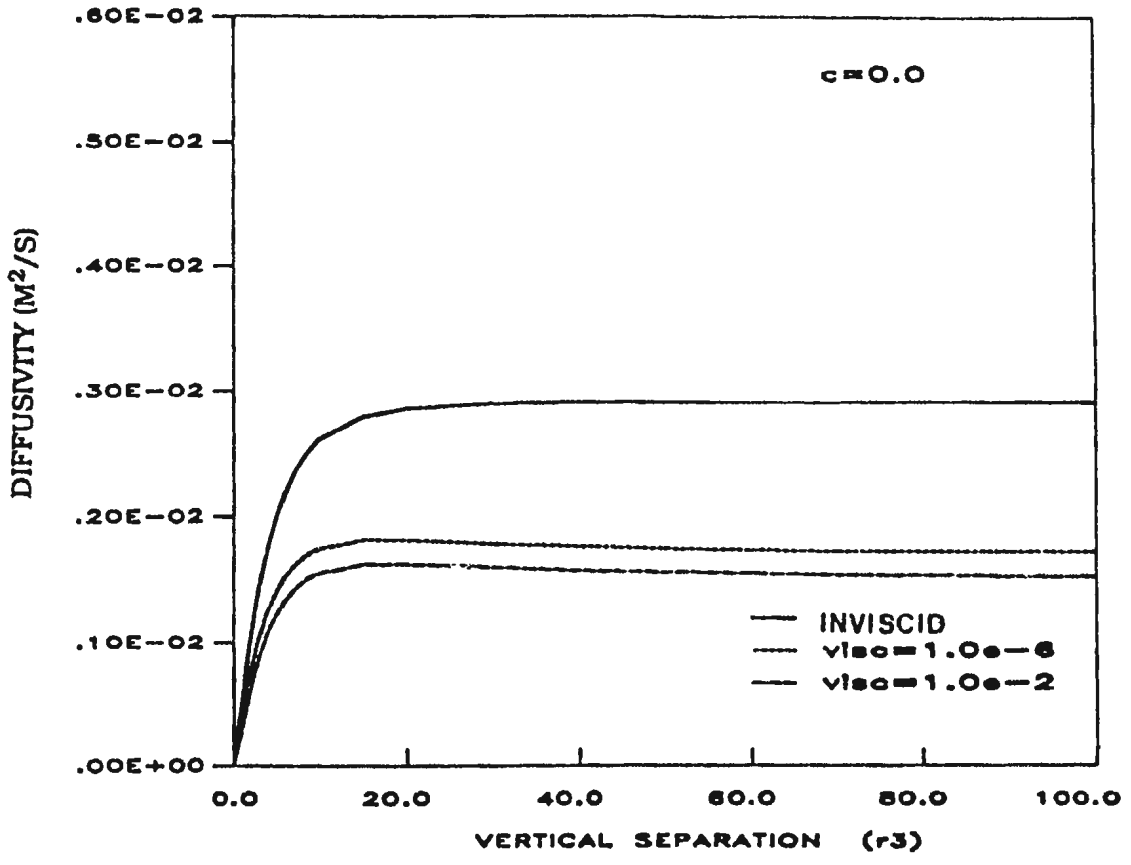

Figure 5-9: Two-particle diffusivities $D_{11}^{IN(2)}$ and $D_{11}^{VF(2)}$ as a function of vertical separation r_3 for c=0. The solid line is for $D_{11}^{IN(2)}$ and the broken lines are due to $D_{11}^{VF(2)}$ for $\nu=1.0\times10^{-6}$ and $\nu=1.0\times10^{-2}$ m^2/s respectively.

Two-particle diffusivity as a function of vertical separation r_3 is calculated from (5.14) with $\alpha_{i,j}$ replaced by $\alpha'^{IN(2)}_{i,j}$ (5.26). In this case, the diffusivity depends not only on the vertical separation between the two particles but also on the initial depth of the reference particle with respect to which the separation is measured. Figure 5.9 shows the plot of the a-component of the eddy-diffusivities $D_{11}^{IN(2)}$, $D_{11}^{VF(2)}$ against vertical separation r_3. For small separation the diffusivity is zero. As the separation increases the two-particle diffusivities increases reaching to a maximum value which is equal to the single-particle diffusivity at the reference depth c_1, in this case, surface. The reason for this is that the velocity of one of the two particles at large depth goes to zero for large vertical separation. As a result, for vertical separation, two-particle diffusivity is not twice the single-particle diffusivity.

Figure (5.10) shows the plot of the vertical diffusivities $D_{33}^{VF(2)}$ as function of vertical separation r_3. In this case also $D_{33}^{VF(2)}$ is zero when r_3 is small and increases to a maximum value equivalent to the single-particle diffusivity of the reference particle.

Diffusion experiments in the ocean have been performed on a variety of space and time scales (Okubo, 1971; Kawai, 1985; Krauss and Boning, 1987). However, most of them are for horizontal diffusion. Few experiments have been conducted to measure vertical diffusivity. Hardly any, however, has been combined with sufficiently detailed wave measurements to determine how much of the observed diffusion may have been due to waves. Most of the experiments on vertical diffusion in the coastal ocean are reported by Kullenberg (1971, 1976, 1977). Kullenberg (1971) used a dye tracing technique to measure vertical diffusivity in stratified shallow waters in weak to moderate (5 - 10 m/s) wind conditions. At a depth between 2 m and 21 m the vertical eddy-diffusivities observed by Kullenberg are scattered in the range of $(0.08-60)\times 10^{-4}\ m^2/s$. In another set of experiments in the Baltic thermo-

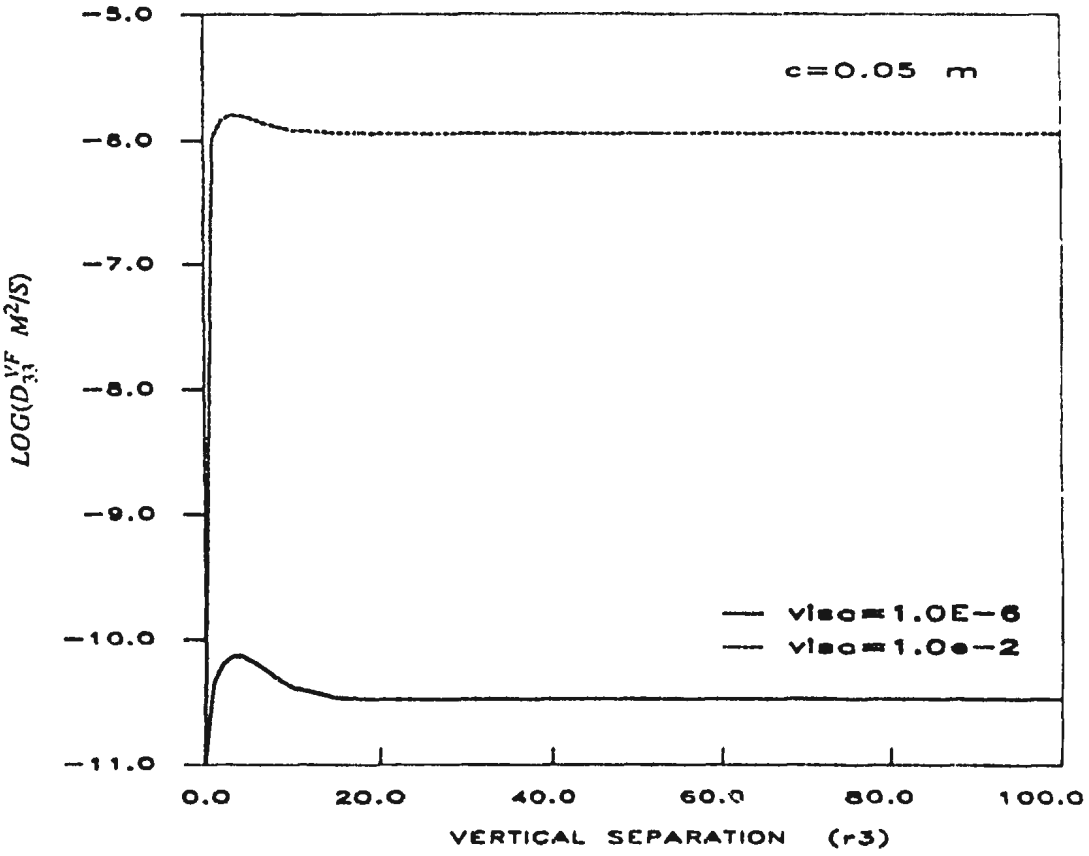

Figure 5-10: Two-particle diffusivity $D_{33}^{VF(2)}$ as a function of vertical separation r_3 for c=0.05 m. The solid line is due to $\nu=1.0\times10^{-6}$ and the broken line is due to $\nu=1.0\times10^{-2}$ m^2/s respectively.

and halocline layer, Kullenberg (1977) obtained vertical diffusivities in the range of $(1.0-4.5)\times10^{-6}\ m^2/s$ in the depth range (30 - 55) m. The Baltic has a stably stratified ($\partial\rho/\partial z<0$) water column having stratification parameter $N^2=-\frac{g}{\rho}\frac{\partial\rho}{\partial z}$ in the range of $(9.0\times10^{-4}-9.0\times10^{-3})\ s^{-2}$. Kullenberg (1971) found an empirical relation connecting vertical eddy-diffusivity (D_{33}) and wind speed (U), stratification parameter N^2 and vertical shear dq/dz given by

$$K_{33}=8.1\times10^{-8}|U^2N^{-2}|dq/dz||$$

where q is the horizontal velocity. Gargett (1984) also observed that vertical eddy-diffusivity (estimated from dissipation rate measurements) is a decreasing function of buoyancy frequency (N).

The vertical eddy-diffusivities estimated from the theoretical calculations are at the lower bound of the above mentioned experimentally observed eddy-diffusivities. This implies that the dynamics in the real ocean is more complex than that described in this model. It is possible that some other mechanism (or mechanisms) may have dominant role in the ocean. For example, wave breaking, vertical shear, internal waves, stratification, etc. may control the dynamics at depth in the real ocean. The theoretical model described here may be appropriate to a small amplitude wave (e.g., swell) travelling through a relatively calm sea.

Chapter 6

SUMMARY AND CONCLUSIONS

Patch diffusion computed from Lagrangian data:

Eddy-diffusion in the ocean has been studied experimentally by using drifter trajectories. The Atlantic Equatorial Undercurrent drogue experiments of Fahrbach et al. (1986) are reanalysed in chapter 2. Eddy-diffusivities were calculated by subtracting: (1) centroid motion (pure diffusion model) and (2) centroid displacement and displacement due to uniform Lagrangian deformations (advection diffusion model). The average diffusivities calculated using (1) are compared with those of Fahrbach et al. (1986). In the meridional direction the assumption C_ρ=0.1 (i.e., integral length scales are one tenth the standard deviation of drifter positions) turns out to be reasonable, thereby confirming relative diffusivities in the meridional direction calculated by Fahrbach et al. (1986). However, the zonal diffusivity is substantially different from that of Fahrbach et al. (1986). The analysis also indicated that a diffusion model described the cluster dispersion every bit as well as an advection diffusion model.

Measurement errors were shown to have little effect upon estimation of eddy-diffusivities but biased Lagrangian integral time and space scales (which were smaller than they should have been). Kinetic energy was increased by the measurement error.

An Eulerian analysis of the relative velocities revealed that

Eulerian integral time scales are slightly larger than the Lagrangian integral time scales. Joint space-time correlations indicated that the eddy velocity changes rapidly compared with time-scales required to advect a particle over the eddy length scale. In the case of experiments D1, D2, D3 (which had large relative velocities) the relative velocity became spatially decorrelated at scales small compared with cluster dimensions. The spatial scales of the relative velocity were larger for the CIPREA experiment which had weaker relative velocities than D1, D2 and D3. Integral time scales for transverse, longitudinal velocity components differed greatly for the x, y velocity components suggesting that the longitudinal-transverse coordinates are more aligned with the eddy causing relative motion between particles than the x–y coordinates.

Diffusion by surface gravity waves:

We have also studied smaller scale ocean diffusion theoretically by solving the Navier-Stokes' equations of motion for deep water surface gravity waves. A perturbation expansion is used to solve the Lagrangian equations of motion analytically for an irrotational, inviscid, homogeneous ocean. The first order solutions are oscillatory in time. The second order momentum equations are solved for the zero-frequency interaction between two primary waves. Other types of solutions with $\omega \neq \omega'$ are also possible. These latter solutions are oscillatory in time and do not cause any diffusion. So they were not studied in the present work.

The second order zero-frequency inviscid solutions are a field of random shearing motions in the horizontal plane but have no vertical motion. These solutions are identical to solutions of Herterich and Hasselmann (1982) who used the Euler-Lagrange transformation to

derive mass transport velocities from the Eulerian solutions. For $\theta=\theta'=0$, the inviscid solutions reduce to Stokes' solutions.

The inviscid dynamics is then extended to include the viscosity (in chapter 4). Surface boundary conditions are derived by considering the balance between vertical and horizontal stresses at the free surface. The solutions are obtained for both nondecaying (permanent primary waves) and decaying waves. In order to maintain the permanent primary waves against decay, a vertical stress is applied to the surface following Weber (1985).

The zero-frequency second order viscous nondecaying solutions are obtained by considering steady state motion. These solutions have both horizontal and vertical random motion that decays with depth. The particular part of these solutions u_2^{VP} and v_2^{VP} reduce to inviscid solutions u_2^{IN} and v_2^{IN} when viscosity set to zero. The second order nondecaying solutions do not, however, reduce to the inviscid solutions when viscosity is set to zero. This is because the homogeneous part of the nondecaying solution is nonzero when viscosity is set to zero. For a monochromatic wave, the a-component of the velocity u_2^{VF} reduces to Weber's (1983b) solution when $\theta=\theta'=0$.

The viscous decaying solutions, were obtained by solving time dependent equations of motion in three dimensions. The homogeneous second order solutions for zero-frequency interactions are obtained subject to an initial condition similar to Weber (1983a). The solutions satisfy boundary conditions at the surface and also at depth. This is in contrast to Chang's (1969) solutions. The second order u_2-component of motion given by the Chang's solution (Chang's equation 121) does not decay with depth. In fact her u_2 solution oscillates sinusoidally up to infinite depth. For $\theta=\theta'=0$, the second order viscous decaying solution u_2^{VD} (4.145a) reduce to Weber's (1983a) solution for a monochromatic

wave situation. Furthermore, setting $\nu=0$, the viscous decaying solutions u_2^{VD}, v_2^{VD} reduce to inviscid solutions u_2^{IN} and v_2^{IN}.

Eddy-diffusivities are calculated from the inviscid and viscous solutions following Herterich and Hasselmann (1982). A Pierson-Moskowitz spectrum (Pierson and Moskowitz, 1964) for a fully developed sea was used in this calculation. The inviscid solutions reproduce Herterich and Hasselmann's (1982) result of directional dependence of eddy diffusivities. The inviscid and viscous horizontal single-particle eddy-diffusivities are highly anisotropic. The inclusion of viscosity, causes a significant change in the horizontal inviscid eddy-diffusivity. At the surface, the viscous decaying diffusivity D_{11}^{VD} is larger than the inviscid diffusivity D_{11}^{IN} and viscous forced diffusivity D_{11}^{VF} by factors of 1.2 and 1.7 respectively for the viscosity equal to 1.0×10^{-2} m^2/s. The viscous decaying diffusivity D_{11}^{VD} and inviscid diffusivity D_{11}^{IN} tend to converge below the depth of the viscous boundary layer. The viscous forcing diffusivity D_{11}^{VF} decays more slowly with depth and remains different from the inviscid diffusivity D_{11}^{IN} even below the Stokes depth which is about 6.6 m.

An analytical expression for the vertical eddy diffusivity due to wave-wave interaction at zero frequency is given for the first time. The vertical eddy-diffusivity due to viscous gravity waves is much smaller than the eddy-viscosity. Changing viscosity has only a small effect on the horizontal eddy-diffusivities (as the eddy-viscosity is increased by an order of 4, the horizontal eddy-diffusivity is changed by less than a factor of 2). However, the vertical eddy-diffusivity was observed to change dramatically (by order of 4) as the eddy-viscosity is changed (increased by order of 4). A linear increase of vertical eddy-diffusivity D_{33}^{VF} with viscosity ν is observed. However, the choice of maximum viscosity is limited by the condition $kl \ll 1$.

The viscous and inviscid single-particle horizontal eddy-diffusivities increase with the wind speed raised to the power of 3. The single-particle vertical eddy-diffusivity D_{33}^{VF}, however, did not show any power-law dependence with the wind speed (although it does increase slightly with increased wind speed). Kullenberg (1971), from dye experiments, reported that the vertical eddy-diffusivity increases with the square of the wind speed coupled with vertical shear and buoyancy frequency.

The theoretically calculated single particle vertical eddy-diffusivities using the nondecaying wave solution in the depth range (1.0-10) m is $(0.62–0.11)\times10^{-6}$ m^2/s for $U=10$ m/s, $\nu=0.01$ m^2/s. There is no report of systematic measurement of vertical diffusivity and wind speed to compare our theoretically calculated eddy-diffusivities with the observations. At depths between 2 m and 21 m, the vertical eddy-diffusivities observed by Kullenberg (1971) are scattered in the range $(0.01–60)\times10^{-4}$ m^2/s. Other estimates of the vertical eddy-diffusivities in the same area (Hansen, 1968) show that the vertical eddy-diffusivities lie in the range $(0.1–0.7)\times10^{-4}$ m^2/s. (Depth range in this case is unknown). The experimental site had stratified water and shallow depth (less than 50 m). Our calculations are for deep water waves in a homogeneous ocean. The wave length corresponding to the peak-frequency ω_m of the Pierson-Moskowitz spectrum is about 71 m. Therefore deep water theory is applicable for these observations. The theoretical estimates of the single particle vertical eddy-diffusivities using the present model are at the lower boundary of the experimentally observed eddy-diffusivities of Kullenberg (1971). It is quite possible that the dynamics causing vertical diffusion in the real ocean are different from those used in this model. Other dynamics such as wave breaking, tertiary inviscid zero-frequency interactions may be important in the real oceanic situation. A wave with small amplitude (e.g., swell moving into a calm sea) may give rise to eddy-diffusivities similar to theoretically calculated values.

Two-particle diffusivities are calculated for horizontal separation r and also for vertical separation r_3. Patch-diffusivity is calculated for horizontal separation r only. Concentration distribution of the patch is taken as Gaussian with horizontal scale $\lambda=200m$ (5.45). For horizontal separation r, the two-particle diffusivity was found to be twice the single-particle diffusivity and patch-diffusivity is in between the two diffusivities similar to Herterich and Hasselmann (1982) and Sanderson and Okubo (1988). For vertical separation (r_3) between a pair of particles, the two-particle diffusivity was observed to increase from zero (at zero separation) to a maximum value (for large separation) which is the single particle diffusivity at the reference depth with respect to which r_3 is measured. This could be explained as follows. The zero-frequency velocity varies sinusoidally with a, b coordinates and decreases exponentially with depth. For two-particle velocity with large vertical separation between the two particles, the velocity of one of the particles at large depth is zero. So the two-particle velocity reduces to a single-particle velocity when one of the particles is at great depth. Consequently, the two-particle eddy-diffusivity reduces to single-particle diffusivity of the particle at shallow depth. For horizontal separation, however, the velocity of a pair of particles (at same depth) separated by a horizontal distance varies sinusoidally as a function of separation (see 5.21, 5.23). As a result, the two-particle eddy-diffusivity is increased by a factor of 2.

The limitation of this model is that the model assumes $\varepsilon^2\varepsilon_1 \gg \varepsilon^3$ which is valid when wave amplitude is small and eddy-viscosity is large. But usually ε^3 is greater than $\varepsilon^2\varepsilon_1$. This implies that the zero-frequency third order inviscid solution will be larger than the zero-frequency second order viscous solutions. It will be interesting to investigate the third order inviscid equations and look for the zero-frequency vertical solution.

The study shows that random surface wave field can produce

both horizontal and vertical diffusion. The observations of Kullenberg (1971) and Hansen (1968) indicate that our vertical diffusive mechanism is only large enough to account for the lower limit of the observed vertical eddy-diffusivity. But our work does agree with measurements of horizontal diffusion at the scale of surface gravity waves. For example, Figure 5.1d shows that at $c=0$, $n=2$, the single-particle horizontal eddy-diffusivity is 0.013 m^2/s. The diffusion diagrams of Okubo (1971) show that we can expect similar range of eddy-diffusivities at 10 - 100 m scale.

BIBLIOGRAPHY

Beauchamp, K., and C. Yuen, 1979: Digital Method for Signal Analysis, George Allen and Unwin, London, 316 pp.

Bowden, K. F., 1965: Horizontal mixing in the sea due to a shearing current, J. Fluid Mech., 21, 83-95.

Chang, M. S., 1969: Mass transport in deep water long-crested random gravity waves. J. Geophys. Res., 74, 1515-1536.

Collin De Verdiere, A., 1983: Lagrangian eddy statistics from surface drifters in the eastern North Atlantic. J. Mar. Sc., 41, 375-398.

Corrsin, S., 1962: Theories of turbulent dispersion. Mechanics of turbulence. Proc. Intern. Symp. National Sc. Res. Center, Marseille, 27-52.

Davis, R. E., 1982. On relating Eulerian and Lagrangian velocity statistics: Single particles in homogeneous flows. J. Fluid Mech. 114, 1-26.

Fahrbach, E., C. Brockmann, and J. Meincke, 1986: Horizontal mixing in the Atlantic Equatorial undercurrent estimated from drifting buoy clusters. J. Geophys. Res., 91, 10557-65.

Gargett, A. E., 1984: vertical eddy diffusivity in the ocean interior. J. Mar. Res., 42, 359-393.

Garrett, C., J. F. Middleton, F. Majaess, and M. Hazen, 1985: Analysis and prediction of iceberg trajectories. Department of Oceanography, Dalhousie University, Nova Scotia, 86 pp.

Hansen, J., 1968: Recipient investigations in the Oresund outside Skovshoved Harbour, Rep. No. 2 (in Danish). The Danish Isotope Centre, Copenhagen, pp. 36.

Hasselmann, K., 1961: On the nonlinear energy transfer in a gravity wave spectrum, part 1: General theory. J. Fluid Mech., 12, 481-500.

Hasselmann, K., T. P. Barnett, E. Bouws, H. Carlson, D. E. Cartwright, K. Enke, J. A. Ewing, H. Gienapp, D. E. Hasselmann, P. Krusemann, A. Meerburg, P. Muller, D. J. olbers, K. Richter, W. sell and H. Walden, 1973: Measurements of wind-wave growth and swell decay during the Joint North Sea Wave Project (JONSWAP). Deutsches Hydrographisches Institut, Hamburg, pp. 95.

Herterich K. and K. Hasselmann, 1982: The horizontal diffusion of tracers by surface waves, J. Phys. Oceanogr.,12,704-711.

Hildebrand, F. B., 1962: Advanced calculus for applications, Prentice-Hall, Inc., Englewood Cliffs, New Jersey, pp646.

Huang, N. E., 1970: Mass transport induced by wave motion, J. Mar. Res., 28, 35-50.

Huang, N. E., 1971: Derivation of Stokes drift for a deep-water random gravity wave field. Deep Sea Res., 18, 225-259.

Jenkins, A. D., 1986: A theory of steady and variable wind and wave induced currents, J. phys. Oceanogr., 16, 1370-1377.

Jenkins, A. D., 1987: Wind and wave induced currents in a rotating sea with depth varying eddy viscosity, J. Phys. Oceanogr., 17, 938-951.

Joseph, J. and H. Sendner, 1958: Uber die horizontale diffusion im Meere. Dt. Hydrogr. Z., 11, 49-77.

Katz, E. J., J. G. Bruce and B. D. Petrie, 1980: Salt and mass flux in the Atlantic Equatorial Undercurrent. Deep Sea Res., 26, suppl. 2, 137-160.

Kawai, H., 1985: Scale dependence of divergence and vorticity of near surface flows in the sea - part 1 & 2, J. Oceanogr. Soc. of Japan, 41, 157-166.

Kinsman, B., 1984: Wind waves: Their generation and propagation on the ocean surface, Dover publication Inc., pp.676.

Krauss W. and C. W. Boning, 1987: Lagrangian properties of eddy fields in teh northern north Atlantic as deduced from satellite-tracked buoys. Journal of Marine Research, 45, 259-291.

Kullenberg, G. E. B., 1971: Vertical diffusion in shallow waters. Tellus, 23, 129-135.

Kullenberg, G. E. B., 1976: On vertical mixing and Energy transfer from the wind to the water. Tellus, 28, 159-165.

Kullenberg, G. E. B., 1977: Observations of the Mixing in the Baltic thermo- and halocline layers. Tellus, 29, 572-587.

Lamb, H., 1932: Hydrodynamics, 6th Ed., Cambridge University Press, 738 PP.

LeBlond, P. H. and L. A. Mysak, 1978: Waves in the ocean. Elsevier Scientific Publishing Company, pp. 602.

Leibovich, S., 1983: The form and dynamics of the langmuir circulations, Annual Rev. in Fluid mech., 15, 391-427.

Longuet-Higgins, M. S., 1953: Mass transport in water waves, Phil. Trans. R. Soc. Lond. A245, 535-581.

Longuet-Higgins, M. S., 1960: Mass transport in boundary layer at a free oscillating surface, J. Fluid Mech., 8, 293-306.

Longuet-Higgins, M. S., 1969: A nonlinear mechanism for the generation of sea waves, Proc. R. Soc., A. 311, 371-389.

Middleton, J. F. and C. Garrett, 1986: A kinematic analysis of polarized eddy fields using drifter data, J. Geophys. Res., 91, 5094-5102.

Munk W., 1981: Internal waves and small-scale processes. In The Evolution of Physical Oceanography: Scientific Papers in Honour of Henry Stommel, Ed. B. A. Warren and C. Wunsch, MIT Press, 264-291.

Okubo, A., 1962: A review of theoretical models of turbulent diffusion in the sea, J. Oceangr. Soc. Japan, 20th Anniv. Vol., 286-320.

Okubo, A., 1967: Study of turbulent dispersion by use of Lagrangian diffusion equation, Phys. Fluids, suppl. 1967, S72-75.

Okubo, A., 1970: Horizontal dispersion of floatable particles in the vicinity of velocity singularities such as convergences, Deep-Sea Res., 17,445-454.

Okubo, A., 1971: Ocean diffusion diagrams, Deep-Sea Research, 18, 789-802.

Okubo, A. and C. C. Ebbesmeyer, 1976: Determination of vorticity, divergence and deformation rates from analysis of drogue observations, Deep-Sea Res., 23, 349-352.

Okubo, A., C. C. Ebbesmeyer and J. M. Helseth, 1976: Determination of Lagrangian deformation from analysis of current followers, J. Phys. Oceanogr., 6, 524-527.

Okubo, A., C. C. Ebbesmeyer and B. G. Sanderson, 1983: Lagrangian diffusion equation and its application to Oceanic dispersion, J. Oceanogr. Soc. Japan, 39, 259-266.

Osborne, A. R., A. D. Kirwan Jr., A. Provenzale, and L. Bergamasco, 1989: Fractal drifter trajectories in the Kuroshio extension. Tellus, 41A, 416-435.

Ozmidov, R. V., 1958: On the calculation of horizontal turbulent diffusion of the pollutant patches in the sea. Doklady Akad. Nauk, SSSR, 120, 761-763.

Ozmidov, R. V., 1960: On the rate of dissipation of turbulent energy in sea currents and on the dimensionless universal constant in the "4/3-power law", (In Russian) Tzv. Akad. nauk SSSR, Geofys. Ser. No. 8, pp. 1234-1237. (Am. Geophys. Union Transl. English Edit., Bull. Acad. Sci. USSR. Geophys. Ser., No. 8, pp. 821-823.).

Pal, B. K. and B. G. Sanderson, 1992: Measurements of drifter cluster dispersion, submitted to Atmosphere-Ocean.

Pierson, W. J., 1962: Perturbation analysis of the Navier-Stokes equations in Lagrangian form with selected linear solutions. J. Geophys. Res., 67, 3151-

Pierson, W. J. and L. Moskowitz, 1964: A proposed spectral form for fully developed wind seas based on the similarity theory of S. A. Kitaigorodoskii, J. Geophys. Res., 69, 5181-5190.

Poulain, P. M. and P. P. Niiler, 1989: Statistical analysis of the surface circulation of the California Current System using satellite-tracked drifters, J. Phys. Oceanogr., 19, 1588-1603.

Russel, R. C. and J. D. C. Osorio, 1957: An experimental investigation of drift profiles in a closed channel. In Proc. 6th Conf. Coastal Energy, Miami, pp.171-993.

Richardson, L. F., 1926: Atmospheric diffusion on a distance neighbour graph, Proc. Roy. Soc. A110, 709-727.

Sanderson, B. G. and A. Okubo, 1986: An analytical calculation of two-dimensional dispersion. J of the Oceangr. Soc. of Japan, 42, 81-94.

Sanderson, B. G. and A. Okubo, 1988: Diffusion by internal waves, J. Geophys. Res., 93, 3570-3582.

Sanderson, B. G., B. K. Pal and A. Goulding, 1988: Computing unbiased estimates of the magnitude of residual velocities from a small number of drogue trajectories, J. Geophys. Res., 93, 8161-8162.

Sanderson, B. G. and B. K. Pal, 1990: Patch diffision computed from Lagrangian data, with application to the Atlantic Equatorial Undercurrent. Atmosphere Ocean., 28, 444-465.

Sanderson, B. G., A. Goulding and A. Okubo, 1990: The fractal dimension of relative Lagrangian motion. Tellus, 42A, 550-556.

Sanderson B. G, and D. Booth, 1991: The fractal dimension of drifter trajectories and estimates of horizontal eddy-diffusivity. Tellus, 43A, 334-349.

Schott, F., M. Ehlers, L. M. Hubrich and D. Quadfasel, 1978: Small scale mixing experiments in the baltic surface mixed layer under different weather condition, Dt. Hydrogr. Z. 31,195-215.

Stokes, G. G., 1847: On the theory of oscillatory waves, Trans. Camb. Phil. Soc., 8, 441-455.

Stommel, H., 1949: Horizontal diffusion due to Oceanic Turbu- lence, J. Mar. Sc., 8, 199-225.

Swan, C. and J. F. A. Sleath, 1990: A second approximation to the time-mean lagrangian drift beneath a series of progressive gravity waves. Ocean Engng., 17, 65-79.

Tamai, N., 1972: Diffusion due to random waves. Proc. Japan Soc. Civil Engineers, 203, 79-91.

Taylor, G. I., 1922: Diffusion by continuous movements, Proc. London Math. Soc. A20, 196-211.

Tennekes, H. and J. L. Lumley, 1972: A First Course in Turbulence, The MIT Press, Cambridge, Mass., 300 pp.

Unluta, U. and C. C. Mei, 1970: Mass transport in water waves. J. Geophys. Res., 75, 7611-7618.

Weber, J. E., 1983a: Attenuated wave-induced drift in a viscous rotating ocean, J. Fluid Mech., 137, 115-129.

Weber, J. E., 1983b: Steady wind- and wave-induced current in the open ocean, J. Phys. Oceanogr., 13, 524-530.

Weber, J. E., 1985: Friction induced roll motion in short-crested surface gravity waves, J. Phys. Oceanogr., 15, 936-942.

Wilson, R. E. and A. Okubo, 1978: Longitudinal dispersion in a partially mixed estuary, J. Mar. Res., 36, 427-447.

Young, W. R., P. B. Rhines and C. J. R. Garrett, 1982: Shear-Flow dispersion, internal waves and horizontal mixing in the ocean, J. Phys. ocean., 12, 515-527.

Zimmerman, J. T. F., 1986: The tidal Whirlpool: a review of horizontal dispersion by tidal and residual currents, Netherlands J. Sea Res., 20, 133-154.